Master's thesis

NTNU
Norwegian University of Science and Technology
Faculty of Natural Sciences
Department of Physics

André Wean Edvardsen

Study of Pair Induced Quenching in Nanosecond-pulsed Holmium-doped Fiber Amplifiers

Master's thesis in Applied Physics and Mathematics
Supervisor: Irina T. Sorokina
Co-supervisor: Lars G. Holmen
June 2022

NTNU
Norwegian University of
Science and Technology

André Wean Edvardsen

Study of Pair Induced Quenching in Nanosecond-pulsed Holmium-doped Fiber Amplifiers

Master's thesis in Applied Physics and Mathematics
Supervisor: Irina T. Sorokina
Co-supervisor: Lars G. Holmen
June 2022

Norwegian University of Science and Technology
Faculty of Natural Sciences
Department of Physics

NTNU
Norwegian University of
Science and Technology

Abstract

Holmium-doped fiber laser amplifiers can operate at a wavelength of $\sim 2.1\,\mu m$, which is an "eye-safe" wavelength that can propagate through the atmosphere with low attenuation. This makes amplifiers of this type promising candidates for a variety of laser applications such as free-space optical communication and remote sensing. However, holmium-doped fiber amplifiers have been found in numerous studies to have a lower efficiency than theoretically expected. The cause of this is often attributed to clustering of the holmium-ions and related pair induced quenching (PIQ).

In this work, PIQ in holmium-doped optical fiber amplifiers is investigated. Specifically, dynamic aspects of the quenching process that occurs on sub-microsecond timescales are studied, which are essential for the understanding of pulsed holmium-doped fiber amplifiers that operate in the nanosecond temporal regime.

A numerical rate equation model for holmium-doped fiber amplifiers was developed, which accounts for dynamic aspects of PIQ. This model was developed to accompany the experimental parts of this project, and it was extensively evaluated by comparing simulations with experimental results. Overall, the numerical model offered good agreement between simulations and experiments.

Spectroscopic measurements were done on holmium-doped optical fibers to measure important parameters of the PIQ process. Specifically, time-resolved fluorescence measurements were done to determine the lifetime of doubly-excited holmium-ion pairs. This lifetime was found to be 460 ns, which notably is almost an order of magnitude larger than the 50 ns lifetime established for erbium.

Additionally, measurements of non-saturable absorption were used to determine the amount of ion-pairs in a holmium-doped fiber sample. This method has for decades been the accepted method used for estimating pair content in erbium-doped fibers. However, numerical simulations in this work reveals that because of the significantly longer pair lifetime in holmium, the method is prone to severely underestimating the pair content of holmium-doped fibers.

The practical impact of PIQ was also investigated in a high power holmium-doped fiber amplifier outputing 20 ns pulses with a wavelength of 2107 nm and

100 kHz repetition rate, achieving an average output power up to 5.4 W. The investigation was done by pumping the amplifier with short 20 ns pulses with a wavelength of 1950 nm, and measuring the optical conversion efficiency when the delay between the pump and seed pulses was varied. It was found that the efficiency decreased with increasing delays on a timescale that corresponds to the holmium-pair lifetime, clearly suggesting that PIQ is the root cause of the reported low efficiency in holmium-doped fiber amplifiers.

The combined results of this work have improved the short-timescale understanding of PIQ occuring in holmium-doped optical fibers, which will aid in the development of next-generation nanosecond pulsed holmium-doped fiber amplifiers.

Sammendrag

Holmium-dopede fiberlaserforsterkere kan operere med en bølgelengde på $\sim 2.1\,\mu m$, som er en "øye-sikker" bølgelengde som kan forplante seg gjennom atmosfæren med lav demping. Dette gjør forsterkere av denne typen til lovende kandidater for en rekke laserapplikasjoner, som for eksempel optisk frittromskommunikasjon og fjernmåling. Holmium-dopede fiber forsterkere har derimot i mange studier vist seg å ha en lavere virkningsgrad enn teoretisk forventet. Årsaken til dette er ofte tilskrevet klynger av holmium-ioner og en relatert tapsmekanisme som kalles "pair induced quenching" (PIQ).

I dette arbeidet undersøkes PIQ i holmium-dopede optiske fiberforsterkere. Spesifikt blir dynamiske aspekter av PIQ-prosessen som skjer på tidsskalaer kortere enn mikrosekund studert, noe som er avgjørende for forståelsen av pulsede holmium-dopede fiberforsterkere som opererer i nanosekund-tidsregimet.

Det ble utviklet en numerisk rateligningsmodell for holmium-dopede fiberforsterkere som tar med i betraktning dynamiske aspekter ved PIQ. Denne modellen ble utviklet for å følge de eksperimentelle delene av dette prosjektet, og den ble grundig evaluert ved å sammenligne simuleringer med eksperimentelle resultater. Overordnet sett viser den numeriske modellen god enighet mellom simuleringer og eksperimenter.

Spektroskopiske målinger ble gjort med holmium-dopede optiske fibre for å måle viktige parametere i PIQ-prosessen. Nærmere bestemt ble det utført tidsoppløste fluorescensmålinger for å bestemme levetiden til dobbelt-eksiterte holmium-ionepar. Denne levetiden ble målt til å være 460 ns, som er nesten en størrelsesorden større enn den etablerte levetiden på 50 ns for erbium.

I tillegg ble målinger av ikke-blekbar absorpsjon brukt til å bestemme mengden ionepar i en holmium-dopet fiberprøve. Denne metoden har i flere tiår vært den aksepterte metoden som brukes for å estimere parinnhold i erbium-dopede fibre. Numeriske simuleringer i dette arbeidet viser imidlertid at på grunn av den signifikante lengre parlevetiden i holmium, kan metoden være utsatt for å underestimere parinnholdet i holmium-dopede fibre.

Den praktiske innvirkningen av PIQ ble også undersøkt i en høyeffekts holmium-dopet fiberforsterker som leverte 20 ns lange pulser med bølgelengde 2107 nm med

en repetisjonshastighet på 100 kHz og oppnådde en gjennomsnittseffekt opptil 5.4 W. Undersøkelsen ble utført ved å pumpe forsterkeren med korte 20 ns pulser med en bølgelengde på 1950 nm, for så å måle den optiske virkningsgraden når forsinkelsen mellom pumpe- og signal-pulsene ble variert. Det ble funnet ut at virkningsgraden falt med økende forsinkelser på en tidsskala som tilsvarer holmium-parlevetiden, noe som tyder på at PIQ er hovedårsaken til den rapporterte lave virkningsgraden i holmium-dopede fiberforsterkere.

De kombinerte resultatene av dette arbeidet har forbedret korttidsskala-forståelse av PIQ som forekommer i holmium-dopede optiske fibre, og vil bidra til utviklingen av neste generasjons nanosekund-pulsede holmium-dopede fiber-forsterkere.

Preface

This thesis is submitted in partial fulfillment of the requirements for the degree of Master of Science in Applied Physics and Mathematics with a specialization in Applied Physics at the Norwegian University of Science and Technology (NTNU). This Master's project was supervised by Lars G. Holmen (FFI) and Irina T. Sorokina (NTNU). The research presented in this thesis was conducted at the Norwegian Defence Research Establishment (Forsvarets Forskningsinstitutt – FFI) at Kjeller, during the spring of 2022.

This thesis builds upon the work and results of a single-semester specialization project that was carried out during the fall of 2021 [1] This thesis is targeted towards an audience that possesses an understanding of physics and mathematics that corresponds to a fifth year physics student.

All of the presented experimental and numerical work was done by the author with the following exceptions:

- The 2.1 µm seed channel presented in Section 4.3 was developed by Lars G. Holmen as part of his PhD project [2].
- The holmium-doped optical fibers that were studied in this project were manufactured by external research groups and commercial manufacturers, and the information about these fibers summarized in Tables 4.1-4.2 was kindly provided by these groups.

Acknowledgements

I would like to extend my gratitude to my supervisor Lars G. Holmen. I have learned incredibly much from our many discussions. Everything from fiber lasers and electro-optics to scientific writing and much more. All the hours you have spent guiding me throughout this project have not gone unnoticed and are greatly appreciated.

I would also like to thank the other members of the laser group at FFI; Espen Lippert, Arne M. T. Løken and Helge Fonnum. The numerous instruments and program automatisations needed for the experimental part of this work would be difficult to master in the time frame of one semester without the effort of these people. Furthermore, I would like to thank Fonnum for great feedback on this thesis.

I thank my group of friends during these five years in Trondheim for making these years such a wonderful time! I thank you, Kristine, for your unconditional support and comfort throughout our time in Trondheim.

Lastly, I would like to thank my family for their continued support and encouragement.

Contents

List of Figures

List of Tables

List of Abbreviations

AOM Acousto-optic modulator

APD Avalanche photo diode

ASE Amplified spontaneous emission

BPF Bandpass filter

EM Electromagnetic

ETU Energy transfer upconversion

FBG Fiber Bragg grating

FUT Fiber under test

FWM Four-wave mixing

FWHM Full width at half maximum

LP Long pass

MM Multi-mode

MOPA Master oscillator power amplifier

NA Numerical aperture

NP Nanoparticle-doping

PIQ Pair induced quenching

RK45 Runge-Kutta4(5)

SBS Stimulated Brillouin scattering

SD Solution-doping

SM Single-mode

SP Short pass

SRS Stimulated Raman scattering

TIR Total internal reflection

WDM Wavelength division multiplexer

Chapter 1

Introduction

The word *laser* is an acronym for light amplification by stimulated emission of radiation. It is a process that generates light with extraordinary properties that has found applications in a wide range of fields since its inception in 1960 [3]. One special class of lasers called *fiber laser* is a technology that has quickly been adopted by industries and has seen immense growth in research and development over the last few decades [4]. In fiber lasers, light is confined inside *optical fibers*, guiding the light as it propagates through it. The optical fibers can be doped with ions of *rare-earth elements*, such as for example *ytterbium*, *erbium*, *thulium* and *holmium*. The rare-earth ions can be manipulated such that light that propagates through the doped fiber becomes amplified by the process of stimulated emission.

This work focuses on fiber lasers doped with ions of the rare-earth element holmium. Such lasers operate at a wavelength of $\sim 2.1\,\mu\text{m}$ [4]. This wavelength regime is very attractive for several established and emerging laser applications. Notably, this wavelength propagates through the atmosphere with low attenuation, and it is furthermore considered to be "eye-safe" since it does not penetrate the eye and cannot damage the retina. This makes holmium-doped fiber lasers premier candidates in applications such as long-range optical communication and remote sensing [4].

However, several reports show that holmium-doped fiber lasers operate with a much lower efficiency than what is theoretically expected. Recent studies have suggested that this may be caused by the doped holmium ions forming *clusters* or *pairs* inside the optical fibers. This evokes a detrimental process called *pair induced quenching* (PIQ) [5, 6, 7, 2]. The focus of this work is to increase our understanding of this process, and its implications on holmium-doped fiber amplifiers.

1.1 Pair Induced Quenching in Holmium-doped Optical Fibers

The pair induced quenching process will only briefly be explained in the following, as it will be thoroughly discussed in Chapter 2. In essence, PIQ is a rapid energy transfer process that reduces a fiber amplifier's ability to amplify light. When holmium ions are doped into optical fibers, the ions do not become randomly distributed. Instead, many more ions than statistically expected are in each others immediate vicinity (nearest neighbours only separated by inter-atomic distances), forming pairs or larger clusters. Holmium ions within a pair can interact rapidly with each other, and exchange energy in a way that reduces the gain of an amplifier.

A handful of studies have investigated PIQ in holmium-doped fiber amplifiers and employed numerical models to simulate the effects of the phenomenon [5, 6, 7, 2]. These numerical models have assumed that the interaction rate between paired ions is infinitely fast, in other words that the energy transfer occurs instantaneously. This is a reasonable assumption when considering amplifiers that operate in the "continous wave" regime, but it is expected to fail for amplifiers that operate with short pulses that have a duration comparable to the energy transfer rates characteristic of PIQ. The fast kinetics of PIQ have previously been studied in fiber amplifiers doped with ions of the rare-earth element erbium [8, 9]. These studies found that the *lifetime* (inverse interaction rate) of doubly-excited erbium ion-pairs was 50 ns. To my knowledge, similar studies have not been reported in published literature for holmium-doped fibers, despite such knowledge being essential prerequisites for numerical models suitable for analyzing fiber amplifiers in the nanosecond pulse regime.

1.2 Aim of This Work

The aim of this work is to study PIQ in holmium-doped fiber amplifiers, with particular emphasis on dynamic aspects of the phenomenon and corresponding implications for short pulse fiber amplifiers. This will involve spectroscopic measurements of holmium-doped fibers to measure important properties of PIQ, inspired by the studies done on erbium-doped fiber amplifiers [8, 9]. Specifically, time-resolved fluorescence measurements will be done to determine the lifetime of doubly-excited holmium ion pairs, and measurements of *non-saturable absorption* of holmium-doped fibers are done to estimate the amount of pairs in the fibers. In addition to the direct spectroscopic measurements, the practical impact of PIQ will be investigated in a high power holmium-doped fiber amplifier. Accompanying these experimental studies, a numerical rate equation model for holmium-doped fiber amplifiers will be developed. This model will account for dynamic aspects

of PIQ, with the purpose of forming a numerical framework for simulating and understanding pulsed amplifiers that operate in the nanosecond temporal regime. The experiments conducted in this project are purposely designed to allow comparison with simulation results of equivalent scenarios. This will allow evaluation of the phenomenological credibility and accuracy of the numerical model.

1.3 Thesis Overview

Chapter 2 presents basic theory of lasers, optical fibers and the energy level structure of holmium in silica. This theory will be important for understanding the numerical model, experiments and results of this work. Chapter 3 presents the numerical rate equation model that will be used for simulations and for comparison with the experiments done in this work. Chapter 4 motivates and explains the three experiments done in this work, before describing the experimental procedure and measurement setups. Chapter 5 presents the results of the experiments and numerical simulations. To aid the readability of the thesis, the results in Chapter 5 are discussed as they are presented. Additionally, summaries of the most important findings are included at the end of each main section of this chapter. Chapter 6 finally concludes the most important findings of this work and suggests relevant topics for future studies.

Chapter 2

Theory

This chapter presents the basic theory of optical fibers and lasers necessary for understanding the numerical model developed in this work, experiments performed, and the presented results from these. The chapter begins by explaining the fundamentals of optical fibers, namely their ability to guide light and the resulting electric field distribution inside the fiber. Then, the fundamental energy transitions occuring in lasers are discussed, followed by a simple rate equation model serving as an introduction to the more complex and specialized rate equation model presented in Chapter 3. Lastly, fiber amplifiers are discussed with focus on the energy level structure of holmium in fused silica. Pair induced quenching as an implication of holmium-ions forming clusters is also discussed.

2.1 Optical Fibers

The field of fiber optics has become essensial for the development of modern society. While early research focused mostly on the transmission of light over long distances, for applications such as optical communications, the research focus has later expanded to areas such as fiber amplifiers and fiber lasers. Optical fibers are a type of *waveguide* that can confine light in two dimensions, allowing the light only to propagate in the third. Though optical fibers can be made of a variety of different materials, the most widely used is fused silica glass (amorphous SiO_2). This material has relatively low cost and outstanding properties, such as extremely small optical propagation losses [10]. This makes fused silica optical fibers a good choice for use as the host material for doping of rare-earth elements, and used as the active medium in laser amplifiers.

2.1.1 Waveguiding in the Geometric Approximation

The simplest and most common optical fiber is a so-called step-index fiber. Figure 2.1a illustrates the cross section of a typical step-index fiber. The fiber consists of a *core* and a *cladding* surrounding it. The cladding itself is usually surrounded by a polymer coating, protecting the fiber. The core is doped with a substance that slightly increases its refractive index relative to that of the cladding. The refractive indices of the core and the cladding are constant, and as Figure 2.1a illustrates, this gives the refractive index profile a step-like shape.

The refractive index difference at the core-cladding interface is what gives step-index fibers their waveguiding property. In the geometrical optics approximation, waveguiding occurs as a result of total internal reflection (TIR). TIR occurs if a ray of light is incident at the core-cladding interface at an angle that is greater than a *critical angle* (θ_c). Generally, what happens to the light ray at an interface is governed by Snell's law of refraction [11]

$$n_1 \sin\theta_1 = n_2 \sin\theta_2, \tag{2.1}$$

where n_1 and n_2 are the refractive indices of the core and cladding, respectively. θ_1 and θ_2 are the angle of incidence and refracted angle from the interface (with respect to the interface normal). Equation (2.1) relates the light ray incident on the core-cladding interface to the ray refracted into the cladding. The outgoing angle of the reflected ray is always the same as the incident angle of the incoming ray. Thus, if the refractive indices of the core and cladding, and the angle of incidence of the incoming ray are known, then Equation (2.1) can be used to find

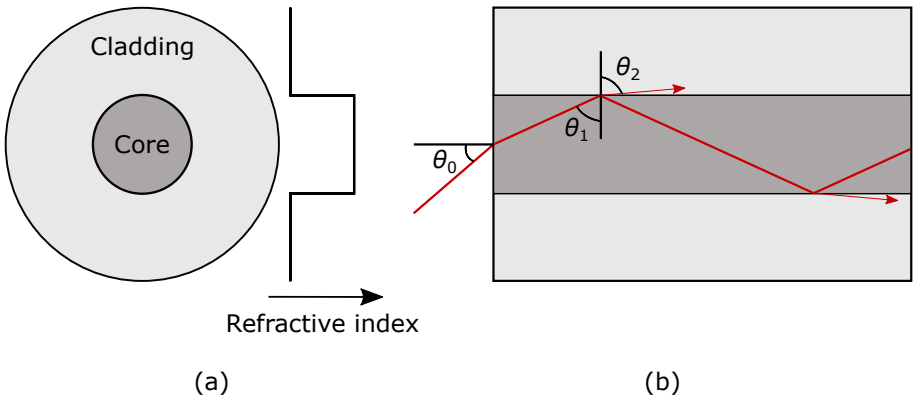

Figure 2.1: (a) A cross section of a step-index fiber together with its refractive index profile, and (b) a side-view of the same fiber illustrating Snell's law of refraction at the core-cladding interface.

the angle of all rays. Snell's law of refraction is illustrated in Figure 2.1b, showing a ray of light being partly refracted and partly reflected at the core-cladding interfaces.

When TIR occurs, no light is refracted into the cladding. The limit for this is when the refracted angle is $\theta_2 = 90°$. Inserting this into Equation (2.1) results in the critical angle

$$\theta_c = \arcsin(n_2/n_1), \tag{2.2}$$

which represents the smallest angle that a light ray can have incident on the core-cladding interface for TIR to occur.

Equations (2.1)-(2.2) can be combined to provide a very useful parameter for optical fibers, namely the *numerical aperture* (NA). Consider a light ray incident onto the input face of the fiber at an angle denoted as θ_0, as shown in Figure 2.1. The angle of the light ray refracted into the fiber core is related to the incidence angle on the core-cladding interface as $90° - \theta_1$. Inserting this angle into Equation (2.1), and substituting the refractive index and refraction angle of the cladding with the refractive index of the surrounding medium n_0 and the input angle θ_0, we get the relation

$$n_0 \sin\theta_0 = n_1 \sin(90° - \theta_1) = n_1 \cos\theta_1. \tag{2.3}$$

To find the largest input angle that will still lead to TIR, called the acceptance angle (θ_a), the critical angle from Equation (2.2) is inserted for θ_1 in Equation (2.3), giving $n_0 \sin\theta_a = n_1 \cos(\arcsin(n_2/n_1)) = \sqrt{1 - \sin[\arcsin(n_2/n_1)]^2} = \sqrt{n_1^2 - n_2^2} \equiv \text{NA}$. Thus, TIR will occur for all input angles satisfying the inequality [10]

$$n_0 \sin\theta_0 < n_0 \sin\theta_a = \sqrt{n_1^2 - n_2^2} \equiv \text{NA}. \tag{2.4}$$

Equation (2.4) describes that light rays entering the fiber core within a cone bounded by the acceptance angle (θ_a) will be guided by the fiber, in principle without any losses. Light rays entering the fiber at angles that do not satisfy this inequality will only be partly reflected, having parts of the light refracting into the cladding each time it is incident onto the core-cladding interface, and eventually dissipate. This is illustrated in Figure 2.1. Thus, the NA represents the optical fibers ability to guide light.

Importantly (and perhaps not intuitively), the fibers ability to guide light only depends on the refractive indices of the core and cladding, and not the size of the fiber core in the geometrical optics approximation. This approximation works reasonably well for optical fibers with a large core diameter compared to the wavelength of light, but begins to break down when the core diameter and the wavelength are comparable. In the latter regime, the wave nature of light must be taken into account.

2.1.2 Waveguiding in the Electromagnetic Approximation

Optical fibers with core diameter comparable to the wavelength of light must be treated with the electromagnetic wave equation based on Maxwell's equations. This treatment will be discussed briefly here. For the most common step-index fibers it can be assumed that the refractive index difference between the fiber core and cladding is small. A simplification that can be made is to assume that the refractive index only depends on the radial distance from the fiber axis r, and not the azimuthal angle ϕ. This approximation is valid for the simplest type of optical fiber that has cylindrical symmetry. Because of this symmetry, it is useful to express the wave equation in cylindrical coordinates r, ϕ and z. The electric field components must then obey the wave equation [12]

$$\frac{\partial^2 E}{\partial r^2} + \frac{1}{r}\frac{\partial E}{\partial r} + \frac{1}{r^2}\frac{\partial^2 E}{\partial \phi^2} + \frac{\partial^2 E}{\partial z^2} + n^2(r)k^2 E = 0, \tag{2.5}$$

where $n(r)$ is the radially dependent refractive index and $k = 2\pi/\lambda$ is called the wavenumber, where λ is the wavelength of the light.

It is useful to decompose the electric field distribution into so-called *modes*, and the total field components can be written as a superposition of these. The shape of these modes stay constant throughout the fiber as the light propagates. The modes only change in their phase, and the change is represented by βz, where β is the *propagation constant* and z is the propagated distance [10]. The electric field mode can be written as

$$E(r, \phi, z) = \Psi(r, \phi)\exp(i\beta z) = F_{lm}(r)\cos(l\phi)\exp(i\beta z), \tag{2.6}$$

where $\Psi(r, \phi)$ is the transverse field distribution, which is further separated into $F_{lm}(r)\cos(l\phi)$. As the modes we look for must have a continous ϕ-dependence, it is clear that l must be an integer. Thus, l describes the azimuthal shape of the electrical field.

Inserting Equation (2.6) into Equation (2.5), one obtains

$$\frac{dF_{lm}(r)}{dr^2} + \frac{1}{r}\frac{dF_{lm}(r)}{dr} + \left(n^2(r)k^2 - \frac{l^2}{r^2} - \beta_{lm}^2\right)F_{lm}(r) = 0. \tag{2.7}$$

For arbitrary values of β, the solutions of Equation (2.7) often diverge when $r \to \infty$. However, for *guided modes* (modes contained within the fiber) one must have the boundary conditions $F_{lm} \to 0$ when $r \to \infty$. The solutions of Equation (2.7), for a given index l, and leads to a guided mode are conventionally labeled by the index m. The solution with the highest value of β is labeled with $m = 1$, and solutions with lower values of β are labeled with higher m-values.

The electric field distribution within the optical fiber can then be written as a linear combination of all the resulting guided modes from Equation (2.7) as

$$E(r, \phi, z) = \sum_{l,m} a_{lm}(z) E_{lm}(r, \phi), \tag{2.8}$$

where $E_{lm}(r, \phi)$ are the modes from Equation (2.6) that produce guided mode solutions of Equation (2.7), where the factor $\exp(i\beta z)$ has been contracted into the complex mode amplitude $a_{lm}(z)$ of mode lm. Equation (2.8) describes a solution of the total elecric field for each polarization direction.

Differing from the results of the geometric approximation, the guided modes extends into the cladding, where they will decrease exponentially. Some optical fibers are so-called *single-mode* (SM), meaning that they only support a single guided mode per polarization direction (in the wavelength region the fiber is intended for). Other optical fibers are so-called *multi-mode* (MM), which are made to support a large number of guided modes. However, all SM fibers will become MM for wavelengths below a certain cut-off wavelength that depends on fiber parameters.

The *V-number* is an important parameter for step-index fibers that can be used to determine how many modes a fiber can guide. It is defined as [10]

$$V = \frac{2\pi}{\lambda} a \mathrm{NA}, \tag{2.9}$$

where λ is the light wavelength, a is the radius of the core and NA is the numerical aperture as defined in Equation (2.4). The V-number can be interpreted as a normalized optical frequency that is rescaled by properties of the fiber. It turns out that for V-numbers lower than ~ 2.405, the fiber is SM. For SM fibers only the "fundamental mode" (denoted LP_{01}, with $l = 0$ and $m = 1$) exists, giving very good beam quality which often is desirable in applications. For V-numbers close to (but still below) ~ 2.405, most of the optical power propagates inside the core. In this regime, the intensity distribution of the optical field can be approximated well by a Gaussian distribution. Figure 2.2 illustrates a Gaussian field distribution together with the refractive index profile of a step-index fiber, where the electric field extends out from the core and into the cladding. For lower values of the V-number, more of the optical power extends out of the core and propagates inside the cladding.

An important parameter describing the radial distance that the optical power extends to is the *mode radius*. For a step-index SM fiber, this can be approximated by Marcuse's formula [10]

$$\frac{\omega}{a} \approx 0.65 + \frac{1.619}{V^{3/2}} + \frac{2.879}{V^6}, \tag{2.10}$$

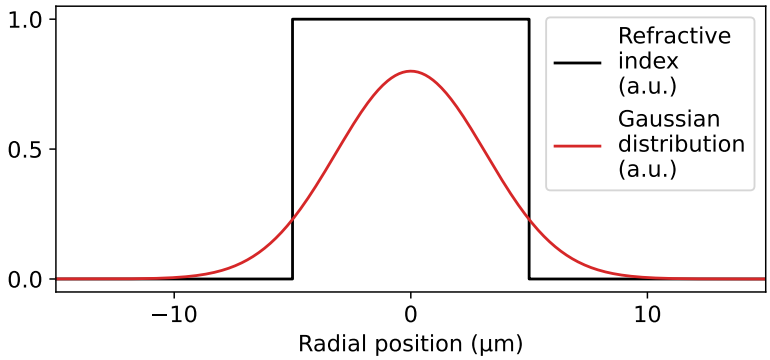

Figure 2.2: A Gaussian field distribution contained mostly inside the fiber core, indicated by the refractive index profile.

where ω is the mode radius. Equation (2.10) approximates the mode radius well for V-numbers between ~ 0.8 and 2.5. The so-called *power filling factor* is a related parameter that gives the ratio of the optical power that propagates inside the core of the fiber. It is given by

$$\Gamma = \frac{\int_0^a I(r) 2\pi r \mathrm{d}r}{\int_0^\infty I(r) 2\pi r \mathrm{d}r} \approx 1 - \mathrm{e}^{-2(a/\omega)^2}, \tag{2.11}$$

where the optical intensity distribution is assumed to be Gaussian in the last approximation.

The optical intensity is related to the electric field of Equation (2.8) by $I = c\epsilon_0 |E|^2/2$, where c is the speed of light in vacuum and ϵ_0 is the vacuum permittivity. Furthermore, the optical intensity distribution is related to the optical power through

$$P = \int_0^\infty I(r) 2\pi r \mathrm{d}r. \tag{2.12}$$

The denominator in Equation (2.11) is thus the total optical power defined here in Equation (2.12).

2.2 Energy Transitions in Lasers

Lasers and amplifiers can be made from optical fibers by doping the core of a fiber with ions of rare-earth elements. To understand the energy transitions occuring in the process of pair induced quenching and why it reduces the gain

of fiber amplifiers doped with holmium, it is important to first understand the fundamental processes and the energy transitions that occur in lasers of this kind.

2.2.1 Radiative Transitions

Absorption, *spontaneous emission* and *stimulated emission* are three fundamental processes that occur in lasers [13]. They are called radiative transitions because they involve either the absorption or emission of a photon. Figure 2.3 illustrates the three processes for a system consisting of two energy states; the ground state 0, and an excited state 1, where the energy of state 1 is larger than for state 0, i.e. $E_1 > E_0$. Let the system represent the states of a rare-earth ion that is doped in an optical fiber, and that the ion is in the ground state 0. If an electromagnetic (EM) wave is present, with a wavelength that matches the energy difference between the two states $\lambda = hc/(E_1 - E_0)$, then there is a finite probability that the ion will become excited to state 1, by absorbing a photon from the wave. This is the process of absorption, and is illustrated in Figure 2.3a. Here, λ represents the wavelength of the photon, h is Planck's constant and c is the speed of light in vacuum.

If the ion is initially excited to state 1 and there is not an EM wave present that matches the energy difference between the two levels, then the ion will eventually decay to the ground state 0 because $E_1 > E_0$. In this case, the energy difference $(E_1 - E_0)$ will be released as a photon that will propagate in a random direction, and with a random phase and polarization. This is the process of spontaneous emission, and is illustrated in Figure 2.3b.

Assume now that the ion again is initially excited to state 1, but now there is an EM wave present with wavelength that matches the energy difference between the two states. Then there is a finite probability that the ion will be forced to transition down to the ground state 0, emitting a photon in the process with the

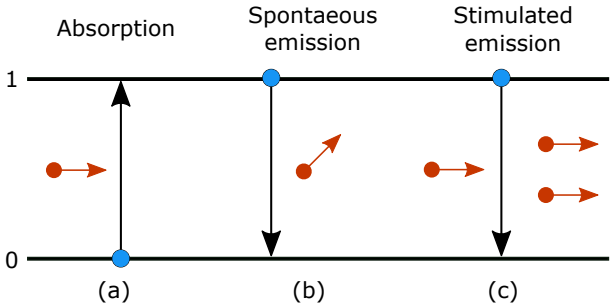

Figure 2.3: The processes of (a) absorption, (b) spontaneous emission and (c) stimulated emission.

same wavelength, polarization, phase and propagation direction as the present EM wave. This is the process of stimulated emission and is illustrated in Figure 2.3c.

2.2.2 Non-radiative Transitions

Non-radiative energy transitions are transitions that do not involve the absorption or emission of photons. When a rare-earth ion is doped into a host material, such as a crystal or glass, the ion and host can exchange energy non-radiatively.

Non-radiative decay is when an initially excited ion decays to a lower energy state, exciting lattice vibrations (*phonons*) in the host material in the process. If the energy difference between the excited state and the next lower energy state is larger than the phonon energy of the host material, then the process is possible by excitation of multiple phonons. The rate at which the ions decay by a multiphonon decay process depends on the number of phonons required to bridge the energy gap. Non-radiative decay is thus faster for energy states that are close in energy than states that are far appart [14].

All optical fibers used in this work are made of fused silica (amorphous SiO_2) as the host material. This material has a large maximum phonon energy compared to the separation between energy levels of the active doped ions. This means that only a few phonons are needed for nonradiative decay to occur, and the process occurs very efficiently.

Non-radiative energy exchange between rare-earth ions can also occur. Two ions in close proximity can interact in many ways via electrical multipole interactions if at least one of the ions are in an excited state. Three commonly occuring multipole interactions in rare-earth ion-doped fibers are *energy migration*, *energy transfer upconversion* (ETU) and *cross relaxation*. These three processes are illustrated in Figure 2.4. Energy migration is when an excited ion simply transfers its excitation to a nearby ion. This is illsutrated in Figure 2.4a. ETU and cross-relaxation are processes that involve a third energy state as ewell. In ETU, two excited ions that are in close proximity can interact such that one ion is demoted to the ground state, giving its energy to the other ion that is promoted to a higher lying energy state. This is illustrated in Figure 2.4b. Cross-relaxation is essentially the opposite process of ETU. One ion that is initially excited to a high lying energy state can interact with a nearby ground state ion, exchanging energy such that both ions end up in the middle lying state. This process is illustrated in Figure 2.4c. The rate at which these multipole interactions occur decreases significantly for increasing separation between the ions.

Energy migration is always energy matched because it involves the same energy levels of the two involved ions. ETU and cross-relaxation on the other hand are not necesserily completely energy matched as the energy transitions involved are different for the two interacting ions. In the general case these processes might need to be phonon assisted to occur. A term that describes how well matched

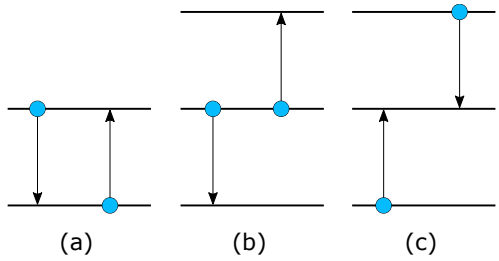

Figure 2.4: Illustration of (a) energy migration, (b) energy transfer upconversion and (c) cross-relaxation.

the transitions are is the degree of *resonance*. If a process only need assistance from a low energy phonon then the process has a high degree of resonance and can occur at a rapid rate. If a process need assistance from one or multiple high energy phonons, then the process has a low degree of resonance and will occur at a slow rate.

2.3 Three-level Laser

A three-level laser is the simplest energy level system that can produce amplification of incoming light [13]. The dynamics of such a system can be modelled by using a system of rate equations. Rate equations are first order differential equations that describe how the *population* of the energy levels change with time. These equations take into account the energy transfer mechanisms that are involved, such as absorption, stimulated emission, spontaneous emission and non-radiative transitions.

2.3.1 Rate Equations for a Three-level Laser

Figure 2.5 shows an energy level scheme of a generic three-level laser system. N_0-N_2 represent the populations of the energy levels with energy E_0-E_2, respectively, and where $E_2 > E_1 > E_0$. The population of an energy level is the number of ions per unit volume that occupy that state. The rate of change of these populations are given by dN_i/dt, for $i = 0, 1, 2$. Thus, there are three rate equations that describe this system, one for each state. To illustrate how rate equations can model a laser amplifier system such as this, the equations will be explained one by one, beginning with the rate equation for the population of the upper state 2.

State 2 is populated by a *pump* EM wave that excites ions from the ground state 0. This pump can be a beam from a laser that outputs light with a wavelength that matches the energy difference between state 2 and 0. The rate at

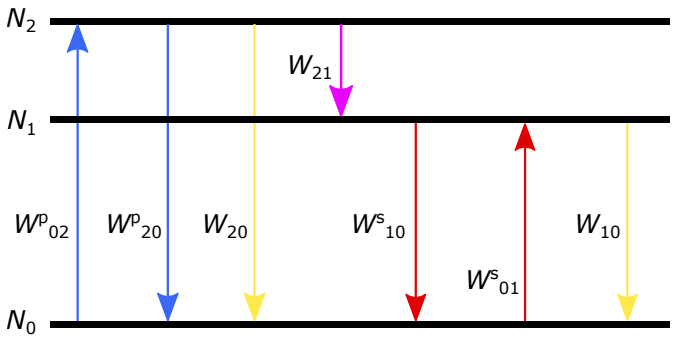

Figure 2.5: Energy transitions and the corresponding rates of a three-level laser system. The rates are from left to right: pump absorption, pump stimulated emission, spontaneous decay from level 2 to 0, spontaneous decay from level 2 to 1, signal stimulated emission and finally, spontaneous decay from level 1 to 0.

which this pump populates state 2 is proportinal to the population of state 0, N_0, as the pumping rate depends on the number of ions available for absorbing pump photons. The proportionality constant, called a rate, is denoted as W^{p}_{02}, where "p" signifies that the process involves the pump light. The convention used for the subscript is that ij denotes a transition from state i to state j. The very same pump beam can also force ions in state 2 to undergo stimulated emisson, i.e. the transition $2 \to 0$ where a photon is added to the pump beam in the process. This process thus increases the population N_0 and depopulates N_2. The rate at which this occurs is proportional to N_2 and is denoted as W^{p}_{20}. Ions populating state 2 can also undergo the transition $2 \to 0$ via spontaneous emission or multiphonon non-radiative decay. This process is also proportional to N_2 and is denoted as $W_{20} = W^{\mathrm{sp}}_{20} + W^{\mathrm{nr}}_{20}$, where the two process are combined into one rate. Here "sp" and "nr" represents spontaneous emission and non-radiative decay, respectively. Lastly, the population N_2 can be depopulated by ions decaying down to state 1 either via spontaneous emission or non-radiative decay. The rate of these processes are also combined and denoted as W_{21}. The rate equation governing the population of state 2 can thus be written as

$$\frac{\mathrm{d}N_2(t)}{\mathrm{d}t} = W^{\mathrm{p}}_{02}N_0(t) - (W^{\mathrm{p}}_{20} + W_{20} + W_{21})N_2(t). \tag{2.13}$$

Consider next the rate of change of the population of state 1. Because the states 2 and 1 are assumed to be much closer in energy than states 2 and 0 (i.e. $\Delta E_{21} \ll \Delta E_{20}$ where $\Delta E_{ij} = E_i - E_j$), the ions pumped to state 2 will rapidly decay down to state 1. Thus, the term $-W_{21}N_2$ in Equation (2.13) is also present in the rate equation for the population N_1, but with opposite sign as this process

populates state 1. Ions in state 1 can undergo stimulated emission by a *seed* EM wave. In an amplifier, this seed can be a beam from a laser with wavelength that matches the energy difference between state 1 and 0. This process occurs at a rate proportional to the population N_1 and is denoted as W_{10}^{s}, where "s" signifies that the process involves the seed light. This seed light is alternatively often denoted "signal" in context of laser amplifiers, and these terms are used interchangeably in this text. State 1 is called the *upper laser level*, because it is from this energy level that laser action is meant to occur. However, the signal beam can also excite ions that are in state 0 up to state 1. This process is proportional to the population of state 0 (N_0) and its rate is denoted as W_{01}^{s}. Finally, ions in state 1 can decay down to state 0 through spontaneous emission and non-radiative decay. These processes are proportional to N_1 and their rates are combined and denoted as W_{10}. Because the energy difference ΔE_{10} is relatively large, the ions in state 1 will decay slowly, and energy can thus be "stored" on this level long enough so that it can be extracted by the seed. The rate equation governing the population of state 1 is given by

$$\frac{\mathrm{d}N_1(t)}{\mathrm{d}t} = W_{01}^{\mathrm{s}} N_0(t) + W_{21} N_2(t) - (W_{10}^{\mathrm{s}} + W_{10}) N_1(t). \tag{2.14}$$

State 0 is the ground level, which by definition does not have any lower lying energy levels. If the electrical multipole interactions described in Section 2.2.2 are neglected, then the only way for ions in the ground state to become excited to other states is by absorption of either a pump or seed photon. The ground state can be populated by stimulated emission of ions in state 1 or 2 by the seed or pump beams, or by radiative or non-radiative decay from these states. These rates were discussed above and the rate equation governing the population of state 0 is given by

$$\frac{\mathrm{d}N_0(t)}{\mathrm{d}t} = (W_{20}^{\mathrm{p}} + W_{20}) N_2(t) + (W_{10}^{\mathrm{s}} + W_{10}) N_1(t) - (W_{02}^{\mathrm{p}} + W_{01}^{\mathrm{s}}) N_0(t). \tag{2.15}$$

The total population of ions in a laser system is constant, thus the equality $N_{\mathrm{tot}}(t) = N_0(t) + N_1(t) + N_2(t)$ holds true and one of the Equations (2.13)-(2.15) can be considered redundant, and can be substituted for the equation $\mathrm{d}N_0/\mathrm{d}t + \mathrm{d}N_1/\mathrm{d}t + \mathrm{d}N_2/\mathrm{d}t = 0$.

2.3.2 Physical Interpretation of the Rates

The rates for absorption and stimulated emission of the pump and signal is the product of the *cross section* for the given transition, and the *photon flux* of the

pump and signal beams. The rates can be written as

$$W_{ij}^{\mathrm{p}} = \sigma_{ij}^{\mathrm{p}} F^{\mathrm{p}} = \frac{\sigma_{ij}^{\mathrm{p}} I^{\mathrm{p}}}{h\nu^{\mathrm{p}}}, \tag{2.16}$$

$$W_{ij}^{\mathrm{s}} = \sigma_{ij}^{\mathrm{s}} F^{\mathrm{s}} = \frac{\sigma_{ij}^{\mathrm{s}} I^{\mathrm{s}}}{h\nu^{\mathrm{s}}}, \tag{2.17}$$

where $i = 0$ and $j = 2$ or vice versa in Equation (2.16) and $i = 0$ and $j = 1$ or vice versa in Equation (2.17). The photon flux is given by $F = I/h\nu$, where I is the intensity of the optical field and $h\nu$ is the energy of a single photon, where ν is the optical frequency. Thus, the photon flux is the number of photons travelling through a cross section area per unit of time. The transition cross sections σ_{ij}^{p} and σ_{ij}^{s} have the dimensions of area. Physically, they describe the probability of a certain transition to occur. If $i < j$ they represent absorption cross sections and if $i > j$ they represent emission cross sections for the pump and signal wavelength. The absorption cross sections describe the rate at which ions will absorb photons for a given number of photons passing by a cross section area. Likewise, the emission cross sections describes the rate at which excited ions will emit photons by stimulated emission, for a given number of photons passing by a cross section area. For the simple three-level system described here, the energy levels are non-degenerate and the principle of *reciprocity* says that the absorption and emission cross sections corresponding to transitions between the same levels are equal [15]. However, for reasons that will be explained in Section 2.4, the energy levels in fiber lasers are effectively a continuum of several strongly coupled sub-levels, and the situation becomes more complex. For this reason, the absorption and emission cross sections are distinguished here as this becomes relevant later.

The rate of decay from a given energy level is often represented by its so-called *lifetime*. Consider the three-level system of Figure 2.5, but now there are no optical fields present (Equation (2.16)-(2.17) are zero). Thus, there are no possible ways that state 2 can become populated ($N_2 = 0$). Let state 1 initially be populated with the population $N_1(0)$ at $t = 0$. Equation (2.14), which describes the rate of change of the population N_1, is then reduced to $\mathrm{d}N_1/\mathrm{d}t = -W_{10}N_1$ which has the simple solution

$$N_1(t) = N_1(0)\mathrm{e}^{-W_{10}t}. \tag{2.18}$$

Equation (2.18) shows that the population of state 1 will decay exponentially from its initial value. One can define the lifetime of this state as the characteristic time at which the initial population $N_1(0)$ has been reduced by a factor 1/e. This occurs for $t = \tau_1$, where τ_1 is given by

$$\frac{1}{\tau_1} = \frac{1}{\tau_{10}^{\mathrm{sp}}} + \frac{1}{\tau_{10}^{\mathrm{nr}}} = W_{10} = W_{10}^{\mathrm{sp}} + W_{10}^{\mathrm{nr}}. \tag{2.19}$$

In Equation (2.19) the lifetimes τ_{10}^{sp} and τ_{10}^{nr} represents the decay time for for radiative and non-radiative decay from state 1 to 0.

One can define the lifetime of all energy states above the ground state by the same method as done here for state 1. For state 2, the lifetime is defined by

$$\frac{1}{\tau_2} = \frac{1}{\tau_{20}^{\mathrm{sp}}} + \frac{1}{\tau_{20}^{\mathrm{nr}}} + \frac{1}{\tau_{21}^{\mathrm{sp}}} + \frac{1}{\tau_{21}^{\mathrm{nr}}} = W_{20} + W_{21}. \tag{2.20}$$

The lifetime of state 2 defined by Equation (2.20) depends on the decay rates to both energy states below it. However, because state 2 and 1 are much closer in energy, the rate describing this rapid decay will be the dominating contributor [13].

2.3.3 Power Amplification

The optical power was related to the field intensity by Equation (2.12), and further related to the fields photon flux by Equations (2.16)-(2.17). The evolution of the optical power of the signal beam along the propagation direction z through the amplifying medium is described by the differential equation

$$\frac{\mathrm{d}P_{\mathrm{s}}(z,t)}{\mathrm{d}z} = \left[\sigma_{10}^{\mathrm{s}} N_1(z,t) - \sigma_{01}^{\mathrm{s}} N_0(z,t)\right] P_{\mathrm{s}}(z,t) = g(t) P_{\mathrm{s}}(z,t), \tag{2.21}$$

where now the z dependence of the populations are specified as well. The factor g is called the *gain coefficient* and describes the amount of gain per unit length in the amplifying medium. Equation (2.21) shows that the optical power will be amplified when $g > 0$ which occurs for $N_1 > N_0 \sigma_{01}^{\mathrm{s}} / \sigma_{10}^{\mathrm{s}}$. When this occurs, it is called a *population inversion* and the seed power will increase exponentially as it propagates throught the amplifying medium [13]. This is the basic working principle of laser amplifiers. A population inversion can be created by a significantly powerful pump beam that excites ions from state 0 to state 2, which then rapidly decays to state 1.

The evolution of the pump power through the amplifying medium can be similarily described by the equation

$$\frac{\mathrm{d}P_{\mathrm{p}}(z,t)}{\mathrm{d}z} = \left[\sigma_{20}^{\mathrm{p}} N_2(z,t) - \sigma_{02}^{\mathrm{p}} N_0(z,t)\right] P_{\mathrm{p}}(z,t) = a(t) P_{\mathrm{p}}(z,t), \tag{2.22}$$

where the cross sections and populations have been substituted for those relevant for the transitions between state 0 and 2, and the *absorption coefficient* ($a(t)$) is used instead of the gain coefficient as the pump beam usually experiences absorption, rather than gain.

The behavior of a laser amplifier can be predicted from simultaneously considering the power evolution of the pump and signal fields, and the populations of the relevant energy levels. This method of rate equation modelling is expanded to a more complex model of a holmium-doped fiber amplifier in Chapter 3.

2.4 Fiber Amplifiers

As mentioned in Chapter 1, optical fibers can be doped with ions of rare-earth elements such as ytterbium, erbium, thulium and holmium. This section describes the energy level structure of holmium when doped into fused silica, and the energy transitions relevant for holmium laser action. The energy transfer upconversion process between holmium ions and how this relates to pair induced quenching is addressed in particular detail. Although this work studies holmium-doped fibers, a brief description of the thulium energy levels is given as this has relevance for the experimental work in this project. Finally, certain additional aspects of fibers amplifiers that are important in this project are explained.

2.4.1 Energy Level Structure of Holmium

Holmium has the atomic number 67 and belongs to the lanthanides in the periodic table of elements. The electrically neutral holmium atom has electron configuration $[Xe]4f^{11}6s^2$. The most stable ionized state is the trivalent state Ho^{3+} which has the two 6s-electrons and one 4f-electron removed [4]. This gives the ionized state the electron configuration $[Xe]4f^{10}$.

Splitting of the Energy Levels

The energy levels of interest for laser action in holmium-ions originate from the 4f-electrons. The states of these electrons are determined by the three parameters *total orbital angular momentum* L, *total spin momentum* S and *total angular momentum* J. L and S are the vector sums of the orbital and spin quantum numbers, respectively, of all 10 4f-electrons. Whereas J is the vector sum of L and S, and describes the *spin-orbit coupling*. The so-called *term symbol* is used to denote the resulting energy states and is given by $^{2S+1}L_J$, where L is for historical reasons denoted by letters instead of numbers. The letters corresponding to the seven lowest values of L are S, P, D, F, G, H and I [16].

How the electron configuration $4f^{10}$ is split into multiple energy levels is illustrated in Figure 2.6. First the electrostatic interaction between the 4f-electrons leads to a degeneracy in L and S. Furthermore, the spin-orbit interaction lifts the degeneracy in J, splitting the states into J *multiplets*. It is these lowest lying multiplets that are relevant for laser action in holmium-doped fiber amplifiers. The level $^5I_8$ is the ground state and $^5I_7$ is the upper laser level (see Figure 2.6). It is stimulated emission from the transition $^5I_7 \rightarrow {}^5I_8$ that produce amplication of light in such amplifiers.

Finally, the holmium-ions interact with the static field from the host material. This interaction further splits the multiplets into *manifolds* of sub-levels. This is referred to as *Stark splitting* and the number of *Stark levels* in the manifolds

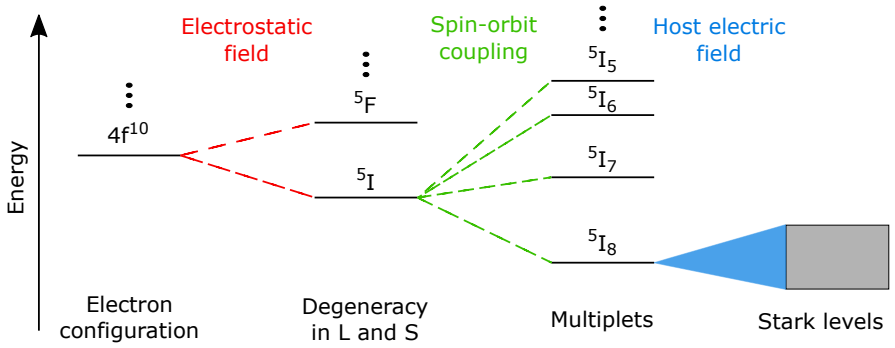

Figure 2.6: Illustration of the splitting of the electron configuration $4f^{10}$ into manifolds of levels when holmium-ions are doped into silica.

depends on the symmetry of the static field of the host. For an amorphous material such as silica there will be site-to-site variations for all doped ions. Thus, every ion will experience a unique electric field, and this will result in splitting of the Stark levels. This is known as *inhomogeneous broadening*. Furthermore, the rapid phonon-induced transitions between Stark levels within the same manifold leads to additional broadening. This is known as *homogeneous broadening* [4]. These broadening mechanisms effectively smears out the Stark levels into a continuum of energy levels.

Effective and Net Transition Cross Sections

The principle of reciprocity holds also here for absorption and emission between a single pair of sub-levels of the manifolds. However, when considering transitions between the upper laser manifold and ground state manifold, multiple transitions are possible between any pairs of sub-levels. It is then convenient to use so-called *effective transition cross sections*. These take into account both the transition strength between all pairs of sub-levels, and the occupation distribution of the different sub-levels of the upper laser level manifold and the ground state manifold.

The occupation distribution of a manifold can be described by Boltzmann statistics [13]. For a sub-level i with energy E_i in a manifold of m strongly coupled and rapidly thermalizing Stark levels, the occupation probability is given by

$$p_i = \frac{\mathrm{e}^{-E_i/k_\mathrm{B}T}}{\sum_m \mathrm{e}^{-E_m/k_\mathrm{B}T}}, \tag{2.23}$$

where k_B is the Boltzmann constant and T is the temperature. The *McCumber relation* generalizes the reciprocity principle to broadband transitions, by connecting

the frequency-dependent absorption and emission cross sections through [17]

$$\sigma_{\mathrm{a}}(\nu) = \sigma_{\mathrm{e}}(\nu) \exp\left(\frac{h\nu - E_0}{k_{\mathrm{B}}T}\right). \tag{2.24}$$

In Equation (2.24) ν is the optical frequency and h is Planck's constant. E_0 is the energy where the absorption and emission cross sections are equal, i.e. when $h\nu = E_0$.

Consider the energy level scheme in Figure 2.7. The figure shows the four lowest lying energy manifolds ($^5\mathrm{I}_8$, $^5\mathrm{I}_7$, $^5\mathrm{I}_6$ and $^5\mathrm{I}_5$) of Ho^{3+} in silica, and the most important energy transitions. The holmium-ions can be pumped from the ground state $^5\mathrm{I}_8$ towards the top of the upper laser level $^5\mathrm{I}_7$ by a beam with wavelenght of 1.95 µm. A pump source that can output this wavelength is e.g. a thulium-doped fiber laser. The ions excited to $^5\mathrm{I}_7$ are rapidly thermalized towards the bottom of the manifold according to Equation (2.23). The fluorescent lifetime of $^5\mathrm{I}_7$ is dominated by non-radiative multi-phonon decay to the ground state, and the lifetime is usually in the range $0.6 - 1.3$ ms [18, 19]. Thus, the ions will be stored in this energy manifold for a relatively long time. The variation of the lifetime seen in different reported holmium-doped optical fibers is attributed to incorporation of different kinds and amounts of co-dopants that affect the local environment around the holmium-ions. Ions in the upper laser level can be demoted back to the top of the ground state manifold via stimulated emission by a signal beam with a wavelength of ~ 2.1 µm. The type of pumping scheme discussed here is known as *in-band pumping*, where the pump transition and laser action (stimulated emission) occurs between the same energy manifolds.

The type of laser media discussed above are referred to as a *quasi three-level media* [20] and should be compared to the three-level laser scheme discussed in Section 2.3. The probabilities for whether absorption or stimulated emission occurs for the pump and signal beams are governed by the effective absorption- and emission cross sections for the transition $^5\mathrm{I}_8 \leftrightarrow {}^5\mathrm{I}_7$, as defined by Equation (2.24). Figure 2.8 shows the effective absorption ($\sigma_{\mathrm{a}}(\lambda)$) and emission ($\sigma_{\mathrm{e}}(\lambda)$) cross sections for holmium-ions in silica at room temperature. The figure shows that the effective cross sections are not equal. The Boltzmann distributions of the ions occupying the manifolds are temperature dependent. Thus, so are the effective cross sections. Figure 2.8 shows that the effective absorption cross section has a peak at ~ 1.95 µm, and rapidly decreases for longer wavelengths. The emission cross section also has a peak at ~ 1.95 µm, but importantly remains relatively large for longer wavelengths. This makes holmium-doped fiber amplifiers especially suitable for being pumped at 1.95 µm and amplify light at 2.1 µm.

The *net cross section* is an important parameter to consider for a quasi three-level laser media. It is given by [20]

$$\sigma_{\mathrm{net}}(\lambda) = \beta\sigma_{\mathrm{e}}(\lambda) - (1 - \beta)\sigma_{\mathrm{a}}(\lambda), \tag{2.25}$$

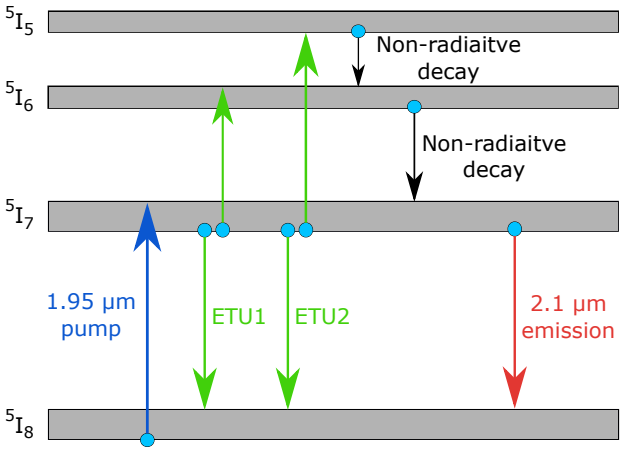

Figure 2.7: Energy level scheme of the four lowest lying energy manifolds of Ho^{3+} in silica, together with the most relevant energy transitions.

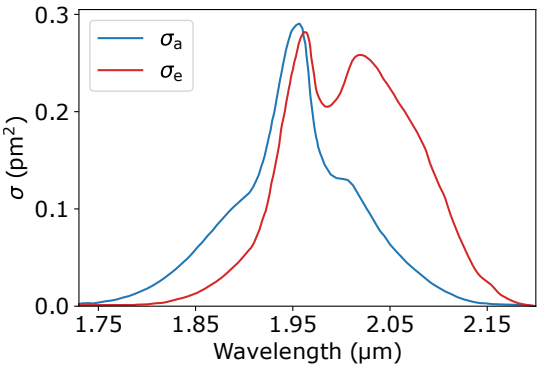

Figure 2.8: Absorption (σ_a) and emission (σ_e) cross sections of holmium-ions in silica at room temperature. Cross section data from Reference [21].

where β is the *inversion level*, i.e. the ratio of the number of ions in the upper laser level to the number of ions in the ground state. Light experiences net absorption when $\sigma_{net}(\lambda) < 0$ and net gain when $\sigma_{net}(\lambda) > 0$. What separates the net cross section in Equation (2.25) from the gain coefficient g in Equation (2.21), is the fact that in a quasi three-level laser media the pump can experience stimulated emission from the same level as the signal.

2.4.2 Energy Transfer Upconversion and PIQ in Holmium

Energy transfer upconversion can occur between two holmium-ions that are in close proximity [22]. This process was discussed in the general case in Section 2.2.2, and is illustrated for the holmium energy manifolds in Figure 2.7. Two holmium-ions that are initially excited to the upper laser level $^5I_7$ can interact with each other such that one ion is demoted to the ground state, giving its energy to the other ion which becomes excited to a higher lying energy state, either the $^5I_6$ or $^5I_5$ manifold. As denoted in Figure 2.7, the transition $^5I_7, ^5I_7 \rightarrow ^5I_8, ^5I_6$ is denoted as ETU1 and $^5I_7, ^5I_7 \rightarrow ^5I_8, ^5I_5$ is denoted as ETU2, following the convention used by Wang and Jackson in References [5, 18]. Neither of these transitions are resonant, thus they need to be phonon assisted. ETU1 has a surplus of energy and can occur by creating a phonon with energy that corresponds to this surplus. ETU2 has an energy deficit and can only occur if a phonon with energy that corresponds to this deficit is absorbed in the process. Thus, ETU1 is an exothermic process and ETU2 is an endothermic process [18].

The fluorescent lifetime of the $^5I_5$ manifold is 22 ns [23]. This lifetime is much shorter than the fluorescent lifetime of $^5I_6$, which is 1.4 µs [23]. Additionally, both $^5I_5$ and $^5I_6$ have a very long radiative lifetime of 14.9 ms and 11.4 ms, respectively [24]. This means that the vast majority of the ions excited to these levels will decay non-radiatively to the next lower energy manifold. Thus, the vast majority of ions excited to $^5I_5$ through ETU2 will rapidly deacay down to $^5I_6$. From here, the majority of the ions, both those excited to $^5I_6$ through ETU1 and the ions that has decayed to this level from $^5I_5$ will decay to $^5I_7$ in a few microseconds. This illustrates why the ETU process is detrimental for holmium-doped fiber amplifiers; for two ions initially excited to the upper laser level $^5I_7$, only one remains. Thus ETU reduces the inversion level, and thus the gain of the amplifying medium. As discussed by Jackson [18], exothermic processes are more likely to occur than endothermic processes, because it is generally more efficient to create a phonon than to rely on a phonon with the correct energy already existing. Thus, ETU1 is more probable than ETU2. Additionally, because the ions excited to $^5I_5$ rapidly decay down to $^5I_6$ as discussed, the ETU process can be well approximated as if ETU1 is the only occuring process.

In addition to ETU, a process known as *excited state absorption* can also promote ions to higher lying energy states. In this process, an initially excited ion becomes further promoted by absorbing a photon. For example, and ion initially excited to $^5I_7$ can absorb a pump or signal photon, becoming further excited to either $^5I_6$ or $^5I_5$ via phonon assistance. The cross-relaxation process described in Section 2.2.2 can also occur between holmium-ions in close proximity. An ion initially excited to either $^5I_5$ or $^5I_6$ can interact and give some of its energy to an ion in the ground state $^5I_8$, such that both ions end up in the upper laser level $^5I_7$. These two processes are however not particularly efficient in in-band pumped

holmium-doped fiber amplifiers.

Homogeneous Upconversion

For energy transfer upconversion between two ions that are not in each others immediate vicinity, the process is called *homogeneous upconversion*. In the dipole-dipole approximation, the ETU interaction rate between two ions is proportional to $1/R^6$, where R is the distance between the ions [9]. The macroscopic effect of homogeneous upconversion is an average of the interaction rate over all the inter-ionic distances inside the host material. In models one usually assigns a single rate for the homogeneous ETU process, which gives a good approximation in most cases. If we assume that the holmium-ions are randomly distributed inside the core of the fiber, then the average distance between ions will decrease with increasing doping concentration. Thus, the homogeneous ETU rate will increase with increasing doping concentration.

Inhomogeneous Upconversion and Pair Induced Quenching

The assumption that the holmium-ions become randomly distributed when doped into the fiber core is not correct. It so happens that many more ions reside in close proximity than what is statistically expected. This is attributed to interactions such as *local charge compensation*, which forces the ions to form clusters where two or more ions are in immediate vicinity [4]. Figure 2.9 illustrates the difference between a single ions and ion-pairs (i.e. clusters consisting of two ions). Because the ETU interaction rate strongly depends on the distance between the ions, upconversion between ions within a cluster is much more rapid than homogeneous upconversion occurring between single ions. Thus, upconversion between two ions within the same cluster is distinctly different from single-ion upconversion, and often referred to as *inhomogeneous upconversion* [9].

To illustrate why ion-clustering is so detrimental for holmium-doped fiber amplifiers, consider a cluster of an arbitrary number of holmium-ions. If a CW pump is launched into the core of the fiber, the ions in the cluster will become excited to the upper laser level $^5\mathrm{I}_7$ as they absorb pump photons. Rapid inhomogeneous ETU will occur between pairs of holmium-ions in the cluster, leaving only one of the two ions in the excited state. This process will repeat rapidly until only one ion is left in the upper laser level. This is called pair induced quenching, and reduces the inversion level (hence the gain) in the holmium-doped fiber. The pump will continue to excite the ground state ions which will rapidly be quenched back down to the ground state again. Thus, much of the pump power is "wasted" on exciting ions that will not be available for amplification of a signal.

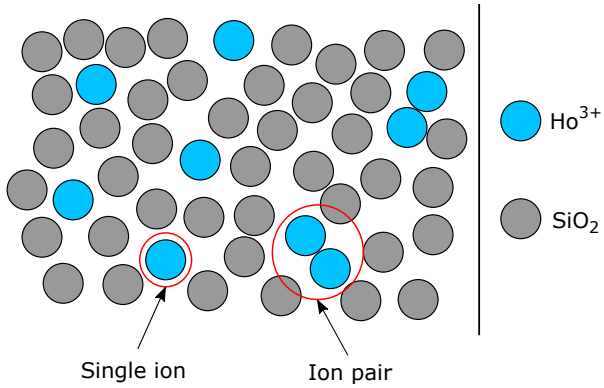

Figure 2.9: Illustration of holmium-ions doped into fused silica, demonstrating the difference between single ions and ion-pairs/clusters.

The ion-clusters can be approximated as being in its simplest form, namely an ion-pair, as it can be argued that a cluster of two ions is the most likely to be formed when doping holmium-ions into the fiber. In a similar manner as was done in Section 2.3.2, one can define a lifetime of *doubly-excited pairs* (i.e. pairs where both ions are excited to $^5I_7$) as the time it takes for $1 - 1/e \approx 63\%$ of the doubly-excited pairs to undergo inhomogeneous ETU. This lifetime describes how rapid the inhomogeneous ETU process occurs. The lifetime of doubly-excited erbium-pairs has been established to be 50 ns [8], which prior to this project served as a suggestion for how rapid this process is expected to be also in holmium.

As previously mentioned, the pump will experience net absorption until the inversion level $\beta = \sigma_a/(\sigma_e + \sigma_a)$ is reached, where the amplifying medium becomes transparent to the pump. However, as illustrated here, PIQ will prevent this inversion level from ever occurring as the pump can always be absorbed by the ions in clusters. Thus, PIQ prevents the absorption from being saturated, and this is called *non-saturable absorption*.

2.4.3 Energy Level Structure of Thulium

As previously mentioned, the pump source used in this work to excite holmium-ions to the upper laser level is a thulium-doped fiber amplifier that outputs light with a wavelengt of 1.95 µm, corresponding to the peak of the effective absorption cross section of holmium shown in Figure 2.8. The amplification properties of thulium-doped fibers will become important in the experiment discussed in Section 4.3, and for this reason the energy level structure and transition cross sections of thulium will be briefly discussed here.

Thulium has the atomic number 69, and similarly to the case of holmium, the energy level structure of interest for thulium-doped fiber amplifiers originate from the 4f-electrons. The four lowest lying energy level manifolds of thulium in silica ($^3H_6$, $^3F_4$, $^3H_5$ and $^3H_4$) are illustrated in Figure 2.10a. In contrast to the laser scheme of in-band pumped holmium-doped fiber lasers, thulium-doped fiber lasers are not pumped directly to the upper laser level. The ions in the ground level $^3H_6$ are excited by a pump with a wavelength of 790 nm to the upper state $^3H_4$. Additionally, in contrast to the three-level laser scheme discussed in Section 2.3, the upper laser level does not become populated by ions in a higher lying state decaying through rapid non-radiative decay. Instead, the upper laser level $^3F_4$ is populated by the cooperative process of cross-relaxation occurring between two thulium-ions in close proximity [24]. It so happens that the energy difference for the transition $^3H_4 \rightarrow {}^3F_4$ matches the transition $^3H_6 \rightarrow {}^3F_4$, but with opposite sign. Thus, a thulium-ion excited to $^3H_4$ by the pump can undergo the transition $^3H_4 \rightarrow {}^3F_4$, transferring the residual energy to a nearby ground state thulium-ion such that both ions end up in the upper laser level. If the optical fiber is highly doped with thulium-ions, such that the average distance between thulium-ions is small, then the cross-relaxation process will occur rapidly and the upper laser level will be populated very efficiently as two ions end up populating this level for each absorbed pump photon [4, 18]. For these reasons, and in sharp constrast to holmium-doped fibers, ion-clustering of thulium is actually beneficial (when utilizing this pumping scheme) as it only increases the rate at which the upper laser level becomes populated. The ions in the upper laser level can be stored there for a relatively long time, because of the long fluorescent lifetime.

Figure 2.10b shows the effective absorption and emission cross sections of the $^3H_6 \leftrightarrow {}^3F_4$ transition. The emission cross section can be seen to cover a broad wavelength range. Thus, even though the thulium-doped fiber amplifier used as a pump source in this work delivers light with wavelength of 1.95 µm, even the 2.1 µm signal for holmium-doped fiber amplifers will experience gain if it is propagated through an excited thulium-doped fiber. This fact will become important in the experiment described in Section 4.3.

2.4.4 Saturation of Absorption

Absorption of pump light occurs as mentioned when $\sigma_{\text{net}} < 0$ at the pump wavelength. This corresponds to an inversion level of $\beta < \sigma_a/(\sigma_e + \sigma_a)$. As seen from Figure 2.8, $\sigma_a > \sigma_e$ for the pump wavelength 1.95 µm. Thus, the pump light experiences net absorption even for low inversion levels. If the pump power is raised such that the inversion level increases, the pump will experience net absorption until the inversion level reaches $\beta = \sigma_a/(\sigma_e + \sigma_a)$, and thus $\sigma_{\text{net}} = 0$. When this inversion level is achieved, the absorption and stimulated emission experieced by the pump balance each other, such that the pump experiences no

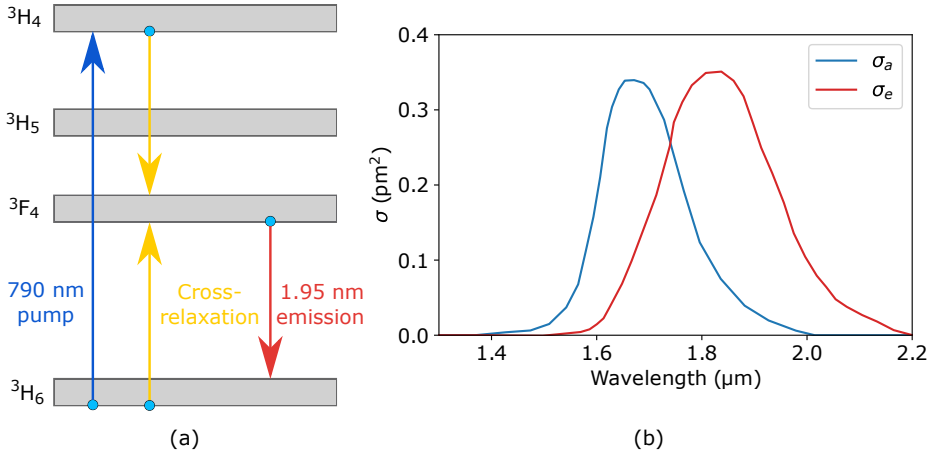

Figure 2.10: (a) Energy level diagram of thulium-ions doped in silica, showing the four lowest lying energy manifolds and the most relevant energy transitions. (b) Absorption and emission cross sections for thulium. Cross section values from Reference [25].

net absorption or gain. Thus, the laser medium has become transparent to the pump light, and increasing the pump power further will not lead to a higher inversion level. It is then said that the absorption has become *saturated*.

An important parameter that describes what energy a pulse would need to create a significant inversion level in a fiber is the *saturation energy*. Assuming that the doped area of the fiber is the same as the fiber core, the saturation energy is given by [4]

$$E_{\text{sat}} = \frac{h\nu A}{(\sigma_{\text{e}} + \sigma_{\text{a}})\Gamma}, \tag{2.26}$$

where A is the doped area, σ_{e} and σ_{a} are the emission and absorption cross sections, and Γ is the power filling factor defined by Equation (2.11). The saturation energy will become important in Chapter 4 in the context of spectroscopic measurements.

2.4.5 Optical Conversion Efficiency

The optical conversion efficiency is an important property of a laser. It is a measure of the optical to optical conversion ratio from the pump to the signal. It can be written as

$$\eta = \frac{P_{\text{s}}^{\text{out}} - P_{\text{s}}^{\text{in}}}{P_{\text{p}}^{\text{out}} - P_{\text{p}}^{\text{in}}}. \tag{2.27}$$

The numerator in Equation (2.27) is the difference between the output signal power and the input signal power. Thus it is the power that is a result only of

the conversion from the pump. The denominator is the difference between the pump power output from the doped-fiber (i.e. the unabsorbed pump power) and the pump power sent into the fiber.

2.4.6 Amplified Spontaneous Emission

It is not only the signal and pump beams that can undergo stimulated emission in a laser media. In holmium-doped fibers, spontaneously emitted light from the transition $^5I_7 \rightarrow {}^5I_8$ can also become amplified. If the spontaneously emitted light has a direction such that it becomes guided by the optical fiber, and a wavelength such that the net cross section is positive, then the light will become amplified as it propagates through the doped-fiber. This is known as *amplified spontaneous emission* (ASE), and is usually undesired in fiber amplifiers. ASE wil reduce the inversion level created by the pump which reduces the gain experienced by the signal. Furthermore, ASE effectively broadens the optical spectrum of the amplifier's output.

Chapter 3

Numerical model

This chapter describes the numerical rate equation model developed in this work for simulating holmium-doped fiber amplifiers. The model accounts for the presence of ion pairs and associated pair induced quenching that is known to be detrimental for the efficiency of such fiber amplifiers. Notably, this model will not make use of the common simplification where PIQ is assumed to occur instantaneously. Thereby, the overall aim with the model is to offer a numerical framework for simulating and understanding pulsed amplifiers that operate on timescales comparable to the PIQ-dynamics.

3.1 Model Overview

3.1.1 Single and Paired Ions

The main idea of this model is to separate the holmium-ions into two separate classes; single ions and clustered ions. The single ions can interact with other single ions through homogeneous energy transfer upconversion, where the upconversion rate is the same for all single ions. All the single ions have the same rate equations. The ion-clusters are approximated as being in its simplest form, namely a pair of two holmium-ions. In this class, an ion-pair is treated as a single unit with entirely different rate equations than the single ions. The states that the ion pair can be in is a combination of all the possible states that each individual ion within the pair can occupy. The single ions and the paired ions can not interact with each other directly, and ion pairs can not interact directly with other ion pairs. However, the single ions and paired ions interact with the same optical pump and signal beams that are present. The two ions within a pair are assumed to be in each other immediate vicinity, thus they can undergo inhomogeneous energy transfer upconversion, as described in Section 2.4.2.

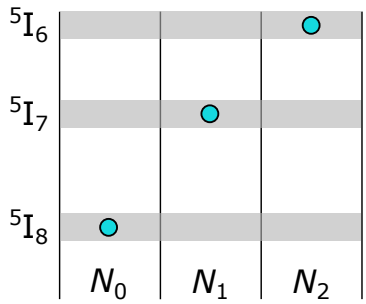

Figure 3.1: The energy states that single ions can occupy in the numerical model. The parameters N_0, N_1 and N_3 are the populations of single ions in the given energy states.

3.1.2 Model Assumptions

For simplicity, it is assumed that all upconverted ions goes to $^5I_6$ and not to $^5I_5$. As discussed in Section 2.4.2, this can be justified by the fact that the transition $^5I_7, ^5I_7 \rightarrow ^5I_8, ^5I_6$ is an exothermic process and $^5I_7, ^5I_7 \rightarrow ^5I_8, ^5I_5$ is an endothermic process. Assuming that $^5I_6$ is the highest reachable level also means that the process called excited state absorption is neglected. This means that ions excited to either $^5I_7$ or $^5I_6$ can not absorb a pump or signal photon. It is assumed that photons spontaneously emitted from any of the levels can not be re-absorbed. It is also assumed that spontaneously emitted photons can not cause stimulate emission of any radiative transitions. Thus, the model does not need to keep track of spontaneously emitted photons and it also means that effects of amplified spontaneous emission are neglected. Additionally, we neglect the effects of the non-radiative energy transfer processes energy migration and cross-relaxation that were described in Section 2.2. Thus, the only way to excite ions to $^5I_7$ is through absorption of photons. It is assumed that non-radiative decay only occurs between adjacent energy levels, because the rate of multiphonon quenching decreases rapidly with the number of phonons needed to bridge an energy gap. Thus, spontaneous decay in the transition $^5I_6 \rightarrow ^5I_8$ comes only from spontaneous emission.

3.1.3 Energy States of Single and Paired Ions

Figure 3.1 shows the energy states that single ions can take. The population of the different states are denoted as N_0, N_1 and N_3, and correspond to the three lowest energy states of holmium, namely $^5I_8$, $^5I_7$ and $^5I_6$.

Each ion in a pair can also occupy these same energy states. However, because the two ions in a pair can exchange energy so rapidly through inhomogeneous ETU, the two ions should be considered collectively. Thus, the states to keep

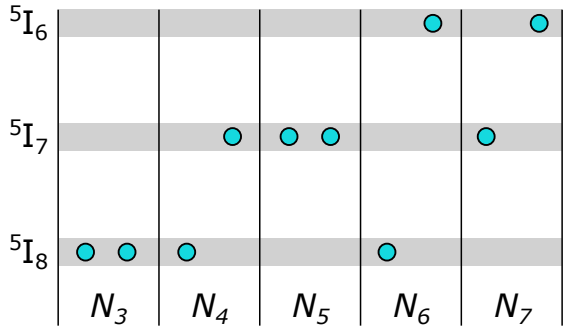

Figure 3.2: Illustration of possible energy states that an ion pair can take in the numerical model. The parameters N_3-N_7 are the populations of paired ions in the given energy states.

track of are all the combinations of states that the two ions in the pair can take. Figure 3.2 shows all the five possible combinations that remain after making the assumptions previously discussed.

The pair states are labeled N_3-N_7 and are as follows: In N_3, both ions are in the ground state $^5I_8$. In N_4, one of the ions is excited to the upper laser level $^5I_7$ and the other is in the ground state $^5I_8$. N_5 is a state where both ions are excited to the upper laser level $^5I_7$, i.e. this is the doubly-excited state and is the primary interest of this model. The doubly-excited state can undergo inhomogeneous ETU with a rate that is the reciprocal of the doubly-excited pair lifetime. N_6 is the state that a pair transforms into after undergoing ETU. It has one ion in the ground state $^5I_8$ and the other in the upper state $^5I_6$. N_7 has one ion in the upper laser level $^5I_7$ and the other ion in the upper state $^5I_6$.

It is assumed that $2k$ is the ratio of ions that reside within a pair. Thus, the concentration of single ions in the fiber is $(1-2k)N_{\mathrm{Ho}}$ and the concentration of ion pairs is kN_{Ho}, where N_{Ho} is the holmium-doping concentration in units of ions/m^3. Note that kN_{Ho} is the concentration of pairs and $2kN_{\mathrm{Ho}}$ is the concentration of ions reciding in pairs.

3.1.4 Transition Rates

The rates of the energy transitions that are assumed to be possible in this rate equation model are illustrated in Figure 3.3. The rates follow the notation established in Section 2.3.1, where W_{ij}, means a transition from the holmium energy state i to j (i $\rightarrow$ j). The subscripts 0, 1 and 2 corresponds to the holmium energy states $^5I_8$, $^5I_7$ and $^5I_6$, respectively. If i $<$ j, W_{ij} represents a rate of absorpion. If i $>$ j then W_{ij} represents a rate of stimulated emission, or

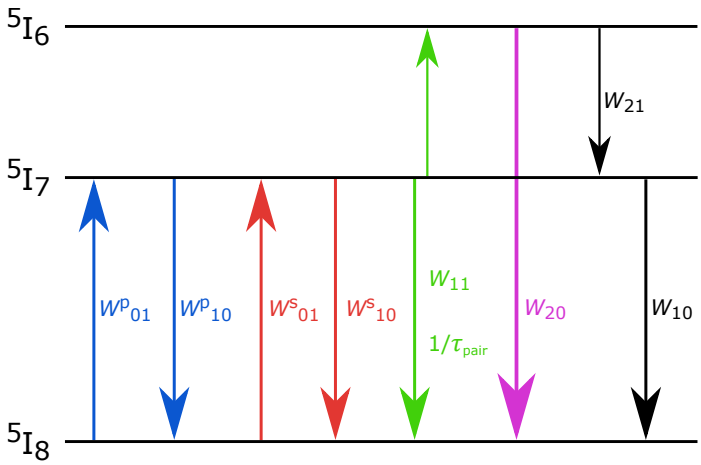

Figure 3.3: Possible energy transitions and their corresponding rates. The rates are from left to right: pump absorption, stimulated pump emission, signal absorption, stimulated signal emission, homogeneous and inhomogeneous energy transfer upconversion, radiative decay from $^5I_6$ to $^5I_8$, spontaneous decay from $^5I_6$ to $^5I_7$ and finally, spontaneous decay from $^5I_7$ to $^5I_8$.

spontaneous decay. In this model there is only one rate W_{ij} where $i > j + 1$, and that is the rate W_{20}. This rate describes spontaneous emission from $^5I_6$ to $^5I_8$. This rate is calculated from the radiative lifetime of $^5I_6$ (which includes the effect of $^5I_6$-ions radiatively decaying to $^5I_7$ as well) and its respective *branching ratios*. The branching ratios represent the ratio of the radiatively decaying $^5I_6$-ions going to $^5I_7$ and $^5I_8$, respectively. The superscripts p and s correspond to a transition induced by the pump or signal field.

Consider the rates in Figure 3.3, W^{p}_{01} and W^{p}_{10} represent absorption and stimulated emission of the pump, respectively. W^{s}_{01} and W^{s}_{10} represent absorption and stimulated emission of the signal, respectively. These four rates are given by the equations

$$W^{\mathrm{p}}_{01} = \frac{\Gamma_{\mathrm{p}}\sigma^{\mathrm{p}}_{01}\lambda_{\mathrm{p}}}{hcA}P_{\mathrm{p}}(z,t), \tag{3.1}$$

$$W^{\mathrm{p}}_{10} = \frac{\Gamma_{\mathrm{p}}\sigma^{\mathrm{p}}_{10}\lambda_{\mathrm{p}}}{hcA}P_{\mathrm{p}}(z,t), \tag{3.2}$$

$$W^{\mathrm{s}}_{01} = \frac{\Gamma_{\mathrm{s}}\sigma^{\mathrm{s}}_{01}\lambda_{\mathrm{s}}}{hcA}P_{\mathrm{s}}(z,t), \tag{3.3}$$

$$W^{\mathrm{s}}_{10} = \frac{\Gamma_{\mathrm{s}}\sigma^{\mathrm{s}}_{10}\lambda_{\mathrm{s}}}{hcA}P_{\mathrm{s}}(z,t), \tag{3.4}$$

where Γ_p and Γ_s are the power filling factors for the pump and signal fields as defined in Equation (2.11). σ_{01}^p and σ_{10}^p are the absorption- and emission cross sections for the pump wavelength, respectively. σ_{01}^s is the absorption cross section for the signal wavelength, and σ_{10}^s is the emission cross section. λ_p is the pump wavelength and λ_s is the signal wavelength. h is Planck's constant, c is the speed of light in vacuum, and A is the cross section area of the fiber core. $P_\mathrm{p}(z,t)$ is the optical power of the pump beam, and $P_\mathrm{s}(z,t)$ is the optical power of the signal beam at position z in the fiber at time t.

In the following Sections 3.2-3.3, the rate equations of single and paired ions are defined and explained thoroughly. The equations are not mathematically complex, but they involve a lot of bookkeeping. The rate equations themselves will not be important for understanding the results of the simulations. The focus of the reader should therefore lie on understanding the energy states of Figure 3.1-3.2 in conjunction with the energy transitions illustrated in Figure 3.3, rather than the exact details of Equations (3.5)-(3.13).

3.2 Rate Equations for Single Ions

Given the energy states of Figure 3.1 and the possible energy transitions of Figure 3.3, the rate of change of the populations N_0-N_2 are given by

$$\begin{aligned}\frac{\mathrm{d}N_0(z,t)}{\mathrm{d}t} =& W_{11}N_1(z,t)^2 + (W_{10} + W_{10}^\mathrm{p} + W_{10}^\mathrm{s})N_1(z,t) \\ &+ W_{20}N_2(z,t) - (W_{01}^\mathrm{p} + W_{01}^\mathrm{s})N_0(z,t), \qquad (3.5)\\ \frac{\mathrm{d}N_1(z,t)}{\mathrm{d}t} =& (W_{01}^\mathrm{p} + W_{01}^\mathrm{s})N_0(z,t) + W_{21}N_2(z,t) \\ &- (W_{10} + W_{10}^\mathrm{p} + W_{10}^\mathrm{s})N_1(z,t) - 2W_{11}N_1(z,t)^2, \qquad (3.6)\\ \frac{\mathrm{d}N_2(z,t)}{\mathrm{d}t} =& W_{11}N_1(z,t)^2 - (W_{21} + W_{20})N_2(z,t). \qquad (3.7)\end{aligned}$$

For brevity, the z- and t-dependencies of the populations N_0-N_2 are left out in the following explanation of the terms in Equations (3.5)-(3.7).

Beginning with the rate of change of N_0 described by Equation (3.5), $W_{11}N_1^2$ describes the process of populating N_0 as two single ions from state N_1 undergo ETU, hence one of these ions is demoted to N_0. This term is quadratic in N_1 because the rate of homogeneous ETU depends on two ions being in N_1. The state N_0 can also be populated by N_1 by ions undergoing spontaneous decay, or stimulated emission by the pump or signal beams. These three effects are represented by the term $(W_{10}+W_{10}^\mathrm{p}+W_{10}^\mathrm{s})N_1$. The last way N_0 can be populated is by ions from N_2 decaying through spontaneous emission. This corresponds to the term $W_{20}N_2$. Lastly, N_0 can become depopulated by populating N_1 through absorption of a pump or signal photon. This is described by the term

$-(W_{01}^{\mathrm{p}}+W_{01}^{\mathrm{s}})N_0$. These terms are also found in Equation (3.6) describing $\mathrm{d}N_1/\mathrm{d}t$, but with opposite sign as they represent a transition.

In Equation (3.6) there are two new terms not found in Equation (3.5). $W_{21}N_2$ represents spontaneous decay from N_2 to N_1. N_1 is also depopulated by two single ions undergoing ETU, where one of the two ions are demoted to N_0 and the other ion is promoted to N_2. This is described by the term $-2W_{11}N_1^2$, where the factor 2 is precent because two ions are lost from this state for every ETU process.

In Equation (3.7) there are no new terms that have not been described above. The total number of single ions must be constant as single ions cannot disappear or be generated in the system. Thus, one of the Equations (3.5)-(3.7) can be considered as redundant and can be substituted with

$$(1-2k)N_{\mathrm{Ho}} = N_0(z,t) + N_1(z,t) + N_2(z,t), \tag{3.8}$$

which ensures that the total number of single ions is constant.

3.3 Rate Equations for Paired Ions

Each ion in a pair can undergo the same energy transitions as single ions with one exception. Paired ions can not undergo ETU through interaction with other single ions or ions from other pairs. Ions in pairs can only undergo ETU within the pair. The rate at which this occurs differs drastically from homogeneous ETU in Equations (3.5)-(3.7). The ion pair undergoes inhomogeneous ETU with a rate denoted $W_{\mathrm{pair}} = 1/\tau_{\mathrm{pair}}$. In this model, an assumption is that only one of the ions within a pair can undergo a transition at a time, with the exception of ETU which involves both ions. Given this assumption, the energy states of Figure 3.2 and the possible transitions of Figure 3.3, the rates of change of the populations

N_3-N_7 are given by

$$\begin{aligned}
\frac{\mathrm{d}N_3(z,t)}{\mathrm{d}t} =&(W_{10}+W_{10}^{\mathrm{p}}+W_{10}^{\mathrm{s}})N_4(z,t)+W_{20}N_6(z,t)\\
&-2(W_{01}^{\mathrm{p}}+W_{01}^{\mathrm{s}})N_3(z,t), &(3.9)\\
\frac{\mathrm{d}N_4(z,t)}{\mathrm{d}t} =&2(W_{01}^{\mathrm{p}}+W_{01}^{\mathrm{s}})N_3(z,t)\\
&+2(W_{10}+W_{10}^{\mathrm{p}}+W_{10}^{\mathrm{s}})N_5(z,t)\\
&+W_{21}N_6(z,t)+W_{20}N_7(z,t)\\
&-(W_{01}^{\mathrm{p}}+W_{01}^{\mathrm{s}}+W_{10}+W_{10}^{\mathrm{p}}+W_{10}^{\mathrm{s}})N_4(z,t), &(3.10)\\
\frac{\mathrm{d}N_5(z,t)}{\mathrm{d}t} =&(W_{01}^{\mathrm{p}}+W_{01}^{\mathrm{s}})N_4(z,t)+W_{21}N_7(z,t)\\
&-2(W_{10}+W_{10}^{\mathrm{p}}+W_{10}^{\mathrm{s}})N_5(z,t)-W_{\mathrm{pair}}N_5(z,t), &(3.11)\\
\frac{\mathrm{d}N_6(z,t)}{\mathrm{d}t} =&W_{\mathrm{pair}}N_5(z,t)+(W_{10}+W_{10}^{\mathrm{p}}+W_{10}^{\mathrm{s}})N_7(z,t)\\
&-(W_{21}+W_{20}+W_{01}^{\mathrm{p}}+W_{01}^{\mathrm{s}})N_6(z,t), &(3.12)\\
\frac{\mathrm{d}N_7(z,t)}{\mathrm{d}t} =&(W_{01}^{\mathrm{p}}+W_{01}^{\mathrm{s}})N_6(z,t)\\
&-(W_{10}+W_{10}^{\mathrm{p}}+W_{10}^{\mathrm{s}}+W_{20}+W_{21})N_7(z,t). &(3.13)
\end{aligned}$$

Once again, the z- and t-dependence are left out for brevity in the following explanation of the terms in Equations (3.9)-(3.13).

In Equation (3.9), the term $(W_{10}+W_{10}^{\mathrm{p}}+W_{10}^{\mathrm{s}})N_4$ represents the process of populating N_3 through spontaneous decay, and stimulated emission by the pump and signal beams of the ion in N_4 that occupies $^5\mathrm{I}_7$. $W_{20}N_6$ represents the process of populating N_3 by the ion in N_6 that is excited to $^5\mathrm{I}_6$ undergoing spontaneous emission, transitioning to $^5\mathrm{I}_8$. $-2(W_{01}^{\mathrm{p}}+W_{01}^{\mathrm{s}})N_3$ represents a transition from N_3 to N_4 by one of the pair's ions absorbing a pump or signal photon. The factor 2 is present because either of the two ions in N_3 can absorb the pump or signal photon.

In Equation (3.10) there are three new terms. $2(W_{10}+W_{10}^{\mathrm{p}}+W_{10}^{\mathrm{s}})N_5$ represents the process of populating N_4 by one of the ions in N_5 undergoing spontaneous decay, or stimulated emission by the pump or signal beams. Again, the factor 2 is present since either one of the two ions in N_5 can undergo these transitions. $W_{21}N_6$ corresponds to the process of populating N_4 by the ion in N_6 that is excited to $^5\mathrm{I}_6$ undergoing spontaneous decay, transitioning to $^5\mathrm{I}_7$. The term $W_{20}N_7$ represents a transition of a pair occupying N_7 to the state N_4 by the ion in N_7 that occupies $^5\mathrm{I}_6$, decaying to $^5\mathrm{I}_8$ through spontaneous emission. The term $-(W_{01}^{\mathrm{p}}+W_{01}^{\mathrm{s}}+W_{10}+W_{10}^{\mathrm{p}}+W_{10}^{\mathrm{s}})N_4$ represents the depopulating of N_4 by populating N_5 and N_3, where the latter is previously described. The depopulating

of N_4 by populating N_5 occurs by the ion in N_4 that is in the ground state $^5\mathrm{I}_8$, absorbing the pump or signal beams.

Equation (3.11) describes the rate of change of the population of doubly-excited ion pairs. In this equation there are two new terms. $W_{21}N_7$ describes the populating of N_5 by the ion in N_7 that occupies $^5\mathrm{I}_6$ undergoing spontaneous decay to $^5\mathrm{I}_7$. The term $-W_{\mathrm{pair}}N_5$ corresponds to the process of depopulating N_5 as the doubly-excited pair undergoes ETU. The pair thus transitions to N_6 with one ion demoted to $^5\mathrm{I}_8$ as the other ion in the pair is promoted to $^5\mathrm{I}_6$.

In Equation (3.12) there are again two new terms. $(W_{10} + W_{10}^{\mathrm{p}} + W_{10}^{\mathrm{s}})N_7$ represents the process of populating N_6 as the ion in N_7 that occupies $^5\mathrm{I}_7$ becomes demoted to $^5\mathrm{I}_8$ through either spontaneous decay or stimulated emission by the pump or signal. The term $-(W_{21}+W_{20}+W_{01}^{\mathrm{p}}+W_{01}^{\mathrm{s}})N_6$ describes the depopulating of N_6 as the pair transitions to either N_4, N_3 or N_7, where only the latter has not yet been described. N_6 can transitions to N_7 by the ion in N_6 that is in the ground state $^5\mathrm{I}_8$ absorbing the pump or signal beam, becoming excited to $^5\mathrm{I}_7$.

There are no new terms in Equation (3.13) that have not been described above. Similarly to the single ions, the total number of ion pairs is constant. One of the Equations (3.9)-(3.13) are thus redundant and can be substituted with

$$kN_{\mathrm{Ho}} = N_3(z,t) + N_4(z,t) + N_5(z,t) + N_6(z,t) + N_7(z,t). \tag{3.14}$$

3.4 Power Evolution of Pump and Signal

The powers of the pump and signal beams changes throughout the optical fiber as they propagate. This is because the optical beams undergo absorption and stimulated emission by the holmium-ions. In this model, it is assumed that the pump and signal beams can only propagate in the positive z-direction. Thus, reflections that would lead to light being guided in the backwards direction (e.g. by impurities or from the fiber output end) are neglected.

3.4.1 Power Propagation Equations

The equations that describe the power evolution of the pump and signal beams as they propagate through the optical fiber are dependent on the population of ions that are in the upper laser level $^5\mathrm{I}_7$ and the ground state $^5\mathrm{I}_8$. Thus, the equations governing the power propagations involve the populations N_0-N_7 that have one

or more ions in $^5\mathrm{I}_7$ or $^5\mathrm{I}_8$. The power propagation equations are given by

$$\begin{aligned}\frac{\mathrm{d}P_\mathrm{p}(z,t)}{\mathrm{d}z} =&\big\{\Gamma_\mathrm{p}\sigma_{10}^\mathrm{p}[N_1(z,t)+N_4(z,t)+2N_5(z,t)+N_7(z,t)]\\ &-\Gamma_\mathrm{p}\sigma_{01}^\mathrm{p}[N_0(z,t)+2N_3(z,t)\\ &+N_4(z,t)+N_6(z,t)]\big\}\times P_\mathrm{p}(z,t), \qquad (3.15)\\ \frac{\mathrm{d}P_\mathrm{s}(z,t)}{\mathrm{d}z} =&\big\{\Gamma_\mathrm{s}\sigma_{10}^\mathrm{s}[N_1(z,t)+N_4(z,t)+2N_5(z,t)+N_7(z,t)]\\ &-\Gamma_\mathrm{s}\sigma_{01}^\mathrm{s}[N_0(z,t)+2N_3(z,t)\\ &+N_4(z,t)+N_6(z,t)]\big\}\times P_\mathrm{s}(z,t). \qquad (3.16)\end{aligned}$$

The power filling factors, transition cross sections and optical powers in Equations (3.15)-(3.16) are the same as in Equations (3.1)-(3.4). In Equation (3.15), the sum $N_1(z,t)+N_4(z,t)+2N_5(z,t)+N_7(z,t)=N_{^5\mathrm{I}_7}(z,t)$ is the total population density of ions in $^5\mathrm{I}_7$, and the product $\Gamma_\mathrm{p}\sigma_{10}^\mathrm{p}N_{^5\mathrm{I}_7}(z,t)P_\mathrm{p}(z,t)$ describes the increase of pump power per unit distance through stimulated emission. The factor 2 in front of $N_5(z,t)$ is present because both ions in the state N_5 are in $^5\mathrm{I}_7$. The sum $N_0(z,t)+2N_3(z,t)+N_4(z,t)+N_6(z,t)=N_{^5\mathrm{I}_8}(z,t)$ is the total population density of ions in $^5\mathrm{I}_8$, and the product $-\Gamma_\mathrm{p}\sigma_{01}^\mathrm{p}N_{^5\mathrm{I}_8}(z,t)P_\mathrm{p}(z,t)$ describes the decrease of pump power because of absorption. The factor 2 in front of $N_3(z,t)$ accounts for both ions in N_3 being in the ground state $^5\mathrm{I}_8$.

Equation (3.16) is similar to Equation (3.15), with the power filling factor, transition cross sections and optical power changed to be specific for the signal beam.

3.4.2 Model of Optical Fiber

The holmium-doped fiber is discretized into multiple segments. Each fiber segment has a length $\mathrm{d}z=L/n$, where L is the length of the holmium-doped fiber and n is the number of fiber segments. Figure 3.4 illustrates how the fiber is divided into segments and how the optical powers propagate through one segment after another. Each fiber segment has its own set of holmium ions and the number of ions is given by $\mathrm{d}zAN_\mathrm{Ho}$, where A is the cross section area of the fiber core. The temporal dimension is also discretized into times $t_k=t_1,t_2,t_3,...,t_\mathrm{end}$ with step size $\mathrm{d}t=t_k-t_{k-1}$. The step size can be varied throughout the simulations as the importance of a short step size changes depending on how fast the populations of the different states are redistributed by the optical pulses.

Example code that shows how the rate equation model presented in this chapter is solved numerically is provided for the interested reader in AppendixA.

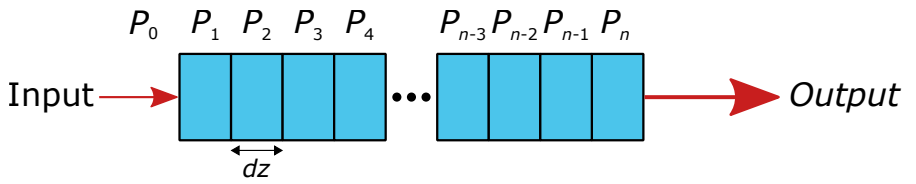

Figure 3.4: The holmium-doped fiber in the model is discretized into segments of length dz. Each fiber segment has its own population of holmium ions, both single ions and pairs.

3.5 Choice of Parameter Values

As evident from Equations (3.1)-(3.14), the numerical model described in this chapter requires input of several parameters that correspond to geometric and spectroscopic properties of the holmium-doped optical fibers under investigation. The spectroscopy experiments described in Chapter 4 investigate twelve different holmium-doped fiber samples. To simplify the numerical investigations of equivalent scenarios as these spectroscopy experiments, most fiber parameters were chosen to be constant for all twelve fibers as these parameters are unknown for the specific fibers and in general very uncertain. The fiber parameters chosen to be constant during simulations of all twelve fibers are summarized in Table 3.1. Varying these parameters slightly does not change the results of the simulations to a significant degree, in the short timescale of interest and relevance for inhomogeneous ETU.

The fiber parameters that are assumed in the simulations to vary from fiber to fiber are: $^5I_7$ lifetime, holmium-doping concentration, core diameter, numerical aperture and fiber lenght. These parameters are provided in Tables 4.1-4.2 in Chapter 4. There are only three fibers where the $^5I_7$ lifetime is unknown, and for these a lifetime of 1 ms was used, which corresponds to the average of the reported values for the other fibers.

Table 3.1: Summary of the constant fiber parameters used in all the simulations.

Parameters	Value
σ_{01}^{p}	$2.85 \times 10^{-25}\,\mathrm{m}^2$ [a]
σ_{10}^{p}	$2.43 \times 10^{-25}\,\mathrm{m}^2$ [a]
σ_{01}^{s}	$0.19 \times 10^{-25}\,\mathrm{m}^2$ [a]
σ_{10}^{s}	$1.25 \times 10^{-25}\,\mathrm{m}^2$ [a]
Radiative lifetime $^5\mathrm{I}_6$	11.46 ms [b]
Branching ratio $^5\mathrm{I}_6 \rightarrow {}^5\mathrm{I}_8$	0.828 [b]
Branching ratio $^5\mathrm{I}_6 \rightarrow {}^5\mathrm{I}_7$	0.172 [b]
W_{20}	$72.25\,\mathrm{s}^{-1}$ [c]
W_{11}	$4.0 \times 10^{-23}\,\mathrm{m}^3\mathrm{s}^{-1}$ [d]
$2k$	8%

[a] Cross section values from Reference [21].
[b] Calculated by Wang et al. with values from Peng et al. [5, 24].
[c] Calculated from radiative lifetime and branching ratio values.
[d] Estimated by Huang et al. in Reference [26].

Chapter 4

Experimental Setup

In this chapter, three different experiments are described. The two first experiments are spectroscopic measurements of holmium-doped fibers that investigates properties of the pair induced quenching process. The third experiment is a laser experiment that investigates how PIQ in practice affects central laser properties such as efficiency in a holmium-doped fiber amplifier. The three experiments will be described in detail in separate sections. Each section starts with some background information to aid the reader in understanding the purpose and details of the given experiment, before the measurement setup is described.

4.1 Lifetime Measurements of Doubly-excited Holmium-ion Pairs

The lifetime of a doubly-excited holmium-ion pair is the time it takes for $1 - 1/e \approx 63\%$ of the doubly-excited pairs to undergo inhomogeneous energy transfer upconversion as described in Section 2.4. When both holmium ions in a pair are excited to $^5I_7$ (a "doubly-excited pair") and undergoes ETU, one of the ions become promoted to either $^5I_6$ or $^5I_5$. However, as discussed in Section 2.4.2, it is a fair approximation to assume that all upconverted ions become excited to $^5I_6$. From these upconverted ions, there is a finite probability that they will spontaneously decay from $^5I_6$ to the ground state, emitting a photon with wavelength $\sim 1.15\,\mu m$ in the process, corresponding to the energy difference between the two states. The intensity of this fluorescence is proportional to the population of ions in this level, and if ETU is assumed to be the only way $^5I_6$ can be populated, then by measuring the time variation of the fluorescence intensity after a short pump pulse has excited the ions, the time course of the upconversion process can be observed.

This experiment concerns the measurement of 1.15 µm fluorescence from holmium-doped optical fibers after being pumped by a short pump pulse at 1.95 µm. Because homogeneous ETU is associated with the square of the population of $^5I_7$, and the lifetime of $^5I_7$ is ~ 1 ms, the population of $^5I_7$ is approximately constant over the sub-microsecond timescale expected to be relevant for inhomogeneous upconversion. Thus, the contribution to $^5I_6$ from homogeneous upconversion will also be constant over this timescale. This means that from the measured time course of the fluorescence intensity, the lifetime of doubly-excited pairs can be deduced. As will be discussed in Section 4.1.3, fiber samples have been chosen, and special measurements are done to verify that the measured fluorescence indeed does originate from doubly-excited pairs undergoing ETU.

4.1.1 Pump Source

A pump source for this experiment needs to output short pulses, much shorter than the lifetime of doubly-excited holmium-ion pairs. Ideally, an infinitely short pulse should be used as a pump pulse, such that all ions are excited at the exact same time. However, the shorter the pump pulse is, the higher its peak power will be for a given pulse energy. High peak powers are problematic in optical fibers, because nonlinear optical effects can degrade the properties of the output pulses, or even be damaging to the pump source itself. Thus, laser sources are often limited by the peak power of the pulses, and the only way to increase the pulse energy is by increasing the width of the pulse. The natural target for the needed pulse energy in this fluorescence experiment is the saturation energy of the fibers. As defined by Equation (2.26), this energy represents the energy that can cause an appreciable depletion of the ground state $^5I_8$, thus populating the upper laser level $^5I_7$. A typical fiber investigated in this experiment has a core diameter of 8 µm, NA = 0.16 and, assuming that the emission and absorption cross sections for the pump wavelength are as given in Table 3.1, the saturation energy is $E_{\text{sat}} = 9.7$ µJ. The wavelength of the pump light should be near the peak absorption wavelength of holmium in silica. As shown in Figure 2.8, the absorption peak of holmium is narrow and centered around 1.95 µm. Thus, the pump light should have a wavelength centered at 1.95 µm and only span some few nanometers.

Thulium-doped Fiber Amplifier

The pump source used for this fluorescence experiment is an all fiber two-stage Tm-doped fiber master oscillator power amplifier (MOPA) that has been developed during this project and has served as a work horse pump source used for all of the spectroscopic measurements and amplifier experiments done with holmium fibers in this work. Although considerable effort has been put into design, construction

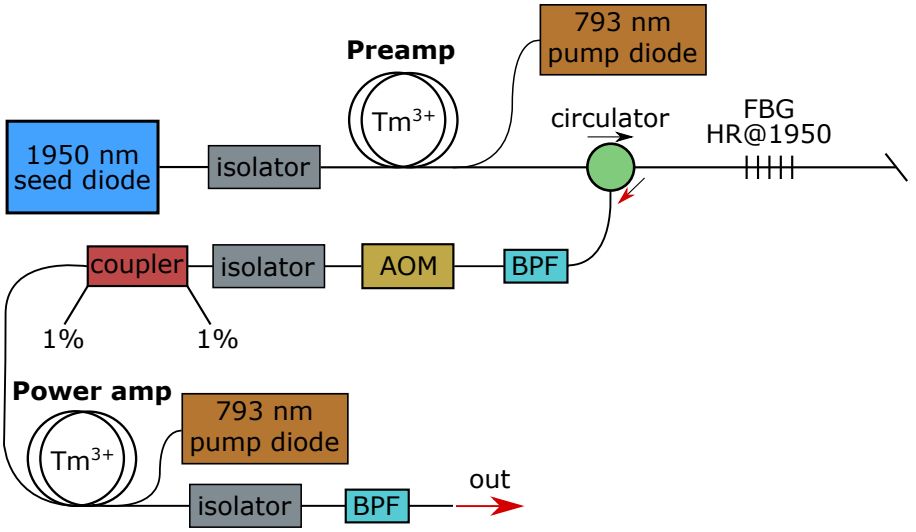

Figure 4.1: Two-stage thulium-doped fiber MOPA. FBG: fiber Bragg grating, HR: high reflectance, BPF: bandpass filter, AOM: acousto-optic modulator.

and characterization of this thulium amplifier, it is regarded as part of the apparatus used for studying holmium fibers, and for that reason, details of its output and performance are considered in this chapter and not as results in Chapter 5.

Figure 4.1 shows a schematic of the pump source, which is comprised of a fiber coupled seed diode laser (master oscillator) followed by two stages of amplification; the preamplifier and the power amlifier. The seed diode emits configurable pulses of 1.95 µm light and is driven by a fast 330 MHz electrical bandwidth pulse generator. A major benefit of using a MOPA as the pump source in this experiment is that the pulse width, shape and repetition rate can be easily adjusted to suit the needs of the experiment. It also provides good pulse to pulse stability, making it possible to average the fluorescence measurements over a large number of pump pulses to lower the noise level.

The 1950 nm seed diode provides pulses with a peak power of only 2.5 mW. For a 30 ns square pulse this yields a pulse energy of only 75 pJ. Thus, to reach the desired pulse energy of 9.7 µJ (saturation energy), the seed pulse must be amplified by a gain of $\sim$ 51 dB. This amplification is provided by the two Tm^{3+}-doped fiber stages. Between the seed diode and each amplification stage, a fiber coupled Faraday isolator is spliced to avoid any unwanted reflections or ASE propagating backwards into the previous amplification stage or to the seed diode. Band pass filtering is included to ensure that the optical spectrum is narrow enough around

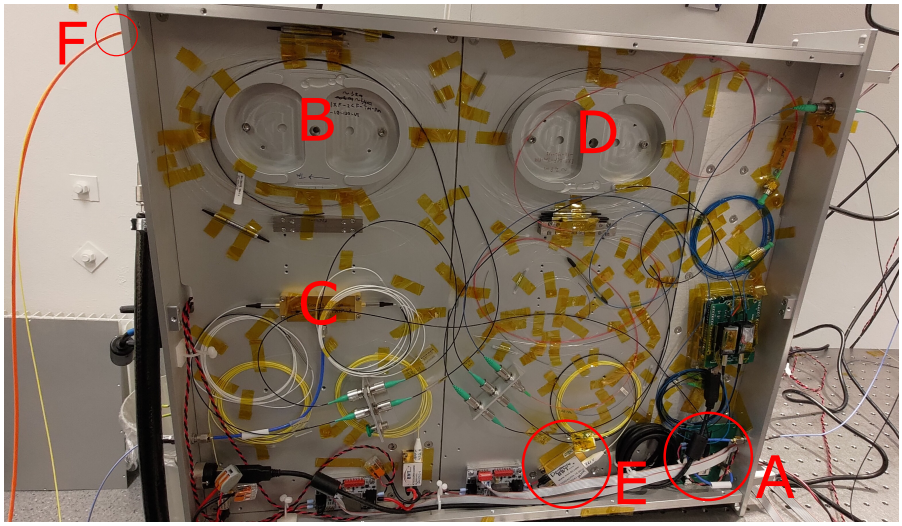

Figure 4.2: Image of the thulium-doped fiber MOPA used as a pump source. Some key elements are highlighted: A: 1950 nm seed diode, B: preamplifier, C: AOM, D: power amplifier, E: pump diode used to pump the power amplifier, and F: the output fiber.

1.95 µm, and to suppress ASE occuring between the seed pulses. A circulator, fiber Bragg grating (FBG) and a dielectric bandpass filter (BPF) are spliced after the preamplifier stage to "clean up" the optical spectrum before the power amplifier stage. The FBG reflects the light centered around 1.95 µm inside a bandwidth of ~ 1 nm. The circulator routes the reflected light towards a fiber-coupled BPF with a bandwidth of 8 nm to lower the unwanted ASE even further. Whereas the circulator, FBG and BPF spectrally removes optical power outside of the pass spectrum, a fiber coupled acousto-optic modulator (AOM) is spliced between the amplification stages to remove optical power in the temporal domain. Specifically, the AOM only transmits light during a small time window around the optical pulse. This is important because without the AOM, any remaining ASE from the preamplifier (after the FBG and BPF) would be amplified by the following power amplifier. The total energy of the resulting ASE could become comparable to the saturation energy, which would cause unwanted excitation of holmium-ions before the actual pump pulse. A fiber optic coupler is spliced between the isolator and pump-signal combiner, allowing signal monitoring. Then follows the power amplifier stage and finally a BPF equivalent to the one previously mentioned. This BPF does the final spectral "clean up" before the pump pulse can be sent into a holmium-doped fiber. An image of this pump source used in all the experiments described in this chapter is shown in Figure 4.2.

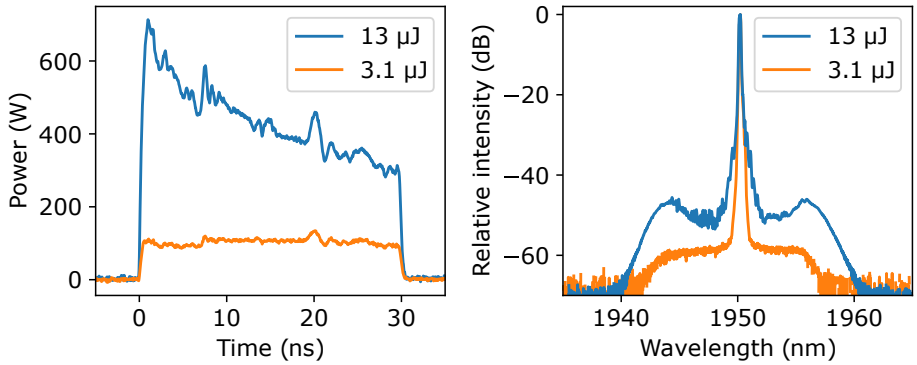

Figure 4.3: Left: Pulse shapes of the 30 ns pulses with energies 13 µJ (blue) and 3.1 µJ (orange). Right: Optical spectra of the pulses.

Pump Pulse Characteristics

The pump pulses chosen for the fluorescence experiment are 30 ns, nearly square pulses at a repetition rate of 100 Hz. The repetition rate is chosen to be low such that the time between the pulses is much longer than the $^5I_7$ fluorescent lifetime (~ 1 ms). This ensures that practically all ions have decayed down to the ground state before the next pump pulse arrives, thus, the measured fluorescence stems from excitation caused by the most recent pulse, and not by any previous pulses.

To see whether the time course of the fluorescence signal depends on the degree of excitation, two different pulse energies were used. The pulse energies are chosen by varying the pump power in the thulium-doped power amplifier stage. The two pulse energies used were 13 µJ and 3.1 µJ. Both the pulse shape and pulse spectrum changes when the gain in the power amplifier is increased by varying the pump power. Figure 4.3 show the temporal shapes and optical spectra of the pump pulses. The temporal form of the two pulses are measured with a fast photodiode and a 1 GHz bandwidth oscilloscope. As can be seen, when the pulse energy is low (3.1 µJ) the pulse shape is nearly square and its spectrum has a large peak at 1950 nm, with a much higher intensity than the ASE between ~ 1942 nm and ~ 1956 nm. This ASE at ~ -60 dB is ocurring mostly in the time between the pulses. When the pulse energy is increased to 13 µJ, the pulse shape and spectrum deteriorates to some extent. The pulse shape becomes less square due to gain saturation where the pulse depopulates the upper laser level to a significant degree such that later parts of the pulse experience less gain compared to the early parts. The temporal oscillations seen in both pulses are attributed to the nonlinear effect *stimulated Brillouin scattering* (SBS) [12]. These SBS induced artifacts do however not have any impact on the results of the measurements.

Because the peak power of the 13 µJ pulse is higher, nonlinear effects become more pronounced. The nonlinear process known as *four-wave mixing* (FWM) converts power from the main peak at 1950 nm to the side lobes located symmetrically around the main peak with peaks at $\sim$ 1944 nm and $\sim$ 1956 nm as can be seen in Figure 4.3. This effect broadens and deteriorates the pulse spectrum, however, the FWM is part of the pulse itself, and the two side lobes are well within the main peak of the absorption cross section of holmium in silica, as can be seen from Figure 2.8. Thus, these pulses are still suitable for the fluorescence experiments. The spectrum of the 13 µJ pulse is also affected by ASE between the pulses, however, the ASE is largely overshadowed by the specral broadening caused by FWM. The two spectra have optical full width at half maximum (FWHM) bandwidths of $\Delta\lambda = 0.17$ nm and $\Delta\lambda = 0.14$ nm for the 13 µJ and 3.1 µJ pulses, respectively.

As mentioned previously, the ASE occuring between the pulses can be disadvantageous if the total energy of the ASE power within the lifetime of $^5I_7$ is large enough to cause significant excitation of the holmium-doped fiber. However, the measured energy of the ASE occuring within 1 ms between the 13 µJ pulses was only $E_{\mathrm{ASE}} \sim 0.1$ µJ, which is much lower than the saturation energy $E_{\mathrm{sat}} = 9.7$ µJ. For the 3.1 µJ pulses the power of the ASE is even lower. Thus, it can be concluded that the influence of ASE is negligible in this experiment.

4.1.2 Measurement Setup

The fluorescence signal to be measured consists of light with wavelength ~ 1.15 µm and stems from the radiative transition $^5I_6 \rightarrow {}^5I_8$. The signal is however expected to be weak, since $^5I_6$ has a radiative lifetime of $\sim$ 11.46 ms [24] and a non-radiative lifetime of ~ 1.4 µs [23]. In other words, most ions excited to $^5I_6$ decay non-radiatively. Additionally, the branching ratio for the radiative transition $^5I_6 \rightarrow {}^5I_8$ in comparison to the radiative transition $^5I_6 \rightarrow {}^5I_7$ is ~ 0.828 [24]. Thus, only a small amount of the upconverted ions undergo the radiative transition that corresponds to 1.15 µm fluorescence.

To measure the weak and rapid fluorescence signal, the detector must be both sensitive and have a high detection bandwidth. In this experiment an InGaAs (indium gallium arsenide) avalanche photo diode (APD) (Excelitas LLAM-1550-R2AH) with a 50 MHz detection bandwidth was used. The measurements with this detector were compared to measurements done with an APD with considerably higher detection bandwidth to verify that the 50 MHz bandwidth was sufficient to capture the signal. The lower detection bandwidth APD was however chosen because it offered a significantly higher signal-to-noise ratio. A schematic of the measurement setup is shown in Figure 4.4, where the 1950 nm pump source is as depicted in Figure 4.1. The pump source output fiber is spliced to the fiber under test (FUT) which is one of the holmium-doped fibers described in

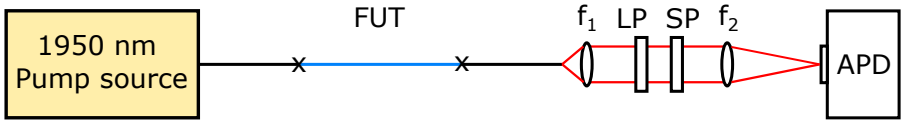

Figure 4.4: A schematic of the measurement setup used in the $^5I_6$ fluorescence experiment. FUT: fiber under test, f: lenses, LP: long-pass filter at 1000 nm, SP: short-pass filter at 1550 nm, APD: avalanche photo diode.

Section 4.1.3. The FUT was in turn spliced to a fiber connector pigtail, and the output signal was collimated by a lens with focal length $f_1 = 8.1$ mm. A long pass filter at 1000 nm and a short pass filter at 1550 nm are placed in the beam path to remove any residual pump and fluorescence stemming from other energy transitions. Following the spectral filters is a lens with focal length $f_2 = 153$ mm focusing the signal beam onto the detector. The spot size on the detector created by the focusing lens and collimating lens was $f_2/f_1 \times 2\omega = 188$ µm, where a mode field radius of $\omega = 5$ µm was assumed, which equals the core radius of most of the fibers used. The spot size of 188 µm is smaller than the diameter of the detector which is 200 µm. The APD is connected to a fast oscilloscope that can capture the time course of the $^5I_6$ fluorescence, and also average over multiple pulse repetitions to increase the signal-to-noise ratio.

4.1.3 Choice of Fibers

Because the rate of inhomogeneous ETU is independent of the doping concentration of the optical fiber, while homogeneous ETU is dependent, both optical fibers with high and low doping concentration are investigated to ensure that the time course of the measured fluorescence signal does indeed originate from upconverted doubly-excited pairs. Twelve different optical fibers, labeled Fibers 1-12, were investigated. Eleven of the fibers were obtained through collaboration with research groups that manufacture rare-earth doped optical fibers and one fiber is a commercially available fiber. Fibers 1-8 are from Kamrádek et al. in Reference [27] and Fiber 9 is from Kamrádek et al. in Reference [19]. The nine fibers correspond to the fibers named, respectively, SD1294, SD1347, SD1412, SD1348, NP1544, NP1557, NP1542, NP1558 and NP1589 in the articles. Fiber 10 is the commercial fiber IXF-HDF-PM-8-125 from iXblue photonics. Fibers 11-12 are provided by the Naval Research Laboratory (USA). The important fiber parameters that were provided by manufacturers are summarized in Tables 4.1-4.2.

The twelve fibers vary in holmium-doping concentration in the wide range $(1.1 - 10) \times 10^{25}$ ions/m^3. Fibers 1-9 are co-doped with alumina (Al_2O_3). The reason for this co-doping is twofold; it lowers the phonon energy of the silica host, and it increases the solubility of the holmium-ions [4]. The effect of increasing the

Table 4.1: Summary of important fiber parameters: Ho^{3+} concentration, Al/Ho ratio, $^5I_7$ fluorescence lifetime and efficiency. Values for Fibers 1-9 are from Reference [27, 19].

Fiber #	Ho^{3+} [ions/m^3]	Al/Ho	$^5I_7$ fluorescence lifetime [µs]	Efficiency [%]
1	1.1×10^{25}	113.2	1217	77.0
2	2.9×10^{25}	42.9	986	72.0
3	5.9×10^{25}	10.3	764	49.1
4	7.0×10^{25}	19.9	815	51.1
5	1.4×10^{25}	110.6	1280	83.1
6	2.3×10^{25}	48.8	1035	74.5
7	4.3×10^{25}	27.9	946	66.9
8	10×10^{25}	8.6	805	41.8
9	5.1×10^{25}	55	1250	81.2
10	3.5×10^{25}	-	-	-
11	2.86×10^{25}	-	-	82.3
12	3.0×10^{25}	-	-	79

Table 4.2: Summary of the fiber parameters: core diameter, small-signal absorption (α_{dB}), numerical aperture (NA), fiber length (L) and absorption (α_{dB}L). The core diameters and small-signal absorption of Fibers 1-9 is from Reference [27, 19].

Fiber #	Core diameter [µm]	α_{dB} [dB/m]	NA	L [cm]	α_{dB}L [dB]
1	10	14.1	-	188	26.5
2	10	37.2	-	68	25.3
3	10	75.6	-	32	24.2
4	10	89.7	-	24	21.5
5	10	17.9	-	153	27.4
6	10	29.5	-	91	26.8
7	10	55.1	-	45	24.8
8	10	128	-	18	23.0
9	10	65.4	-	44	28.8
10	8	45	0.16	58	26.1
11	10	26	0.18	103	26.8
12	10	39	0.174	71	27.7

solubility is that the likelyhood of holmium-ions forming pairs/clusters is decreased. This is especially important for highly-doped fibers. These fibers are manufactured using two different doping methods; Fibers 1-4 are manufactured using the well-known solution doping (SD) technique, and Fibers 5-9 are manufactured using a less conventional approach called nanoparticle-doping (NP).

The holmium-doping concentrations for Fibers 1-9 were calculated from the measured small-signal absorption, α_{dB}, with the formula

$$\alpha_{\mathrm{dB}} = 4.34\sigma_{\mathrm{a}}N_{\mathrm{Ho}}\Gamma, \tag{4.1}$$

where the factor $4.34 = 10\log(\mathrm{e})$, $\sigma_{\mathrm{a}} = 2.954 \times 10^{-25}$ m^2, N_{Ho} is the Ho^{3+} concentration and Γ is the power filling factor from Equation (2.11). In Reference [27, 19] the assumption $\Gamma = 1$ was made for simplicity during calculations. The holmium concentrations of Fiber 10 and 12 were not stated by the manufacturers, therefore it was calculated from the small-signal absorption using Equation (4.1). The numerical aperture of Fibers 1-9 was not given, thus, for simplicity the numerical aperture was assumed to be the same as Fiber 10 (NA = 0.16) in calculations and simulations.

Choice of Fiber Lengths

To avoid re-absorption and re-emission obscuring the time course of the fluorescence signal, it is important to choose short fiber lengths. Ideally, the fiber lengths should be infinitely short, such that the probability of re-absorption and re-emission is zero. However, enough pairs of Ho-ions need to be excited such that the fluorescence signal is detectable. In other words, the fiber lengths must be long enough to get a measurable signal, but short enough to avoid high re-absorption and re-emsission. As holmium-doped fibers are expensive, conserving useful pieces of fiber lengths is also taken into account when choosing the lengths of the fibers. All of these points taken into consideration, a goal absorption of $\alpha_{\mathrm{dB}}L \approx 25\,\mathrm{dB}$ was chosen, i.e. $\sim 99.7\%$ of the pump light being absorbed in the small-signal regime. The chosen fiber lengths and the resulting absorptions for all the fibers can be seen in Table 4.2. The absorption varies between the fibers in the range $21.5 - 28.8\,\mathrm{dB}$. Additionally, a cut-back measurement was done for Fiber 8 to verify that only the signal strength is dependent on the length of the fiber and not the shape of the measured fluorescence time course.

4.2 Measurements of Non-saturable Absorption

Non-saturable absorption is one of the most commonly encountered manifestations of clustered ions, and its strength can be used to quantify the amount of pairs/clusters in the optical fiber. As discussed in Section 2.4.2, the rapid inhomogeneous ETU prevents more than one of the ions in a cluster to be excited at

any given time, when considering timescales much longer than the doubly-excited pair lifetime. Thus, when pumping the holmium-doped fiber there will always be some holmium ions that reside in the ground state $^5I_8$.

Consider the pumping of a holmium-doped fiber with continous wave (CW) 1950 nm light, $^5I_7$ will be populated as $^5I_8$ is depopulated. If there are no ion clusters, and the pump power increases, the degree of excitation will continue to increase until there is a balance between absorbed pump light and pump light generated via stimulated emission. When this excitation is achieved, the holmium-doped fiber becomes transparent to any additional power of pump light. Thus, increasing the pump power further will not lead to additional absorbed light and the absorption is said to be saturated. However, when clusters of holmium ions are present this degree of excitation will never be achieved because there will never be more than one excited ion in a cluster. In other words, there is a non-saturable absorption in the fiber. By measuring the pump transmission of a fiber when pumping with high powers, the amount of non-saturable absorption can be measured. Additionally, and more interestingly, by measuring the non-saturable absorption for multiple fiber lengths, the non-saturable absorption per fiber length can be determined. This is the main quantity of interest in this experiment.

4.2.1 Pump Source

The pump source used in this experiment is the same pump source as was used in the fluorescence experiment in Section 4.1 and illustrated schematically in Figure 4.1. Only a minor modification was done to optimize the source to output high average power CW light, namely, the AOM in Figure 4.1 is bypassed.

4.2.2 Measurement Setup

The measurement setup is shown schematically in Figure 4.5. A fiber optic coupler is spliced to the output of the 1950 nm pump source. The coupler transmits 99% of the input power through one port and the remaining 1% of the power through a second port. The 99% port of the fiber optic coupler at the end of the pump source was spliced to the FUT and the 1% port was used to monitor the power that goes into the the FUT, as this varies depending on variables such as the temperature of the pump source. As the different fibers were tested at several lengths, the fibers must be cut after each measurement and spliced again to the fiber on the right side of the FUT in the figure. Thus, there will be a different and unknown splice loss for each fiber length, which would add uncertainty to the absorption measurements. For this reason, the output of the FUT was spliced to a multi-mode (MM) fiber that has a core diameter of 105 µm. There is essentially zero loss when the light from the SM FUT is sent into the MM fiber, even for relatively low quality splices, since this fiber core is so large compared to the

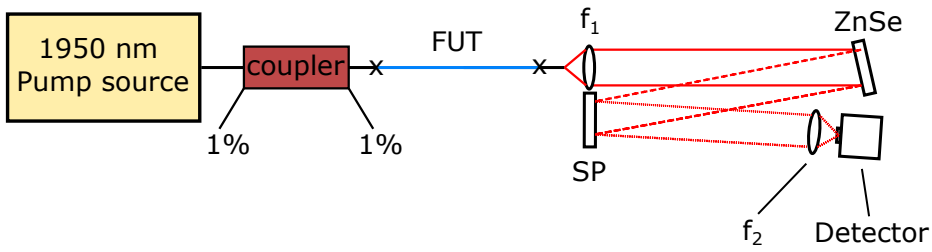

Figure 4.5: A schematic of the measurement setup used in the non-saturable absorption experiment. FUT: fiber under test, f: lenses, ZnSe: zinc selenide wedge, SP: high reflectance filter at 1900-1950 nm.

$\sim 10\,\mu$m diameter core of the SM fiber. This removes any potential variations in splice loss between the FUT and the MM fiber.

The transmission through the FUT was measured for input powers ranging from a few hundred microwatt, which corresponds to the small-signal regime of the FUT, and up to ~ 5 W which was the maximum available power from the pump source.

The detector used for the experiment was an extended InGaAs integrated sphere photodiode (Thorlabs S148C), capable of measuring powers in the range $1\,\mu\text{W} - 1$ W. As the expected maximum power transmitted through the FUT is larger than the 1 W limit of the detector, the light output from the MM fiber was collimated by a lens with focal length $f_1 = 15$ mm and reflected by a zinc selenide (ZnSe) optical wedge, as seen in Figure 4.5. The ZnSe wedge reflects 17.5% of the incoming light, which means that the signal reaching the detector falls within the detector limit even if all of the 5 W pump power is transmitted through the FUT. The wedge was placed in the beam path at near normal incidence to avoid any polarization dependent reflectivity.

To prevent ASE generated in the FUT from obscuring the measurement results, a spectral filter with high reflectance at $1900 - 1950$ nm and low reflectance at $2040 - 2100$ nm was placed in the path of the beam reflected by the wedge. This filter was also placed at near normal incidence. The filter reflects 100% of the 1950 nm pump light and transmits the longer wavelength ASE. A lens with focal length $f_2 = 25$ mm was used to focus the beam onto the detector. If the mode field radius is assumed to be equal to the core radius of the MM fiber, then the collimating and focusing lens created a spot size of $f_1/f_2 \times 2\omega = 175\,\mu$m, which is much smaller than the 5 mm diameter opening of the integrating sphere detector.

The pump source and detector were computer controlled, and the pump power was automatically swept while recording the transmission through the FUT. Importantly, this allowed for quick measurement runs with a high density of data points. Being able to do the measurements for all input powers in a short amount

of time reduces the impact of drift in the pump source and measurement system that would otherwise increase the measurement uncertainty.

4.3 Impact of PIQ on a Nanosecond-pulsed Fiber Amplifier

The reports showing a lower-than-expected efficiency in holmium-doped fiber amplifiers have all used pump sources producing CW light to pump the holmium-doped fiber. It has been suggested that it can be beneficial to implement pulsed pumping if the pump and signal pulse widths are shorter than the doubly-excited pair lifetime [2]. The aim of this experiment is to investigate this strategy for reducing the impact of PIQ on a nanosecond-pulsed holmium-doped fiber amplifier.

This is done by pumping the amplifier with short pulses, and varying the delay between the pump and seed pulses. This delay variation is illustrated in Figure 4.6 for three different values of the delay τ. The figure shows trains of pump pulses at 1950 nm and seed pulses at 2107 nm with repetition rates of 100 kHz (period of 10 µs). In this experiment, measurements of the resulting output power from the amplifier wil be done as the delay between the pulses are swept from essentially no delay, and up to an entire period. However, delays that results in direct overlap between the pump and seed pulses had to be avoided since the nonlinear optical effect *Stimulated Raman Scattering* (SRS) was found to convert optical power from the pump pulse to the seed pulse at the overlapping parts of the pulses. Though interesting, this powerful effect obscures the measurements of PIQ, which is of interest in this work. Although falling outside the scope of this project, the SRS effect and experimental results are briefly described in Appendix B for the curious reader.

4.3.1 Holmium Fiber Amplifier Design

The pulsed holmium-doped fiber amplifier is designed as a MOPA with three amplification stages (two preamplifier stages and a final power amplifier stage). The power amplifier stage employs a so-called tandem setup with a thulium-doped fiber directly preceding a holmium-doped fiber [2]. A schematic of the amplifier design is shown in Figure 4.7. The thulium-doped fiber (manufactured by iXblue Photonics) has a core diameter of 20 µm, a cladding diameter of 300 µm and a numerical aperture of 0.08. This fiber is seeded by 20 ns pulses with wavelength of 1950 nm at a repetition rate of 100 kHz from the 1950 nm channel depicted in Figure 4.7. This 1950 nm channel is the same source as described in Section 4.1. The thulium-fiber is pumped by light from diode lasers at 793 nm which is launched through a pump combiner and into the cladding of the thulium-fiber. The tandem

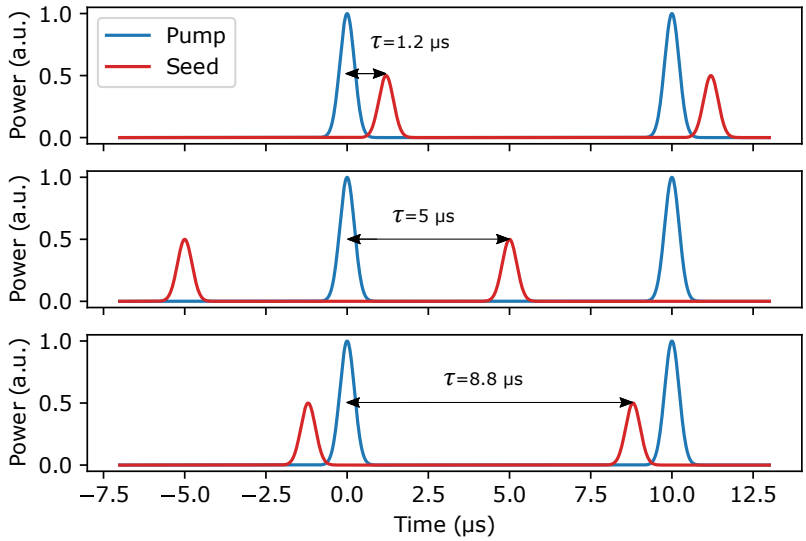

Figure 4.6: Illustration of a 1950 nm pump and 2107 nm seed pulse train with a period of 10 µs, shown for different values of the delay τ.

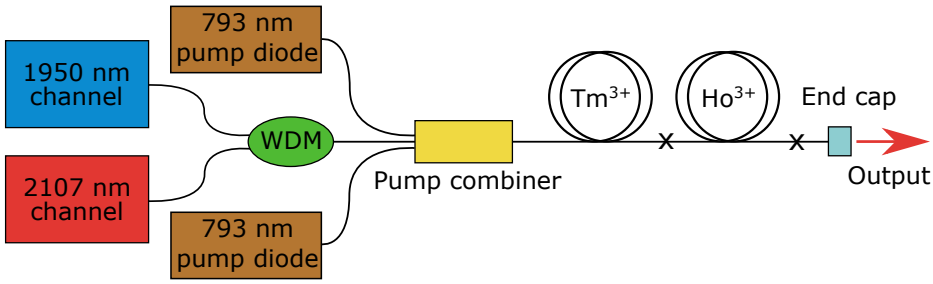

Figure 4.7: Illustration of the holmium-doped fiber amplifier.

setup employed here allows for core pumping of the following holmium-doped fiber.

The 2107 nm seed of the holmium fiber amplifier is delivered by the 2107 nm channel depicted in Figure 4.7. This channel is a two-stage holmium-doped fiber MOPA developed in-house, and corresponds to the two first amplification stages described in Reference [2]. This channel outputs 20 ns pulses, also at 100 kHz repetition rate. The outputs from the 1950 nm and 2107 nm channels are combined into one single fiber by a *wavelength division multiplexer* (WDM).

Pump and Signal Input Power to the Ho-doped Fiber

It is desired to investigate the light amplification occurring in the holmium-doped fiber. This require knowledge of the power of the pump and signal pulses at the input of the holmium-doped fiber, i.e the output of the thulium-doped fiber in the tandem-amplifier. As described in Section 2.4.3, both the 1950 nm and 2107 nm pulses will expericence gain in the thulium-doped fiber. The 1950 nm pulses will obviously experience the most gain in this fiber, but the gain experienced by the 2107 nm pulses is significant. To investigate the impact of PIQ in the following holmium-doped fiber, it is desired that the input powers of the 1950 nm and 2107 nm pulses remain constant when the delay between them is varied. However, the gain that the pulses experiences in the thulium-doped fiber changes with the delay. This is because the degree of excitation in the fiber changes when a pulse propagates through it and extracts gain. For example, if the delay is small such that the 1950 nm pulses propagates through the fiber right before the 2107 nm pulses (see the top plot of Figure 4.6), then the gain is low for the 2107 nm pulses because the 1950 nm pulses have extracted most of the gain. However, if the delay is large such that the 2107 nm pulses arrives right before the 1950 nm pulses (see the bottom plot of Figure 4.6), then the 1950 nm pulses will experience reduced gain while the 2107 nm pulses experiences increased gain (because the 793 nm pump diodes have had a long time to increase the excitation level).

Figure 4.8 shows a measurement of how the average power of the 1950 nm pulses and the 2107 nm pulses output from the thulium-doped fiber changed for delays between 22 ns and 9978 ns. These measurements were done using the measurement setup that is described later in Section 4.3.2. The 1950 nm power is reduced slightly from around 10.12 W to 9.98 W when the delay increases. This is a small $\sim 1\%$ decrease, but if not accounted for will carry over to an uncertainty in the degree of excitation produced in the following holmium-doped fiber. A much larger difference can be seen for the 2107 nm pulses for which the average power increases from about 680 mW to 800 mW. This is a large $\sim 18\%$ increase which will make the resulting measurements of the holmium-doped fiber output incomparable for different delays. The small "jump" seen at 6 µs is attributed to the order that the measurements were done. The measurements were started for a delay of 6000 ns, then incrementally increased up to 9978 ns. From here the delay was set to 22 ns and increased back up to 6000 ns again. Thus, the jump was confirmed to be caused by thermal drift occuring between the first and last measurement.

For the reasons discussed above, the input average power of the 2107 nm pulses had to be compensated for the increased gain at increasing delays. This was done by linearly reducing the power of the 2107 nm pulses input at the thulium-doped fiber. The effects of this compensation are shown in Figure 4.9. As can be seen, when this compensation is made the average power of the 2107 nm pulses only

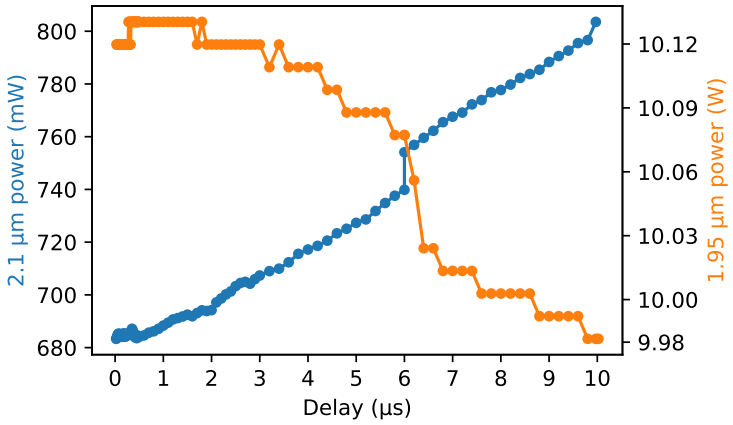

Figure 4.8: The average power of the 2107 nm and 1950 nm pulses output from the thulium-doped fiber when the input powers are constant and only the delay between the pulses are varied.

varies in a range that is ±1% from the average of 690 mW. As a result of the compensation, the change in the average power of the 1950 nm pulses for varying delays becomes less as well. Figure 4.9 shows that when compensated, the average power only falls from 10.12 W to 10.07 W which is a decrease of only ∼ 0.5%.

It should be noted that the exact measured powers vary seemingly random each time this measurement was repeated. A figure showing the variations between five different measurements when the power is compensated is shown in Appendix C. The variations are however small and will not discourage the final results of this experiment. The compensated average powers of the 1950 nm and 2107 nm pulses shown in Figure 4.9 are the average of these five measurements. This power will be assumed to be the input to the following holmium-doped fiber.

The holmium-doped fiber studied in this experiment is IXF-HDF-PM-20-250 manufactured by iXblue photonics. This fiber has a core diameter of 20 µm, a cladding diameter of 250 µm and a NA of 0.08. The length of the fiber was 210 cm. The output light from this fiber consists of residual unabsorbed 1950 nm pump power and the amplified 2107 nm pulses. Because of the high power that is output from the holmium-doped fiber, it is bonded to an anti-reflection coated fused silica end cap. This is done to suppress feedback and to prevent fiber damage, as the light expands inside the end cap before the glass-air interface.

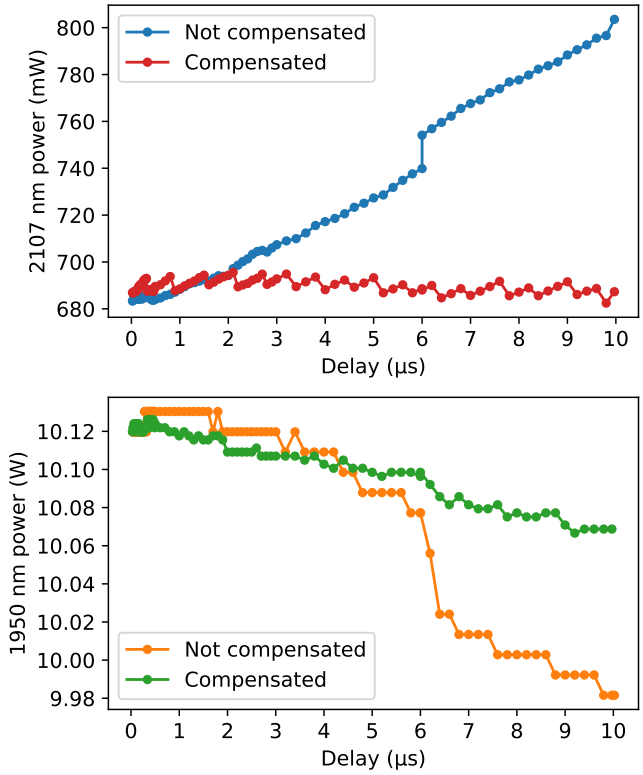

Figure 4.9: (Top) The average power of the 2107 nm pulses exiting the thulium-fiber in Figure 4.7 when the input power is compensated to give a nearly constant average output power, versus when the 2107 nm pulses are not compensation. (Bottom) The average power of the 1950 nm pulses exiting the thulium-fiber in Figure 4.7 when the input 2107 nm power is compensated, versus when it is not compensated.

4.3.2 Measurement Setup

Figure 4.10 shows a schematic of the setup used in this experiment to measure the average power of the 1950 nm and the 2107 nm pulses, as well as the pulse shapes and optical spectra. The output of the end cap was collimated by an anti-reflection coated lens with focal length of 25.5 mm. An uncoated CaF_2 wedge was placed in the path of the collimated beam to create two pick-off beams that allowed for continous monitoring (the angle of the pick-off beams from the main beam is exaggerated, and the beam widths are underexaggerated). These pick-off beams were both focused by lenses with a focal length of 18 mm into optical fibers

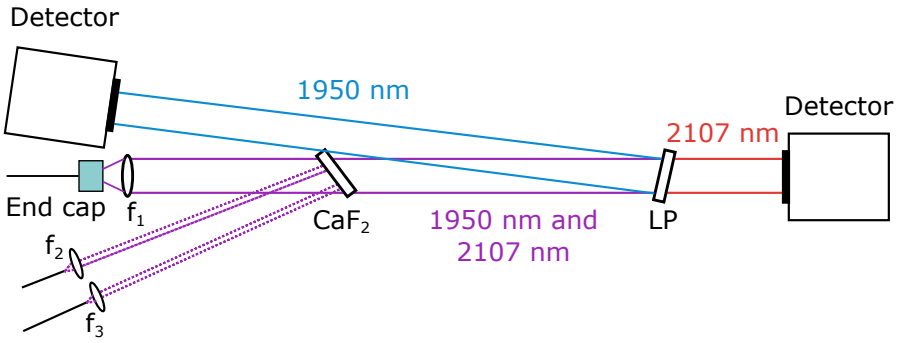

Figure 4.10: A schematic of the setup used to measure the average power output from the thulium- and holmium-doped fibers in the tandem-amplifier in Figure 4.7. f: lenses, LP: long-pass filter with high reflectance at $1900 - 1950\,\text{nm}$.

and were used to measure the optical spectrum and pulse shapes.

The 2107 nm pulses were separated from the 1950 nm pulses by a long pass spectral filter with high reflectance at 1950 nm, and each beam were measured by thermal power detectors.

Chapter 5

Results and Discussion

This chapter presents and discusses the results of the three experiments described in Chapter 4. The fluorescence experiment considered and discussed in Section 5.1, the non-saturable absorption experiment is then described in Section 5.2, and finally the practical experiment of a holmium-doped fiber power amplifier discussed in Section 5.3. In all sections, the experimental findings are compared to results from simulations of equivalent scenarios using the numerical model describe in Chapter 3.

5.1 Lifetime of Doubly-excited Holmium-ion Pairs

As discussed in Section 4.1, the time-course of the measured 1.15 µm fluorescence intensity stemming from the radiative transition $^5I_6 \rightarrow {}^5I_8$ is proportional to the population of $^5I_6$. The time-course of the fluorescence build-up is thus proportional to the energy transfer upconversion process. From this measurement the lifetime of doubly-excited holmium-ion pairs can be determined.

5.1.1 Experimental Results

The measured time-courses of the 1.15 µm fluorescence intensity from the twelve different fibers are shown normalized in Figure 5.1. The signals are averages of 2000 repetitions to increase the signal-to-noise ratio. Figure 5.2 shows the difference between a single shot signal, and when the signal is averaged 2000 times from a measurement of Fiber 10. As can be seen, the signal-to-noise ratio is poor in a single shot measurement. The signal is only barely distinguishable from the noise, however, the signal-to-noise ratio is improved considerably when the signal is averaged. In both figures, a noticable ripple can be seen in the signal occurring close to, but right before, the time is zero. This artifact was confirmed to be

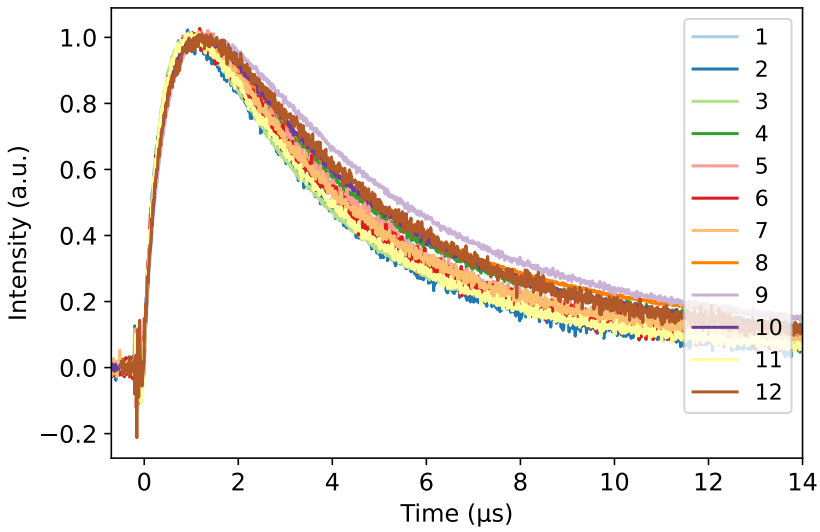

Figure 5.1: Normalized 1.15 µm fluorescence measured from twelve different test fibers after the 30 ns 1950 nm pump pulse.

purely electrical noise from the measurement setup, and not related to actual optical signals.

The build-up of the fluorescence signals from the twelve fibers in Figure 5.1 shows that $^5I_6$ becomes rapidly populated after the holmium-ions in the fiber are pumped to $^5I_7$ by the short 30 ns 1.95 µm pulse at time zero. This shows that the ETU process between ions within a pair occurrs rapidly after the ions become excited. The signal reaches a maximum after ~ 1 µs, signifying that almost all ion-pairs have undergone ETU at this point. In the build-up time from zero up to the maximum, the time course of the twelve signals vary only slightly. This indicates that the lifetime of holmium-ion pairs must be similar for all twelve fibers. After the signals have reached their maxima, the intensity begins to drop as the population of $^5I_6$ decreases. The rate at which the signal intensity decreases is given by the fluorescent lifetime of $^5I_6$. This intensity decrease can be seen to vary notably between the twelve fibers as the signals begin to separate. Notably, the decay rate of the curves in Figure 5.1 reflects the variation in $^5I_7$ lifetime shown for Fibers 1-9 in Table 4.1. The variations in $^5I_6$ and $^5I_7$ lifetimes are attributed to variations of the characteristic phonon energy of the local environment around the holmium-ions.

As can be seen in Figure 5.1, the build-up time and the decrease time of the

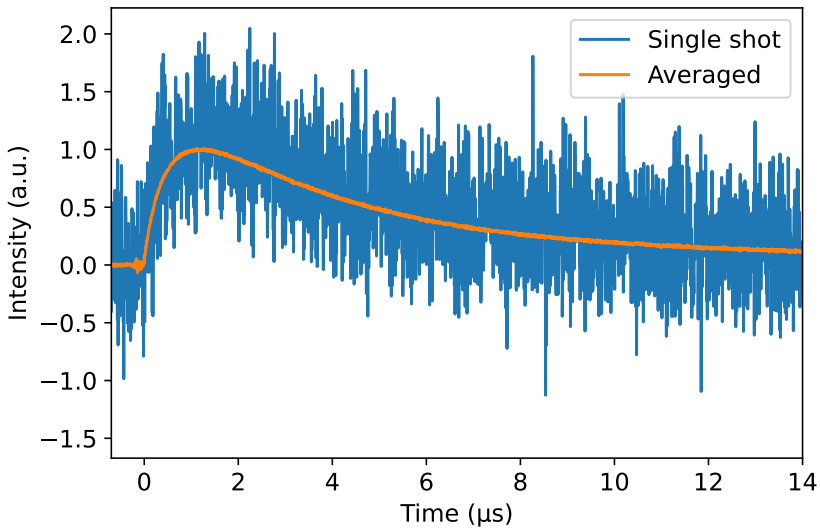

Figure 5.2: Normalized single shot measurement of the 1.15 µm fluorescence intensity from Fiber 10 and a normalized measurement averaged from 2000 repetitions.

fluorescence signal are apparently not that significantly different. Though the build-up time is shorter, it might not be significantly short enough such that it can be assumed that all doubly-excited holmium-ion pairs have upconverted before a significant amount of the already upconverted ions have decayed back down from $^5I_6$. An other way to say this is that it is evidently incorrect to assume that $\tau_{\text{pair}} \ll \tau_{^5I_6}$. This means that neither the doubly excited pair lifetime nor the fluorescent lifetime of $^5I_6$ can be simply taken as the 1/e-crossing points of the curves in Figure 5.1. For reference, this is in contrast to the study of inhomogeneous upconversion in erbium-doped fibers conducted by Myslinski et al. [8, 9], where the lifetime of doubly-excited erbium pairs was measured to be 50 ns and the lifetime of the erbium state $^4I_{11/2}$ that the measured fluorescence signal originated from was in the range 3-7 µs for the tested fibers.

In this work, instead of direct readouts of 1/e-crossings, the lifetimes of doubly-excited pairs and the $^5I_6$ level must be determined by comparing the experimental results of Figure 5.1 to numerical simulations of a holmium-doped fiber, pumped by a 30 ns 1950 nm pulse using the rate equation model described in Chapter 3. These results are discussed in Section 5.1.2.

To verify that the measured fluorescence signals of Figure 5.1 are not obscured by effects such as re-absorption and re-emission, fluorescence measurements were

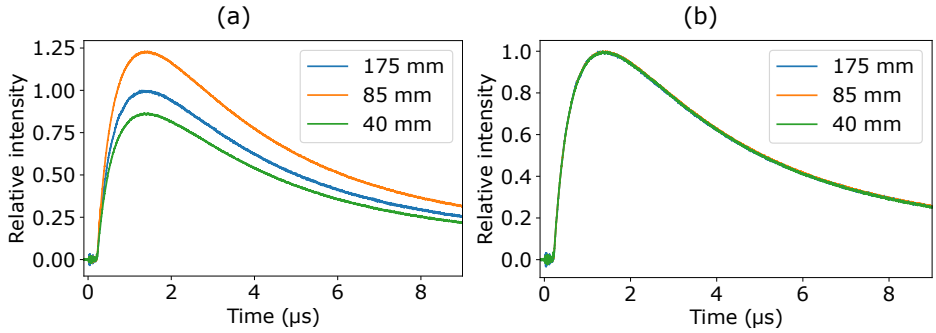

Figure 5.3: (a) Measured fluorescence for three different lengths of Fiber 8. The intensity of the three measurements is relative to the peak intensity of the 175 mm fiber length measurement. (b) The fluoresence measurements from (a), but where all three measurements are normalized.

done on Fiber 8 for three different fiber lengths; 175 mm, 85 mm and 40 mm. Figure 5.3a shows the measured fluorescence intensity for the three fiber lengths relative to the peak intensity of the 175 mm fiber length measurement. The figure shows that the highest intensity is actually achieved with the middle fiber length, and not the longest length. This is attributed to re-absorption of the fluorescence signal, giving a reduced output fluorescence intensity for the longest fiber. The shortest fiber length outputs the weakest signal, which is explained by the fiber being too short for absorbing all the pump light.

Figure 5.3b shows the same fluorescence measurements as Figure 5.3a, after normalization to their respective peak values. The three signals are seen to be virtually indistinguishable. From this measurement it can be concluded that the time course of the fluorescence is independent of fiber length, and hence, re-absorption and re-emission do not affect the measurements in Figure 5.1. Re-absorption in the fibers only affects the intensity of the output fluorescence signals.

It was desired to verify that the measured fluorescence signals of Figure 5.1 do not partly stem from holmium-ions undergoing homogenous ETU, and thus only stems from doubly-excited pairs undergoing inhomogenous ETU. This was done by measuring fluorescence from Fiber 8 after pumping with two different pulse energies (13 and 3.1 µJ). The rate of homogeneous ETU depends on the degree of excitation to $^5I_7$. In the rate equation model presented in Chapter 3, the rate of homogeneous ETU was $W_{11}N_1^2$. It depends quadratically on N_1, thus the homogeneous ETU rate increases with increasing degree of excitation. This is however not true for the upconversion rate (inverse lifetime) of doubly-excited pairs. Pumping the fiber with a lower energy pulse would lead to a lower degree of

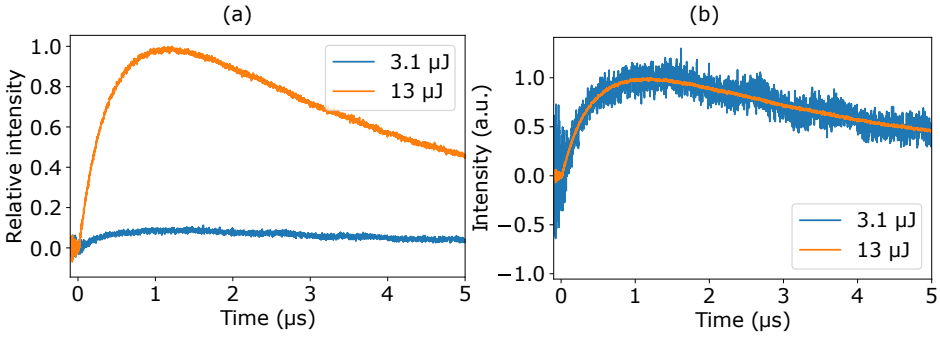

Figure 5.4: (a) Intensity of the measured fluorescence signals from Fiber 8 when pumped by two different pulse energies; 3.1 µJ and 13 µJ. The intensities are relative to the peak of the measurement caused by the 13 µJ pump pulse. (b) The normalized fluorescence signals caused by the 3.1 µJ and 13 µJ pump pulses.

excitation. Because of the lower degree of excitation, it is also expected that the fiber outputs a lower intensity fluorescence signal. However, if the time course of the signal does not change between the two pump pulses, then it can be concluded that the fluorescence stems from upconversion by doubly-excited pairs alone.

Figure 5.4a shows the measured fluorescence signals from Fiber 8 when pumped by a 3.1 µJ pulse and a 13 µJ pulse. As expected, the signal is much weaker when pumped by the 3.1 µJ pulse compared to the 13 µJ pulse. However, when both signals are normalized as shown in Figure 5.4b, the time-course of the fluorescence signals coincide perfectly. From this, it is concluded that the fluorescence signals originate from upconverted doubly-excited pairs and not homogeneous ETU.

5.1.2 Comparison with Simulations

By solving the rate equations from Chapter 3 for a 30 ns 1950 nm square pump pulse, and plotting the temporal variation of the total population of $^5\mathrm{I}_6$, the simulation results can be fitted to the experimental results by varying the doubly-excited pair lifetime and $^5\mathrm{I}_6$ lifetime. Figure 5.5 shows the measured fluorescence from Fiber 1 together with the results of a simulation where the doubly-excited pair lifetime was chosen to be $\tau_{\mathrm{pair}} = 450$ ns and the $^5\mathrm{I}_6$ lifetime was chosen to be $\tau_{^5\mathrm{I}_6} = 3.8$ µs. The results of the simulation matches the experimental measurements well in the time interval shown in the figure (5 µs). In this short time interval, the doubly-excited pair lifetime and the $^5\mathrm{I}_6$ lifetime are the parameters dominating the shape of the simulation results, and other unknown fiber parameters such as the ratio of pairs $2k$ and the homogeneous ETU rate W_{11} have negligible effect. For much longer time intervals, i.e. > 20 µs, these fiber parameters begin to

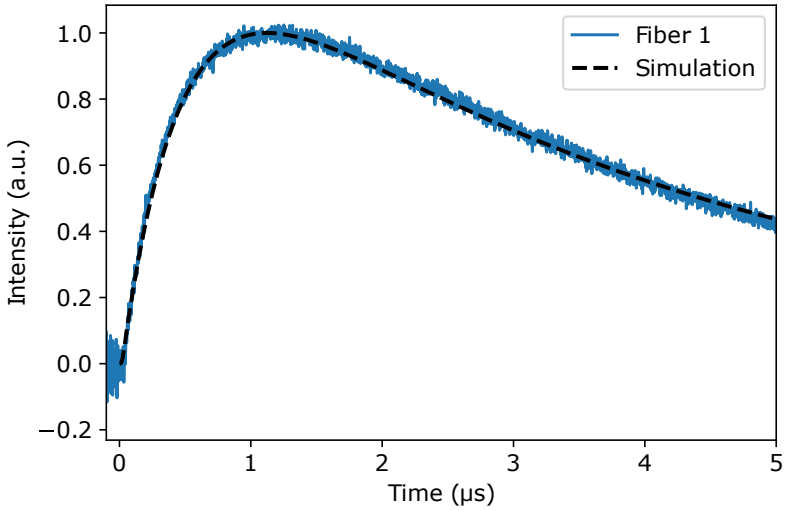

Figure 5.5: Measured 1.15 µm fluorescence from Fiber 1 and the temporal variation of the $^5I_6$ population from a corresponding simulation where the doubly-excited pair lifetime ($\tau_{\text{pair}} = 450\,\text{ns}$) and the $^5I_6$ lifetime ($\tau_{^5I_6} = 3.8\,\mu\text{s}$) were chosen to best fit the experimental measurement.

have a noticable effect. However, their impact can be neglected in the short time interval associated with the doubly-excited pair lifetime. This was confirmed by comparing simulations where these unknown parameters were varied over multiple orders of magnitude, without noteworthy affecting the lifetime values that gave the best fit. Thus, the numerical model is used to fit simulations to the experimental fluorescence measurements from Figure 5.1, to determine the measured doubly-excited pair lifetimes.

The results of the measured doubly-excited pair lifetimes for all twelve fibers, when compared to simulations are shown in Table 5.1, together with the corresponding $^5I_6$ lifetimes that were chosen to best fit the measurements. The doubly-excited pair lifetime for the twelve fibers vary in the range $440 - 520\,\text{ns}$ with most measurements being close to 450 ns. Fiber 9 is the largest outlier, with a somewhat long pair lifetime of 520 ns. This lifetime is 13% above the average pair lifetime of 462 ns. Fiber 6 and Fiber 11 have the shortest measured lifetime of 440 ns, which is 5% below the average. These results substantiate the assumption that inhomogeneous ETU is an isolated process. In contrast to homogeneous ETU, inhomogeneous ETU is not easily affected by the surroundings of the holmium-ion pairs. The results show a narrow span of measured lifetimes even though the fibers have largely varying holmium-doping concentration and doping chemistry.

These findings are analogous to the observations done by Myslinski et al. in

Table 5.1: Summary of the pair lifetimes (τ_{pair}) and $^5I_6$ lifetimes ($\tau_{^5I_6}$) determined from the fluorescence measurements in Figure 5.1.

Fiber #	τ_{pair} [ns]	$\tau_{^5I_6}$ [µs]
1	450	3.8
2	445	2.9
3	450	2.5
4	450	3.1
5	460	3.8
6	440	3.4
7	460	3.1
8	480	2.8
9	520	3.9
10	460	3.8
11	440	3.1
12	490	4.0

their study of ETU whitin clusters/pairs in erbium-doped fibers [8]. However, the measured doubly-excited pair lifetime of holmium (460 ns) is significantly longer than the 50 ns lifetime found for erbium. The two results do however have many qualitative similarities, such as near constant lifetime from fiber to fiber even when the fibers vary greatly in ion-doping concentration and co-doping chemistry.

A difference in degree of resonance for the ETU process between erbium and holmium might be the cause of the large difference in doubly-excited pair lifetime. As previously discussed, the ETU process in holmium is not resonant and require phonon assistance. If the required phonon energy is larger for holmium than for erbium, then this might explain the observed difference in lifetime. Further studies of the accurate position and extent of the energy levels involved in the ETU process would shed further light on this.

It should be expressed that Fiber 9, that had the longest measured doubly-excited pair lifetime (520 ns), was also an outlier in other parameters. The fiber has a high holmium-doping concentration of 5.1×10^{25} ions/m^3 and only a moderate Al/Ho ratio of 55, while exhibiting a very long $^5I_7$ lifetime of 1250 µs [19]. Such a long $^5I_7$ lifetime suggests that the fiber's maximum phonon energy is small compared to fibers with a short $^5I_7$ lifetime, such that a large number of phonons are needed to bridge the gap between $^5I_7$ and the ground state $^5I_8$. It can be speculated that Fiber 9 also has a relatively long pair lifetime from a low phonon energy local environment around the ion-clusters. Thus, the phonon-assisted ETU process in Fiber 9 requires more phonons than for the other investigated fibers. Finally, a different explanation might be that the local environment around the

ion-clusters might increase the inter-ionic distance inside clusters. This would cause electrical multi-pole interactions such as ETU to be less efficient, and would increase the doubly-excited pair lifetime.

5.1.3 Summary

The fluorescence signals was confirmed to originate from doubly-excited pairs undergoing ETU. The lifetime of doubly-excited pairs was measured to be 460 ns varying only −5% to 440 ns and +13% to 520 ns, which was the largest outlying measurement. The measured pair lifetime of holmium is interestingly found to be an order of magnitude larger than that of erbium pairs. One explanation for this might be that the ETU process is less resonant for holmium, and therefore requires more phonon assistance.

5.2 Non-saturable Absorption

The presence of holmium-ion pairs gives rise to non-saturable absorption. As discussed in Chapter 2, the very rapid energy transfer upconversion occurring between two ions in immediate vicinity prevents more than one of the ions in a cluster to be excited during any considerable amount of time. Thus, when considering timescales much longer than the doubly-excited pair lifetime (~ 460 ns as found in Section 5.1), there are always one ion in each pair that can absorb pump light and this leads to non-saturable absorption.

5.2.1 Experimental Results

Measurements of 1950 nm transmission for input powers varying from 120 mW to 5.1 W, were done for two selected fibers out of the twelve available fiber samples specified in Section 4.2. Fiber 1 has a holmium doping concentration of 1.1×10^{25} ions/m^3, which is the lowest concentration among all twelve fibers. The fiber also has the highest Al/Ho ratio (113.2) and is for these reasons expected to be the fiber with the lowest ratio of holmium-ions residing in pairs. The fiber with the highest holmium concentration is Fiber 8 (10×10^{25} ions/m^3) and this fiber also has the lowest Al/Ho ratio (8.6). For these reasons Fiber 8 is expected to have the highest ratio of holmium-ions residing in pairs.

Figure 5.6a shows the 1950 nm transmission of Fiber 8 for the fiber lengths 121 mm, 69 mm and 30 mm. For low input powers, from ~ -10 dBm to ~ 0 dBm, the transmission is approximately flat for the three lengths. This is the so-called small-signal regime of the fiber, where the 1950 nm signal is too weak to significantly change the population distribution of the holmium-ion energy levels. In the range $\sim 10-20$ dBm, the transmission begins to increase as the input pump power becomes large enough to create a significant degree of excitation to $^5I_7$ in

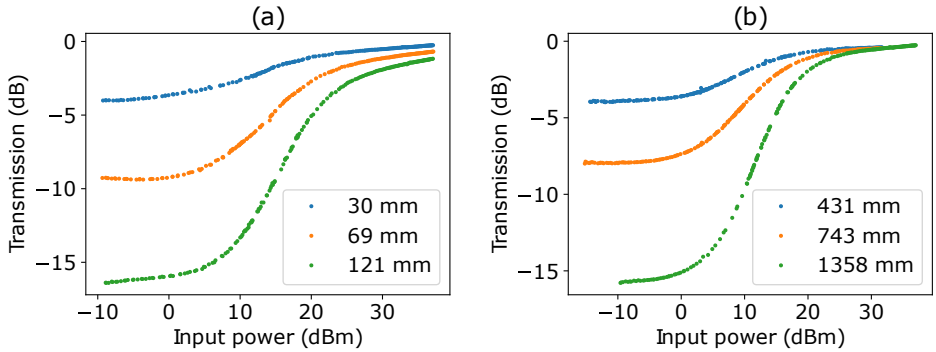

Figure 5.6: Transmission measurements at 1950 nm for (a) Fiber 8 and (b) Fiber 1.

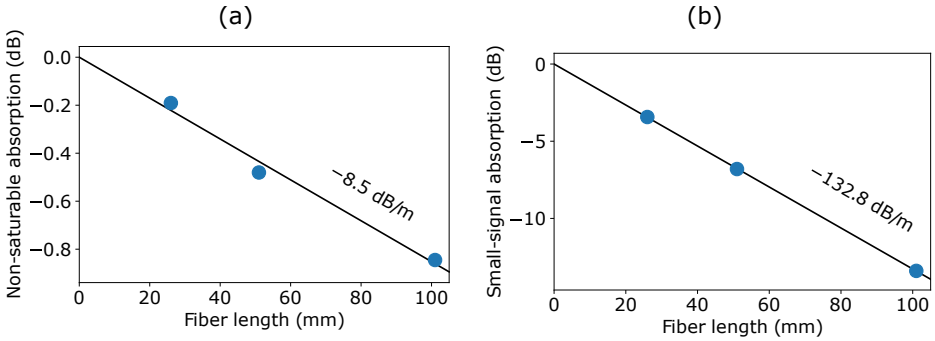

Figure 5.7: (a) A linear regression line fitted to the transmission points of Fiber 8 at high input powers for three fiber lengths. The slope of this line is the non-saturable absorption (α_{ns}). (b) A linear regression line fitted to the transmission points of Fiber 8 at low input powers for three fiber lengths. The slope of this line is the small-signal absorption (α_{ss}).

the fiber. When the degree of excitation increases, so does the transmission as there are fewer ions in $^5\mathrm{I}_8$ that can absorb photons, and more ions in $^5\mathrm{I}_7$ that can undergo stimulated emission. For input powers $> 30\,\mathrm{dBm}$ the transmission begins to flatten once again as the absorption begins to become saturated. However, the transmission is seen to not reach 0 dBm (100%), meaning that the absorption is not completely saturated, i.e. there is a significant amount of non-saturable absorption.

Figure 5.6b shows the 1950 nm transmission of Fiber 1 for the fiber lengths 431 mm, 743 mm and 1358 mm. Much of the same characteristics can be seen for Fiber 1 as with Fiber 8. Fiber 1 also has a small-signal regime where the transmission is flat for low input powers. As the input power becomes signifcantly large, the transmission increases. For high input powers however, Fiber 1 differs qualitatively from Fiber 8. For all three fiber lengths the transmission goes to 0 dBm for high input powers, meaning that the absorption becomes completely saturated. This suggests that Fiber 1 has a very low content of ions residing in pairs, which is as expected. In fact, the fiber has such a small amount of pairs that the non-saturatable absorption is unresolvable with this experimental setup.

The non-saturable absorption per unit length of the fibers can be deduced by fitting a linear reggresion line to the transmission measured at the highest input powers for the three fiber lengths. This is shown for Fiber 8 in Figure 5.7a. The figure shows the three points from Figure 5.6a at the highest input power. The slope of the line fitted to the three points gives the non-saturable absorption per unit length. This shows that Fiber 8 has a non-saturable absorption per unit length of $\alpha_{\mathrm{ns}} = 8.5\,\mathrm{dB/m}$. For completeness, the small-signal absorption per unit

length of the fiber is also determined. This is calculated in the same way, except the points used are taken at the lowest input power. This is shown in Figure 5.7b, where the slope of the fitted line shows that Fiber 8 has a small-signal absorption of $\alpha_{\mathrm{ss}} = 133\,\mathrm{dB/m}$. This is close to the value $\alpha_{\mathrm{dB}} = 128\,\mathrm{dB/m}$, reported by the fiber manufacturer (see Table 4.2).

As previously discussed, the non-saturable absorption of Fiber 1 is below the resolution of this measurement setup. The non-saturable absorption per unit length for Fiber 1 can therefore not be calculated.

The fraction of holmium-ions residing in pairs can be estimated from the measured non-saturable absorption by [9]

$$2k = \frac{\alpha_{\mathrm{ns}}}{\alpha_{\mathrm{ss}}} \times \frac{2\sigma_{\mathrm{a}} + \sigma_{\mathrm{e}}}{\sigma_{\mathrm{a}}}. \tag{5.1}$$

Here, α_{ns} and α_{ss} are the non-saturable absorption per unit length and small-signal absorption per unit length. σ_{a} and σ_{e} are the absorption- and emission cross sections. By using the cross section values from Table 4.1, and the measured values α_{ns} and α_{ss} for Fiber 8, the rato of ions residing in pairs is found to be $2k = 18\%$. This estimation shows that a significant amount of holmium ions in the fiber are residing in pairs.

5.2.2 Comparison with Simulations

By solving the rate equations from Chapter 3, the transmission through the fibers can be simulated for different input powers and fiber lengths. Figure 5.8 shows the same experimentally measured transmissions of Fiber 8 as was shown in Figure 5.6a together with results from a simulation of the same scenario. The fiber parameters used for this simulation are the same as summarized in Table 3.1, except for the following parameters: $\sigma_{01}^{\mathrm{p}} = 4.6 \times 10^{-25}\,\mathrm{m}^2$, $\sigma_{10}^{\mathrm{p}} = 4.4 \times 10^{-25}\,\mathrm{m}^2$, $W_{11} = 4.5 \times 10^{-23}\,\mathrm{m^3 s^{-1}}$ and $2k = 30\%$. Additionally, the holmium-doping concentration was adjusted to $N_{\mathrm{Ho}} = 7.8 \times 10^{25}\mathrm{ions/m^3}$. The doubly-excited pair lifetime and the $^5\mathrm{I}_6$ fluorescent lifetime are as found in the fluorescence experiment described in Section 5.1.2, and summarized in Table 5.1.

Figure 5.8 shows that the fiber parameters can be adjusted such that the simulation fits very well with the experimental measurements. The simulations and experimental data show overall good agreement over the entire input power range. Additionally, because the numerical model is not limited in the available 1950 nm power, the simulation is continued beyond the $\sim 5\,\mathrm{W}$ experimental limit to 100 W. Interestingly, the simulations show that the transmission does not simply continue to flatten, as was assumed in Section 5.2.1 when calculating the non-saturable absorption α_{ns} and from that, the ratio of ions residing in pairs. It appears that the transmission begins to flatten, and then starts to increase again before it finally flattens out at 100% transmission. The first plateau is attributed

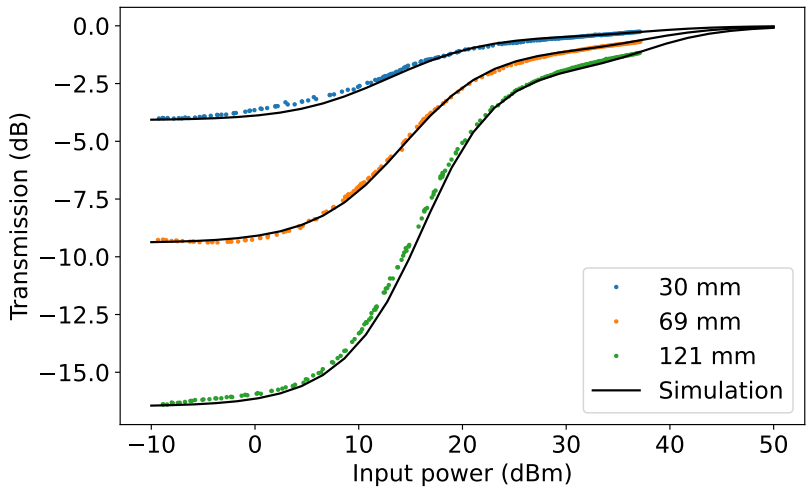

Figure 5.8: Experimentally measured transmission through Fiber 8 for different input pump powers, compared to a simulation of the same scenario.

to saturation of absorption of single ions in the fiber, whereas the second plateau is attributed to saturation of the absorption of paired ions.

Figure 5.9 illustrates this point by plotting the total populations in the fiber of the states N_1, from Figure 3.1, and N_5, from Figure 3.2. In Figure 5.9, N_1 is the total population of single ions in the fiber that are excited to $^5I_7$. N_5 is the total population of doubly-excited pairs in the fiber. The figure shows that the single ions become saturated for input powers larger than $\sim 30\,\text{dBm}$. The ion-pairs become saturated when the input power exceeds $\sim 50\,\text{dBm}$. These observations correspond well with those of Figure 5.8.

These results reveal that the "non-saturable absorption" occurring in holmium-doped fibers actually become saturated to a noticeable degree. Equation (5.1) relies on the assumption that the holmium-pairs do not become excited to a significant degree. However, as Figure 5.9 shows, the input powers that are needed for the single ions to become fully saturated overlaps with the input powers that produce a significant excitation of doubly-excited pairs. This suggests that Equation (5.1) may not be able to estimate the pair-content with high accuracy for holmium-doped fibers. The equation likely underestimates the amount of pairs in the fiber, because the amount of non-saturable absorption is seemingly reduced by the partial saturation of the pair absorption. This is also reflected by the much higher ratio of pairs needed in the simulation ($2k = 30\%$) to give good agreement with the measurements, compared to the estimated value ($2k = 18\%$)

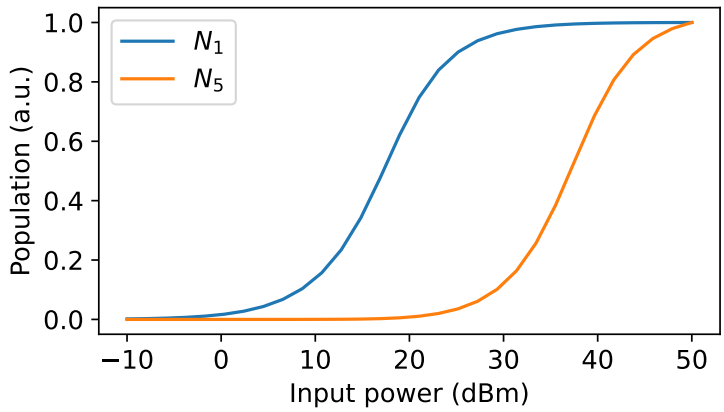

Figure 5.9: Simulated population of single ions excited to $^5I_7$, N_1, and population of doubly-excited pairs, N_5, plotted for a range of input 1950 nm powers. For improved readability, the populations are here shown normalized such that a population of 1 represents the population reached when the absorption is saturated.

from Equation (5.1).

For reference, because the doubly-excited pair lifetime of erbium is almost an order of magnitude lower (50 ns) than for holmium, it is expected that Equation (5.1) gives a better estimation in erbium-doped fibers, as was done by Myslinski et al. [9]. The simplicity of measuring nonsaturable absorption and using Equation (5.1) has made this the standard method used for decades to determine the pair-content in erbium-doped fibers. When considering holmium doped fibers, the findings presented here reveal that the significantly longer holmium-pair lifetime break the central assumptions upon which this method is based. Specifically, the reported pair content will generally be underestimated using this approach, and I expect this to be the case in the many recent publications that have studied PIQ in holmium-doped fibers[5, 6, 7, 2]. Alternative measurement strategies such as comparison of transmission measurements with full rate equation simulations should be used for accurate determination of holmium pair content – despite the reduced convenience of a more cumbersome approach.

5.2.3 Summary

Experimental measurements of the transmission of 1950 nm light were made for different lenghts of two holmium-doped fibers with an order of magnitude difference in doping concentration. From these measurements, the amount of

non-saturable absorption in one fiber was found to be $\alpha_{\mathrm{ns}} = 8.5\,\mathrm{dB/m}$, and less than the resolution of the measurement setup for the other fiber. The results were compared to numerical simulations. The simulations revealed that the holmium-ion pairs do become noticably saturated, at a higher input power than the single ions. It was found that the in input power needed to saturate the pairs overlap to a significant degree with the input powers that saturate the single ions. This result suggests that Equation (5.1) that is conventionally used to determine pair-content in erbium fibers may significantly underestimate the pair content when applied for holmium-fibers.

5.3 Impact of PIQ on a Nanosecond-pulsed Fiber Amplifier

This experiment aims at investigating how the dynamic aspects of pair induced quenching will affect a nanosecond-pulsed holmium-doped fiber amplifier in practice. As described in Section 4.3, a high power holmium-doped fiber amplifier is pumped by pulses at a wavelength of 1950 nm with 20 ns duration, and the gain created by these pulses are extracted by 20 ns long pulses at 2107 nm. The repetition rate of both the seed and pump pulses is 100 kHz (i.e. a period of 10 µs). The impact of PIQ on the efficiency of the amplifier is studied when varying the delay between the pump and seed pulses.

5.3.1 Experimental Results

The holmium-doped amplifier outputs an average power of 5.4 W at 2107 nm for the situation where the seed pulses arrived just after the pump pulses. This corresponded to 22 ns delay between the seed and pump pulses. The pulses have an energy of 54 µJ inferred from the 100 kHz repetition rate. Figure 5.10 shows the pulse shape and optical spectrum of the output. The pulses have a FWHM width of 17.7 ns and a FWHM spectral width of less than the 0.1 nm resolution of the optical spectrum analyzer. The pulses have a near square shape, a very narrow spectral width, and less ASE than it was possible to detect with the measurement setup. The two side loabes located symmetrically on each side of the main 2107 nm peak extending $\pm \sim 4$ nm in Figure 5.10b, are attributed to the nonlinear optical effect four-wave mixing [12]. From numerical integration of the pulse shape scaled to give the correct pulse energy, a peak power of ~ 3.2 kW was found.

The length of the holmium-doped fiber was 210 cm and has not been optimized for maximum output power. The unabsorbed 1950 nm pump output from the holmium-doped fiber was less than 0.01 W, which is the lowest resolvable power in the measurement setup. Thus, the fiber length is longer than optimal, and it is expected that a significant amount of the 2107 nm power was re-absorbed in the fiber. The optimal fiber length could have been determined by the so-called "cut-back" method, but this was not done in this work as it was not necessary for the investigation of PIQ effects.

Figure 5.11 shows the resulting laser efficiency when the delay of the seed pulses compared to the pump pulses was varied from 22 ns to 9978 ns. As can be seen, the laser efficiency decreases from 47% down to 39%, depending on the delay. The efficiency is the highest when the delay is the smallest, and generally decreases with increasing delay. At the lowest efficiency, the amplifier outputs 4.6 W of average 2107 nm power. The efficiency decreases at the highest rate when the delays are low, resembling the "build-up" of the $^5I_6$ fluorescence that

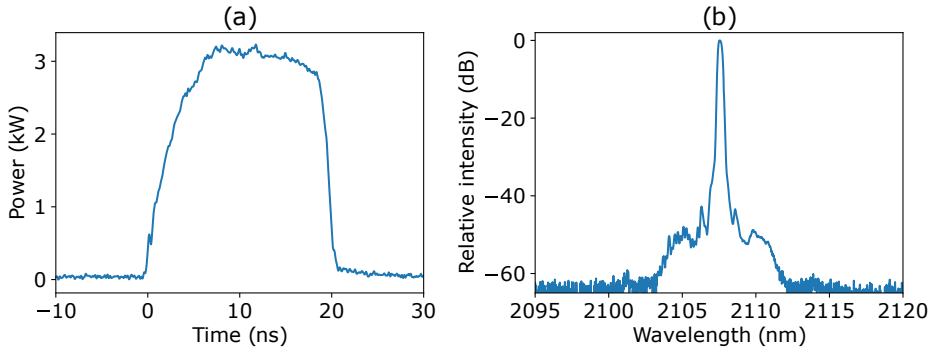

Figure 5.10: The pulse shape (a) and optical spectrum (b) of the 2107 nm pulse after amplification in the holmium-doped fiber amplifier. The optcal spectrum in (b) was measured with a resolution of 0.1 nm.

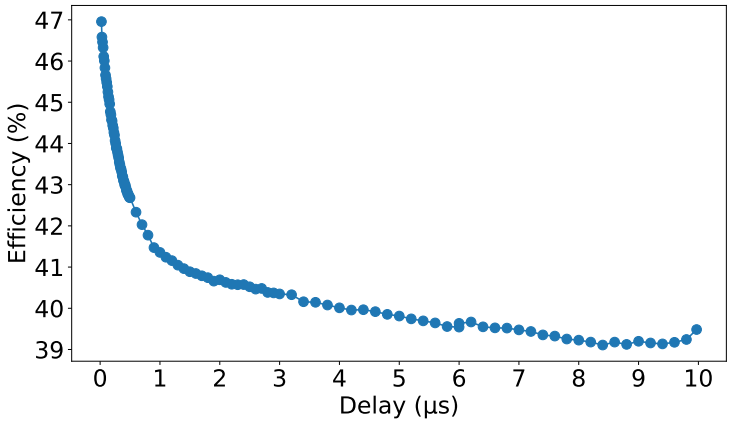

Figure 5.11: Efficiency of a holmium-doped fiber amplifier for different delays between the 1950 nm pump pulses and the 2107 nm seed pulses.

was shown in Figure 5.1. This initially rapid decrese in efficiency can thus be attributed to PIQ occuring in the time between the pump pulses have excited ions to $^5I_7$ and the seed pulses have extracted the gain.

The small "jump" evident at the delay of 6 µs is attributed to the manner the experiment was performed. As described in Section 4.3, the measurements were started at a delay of 6000 ns, then incrementally increased up to 9978 ns. From there, the delay was set to 22 ns and increased incrementally up to 6000 ns again.

The apparent jump was confirmed to be caused by thermal drift occuring in the time between the first and last measurement, and does not represent a real effect.

For delays $> 1\,\mu s$, the efficiency decreases at a rate that is small compared to the PIQ-related decrease at shorter delays, but large compared to the inverse lifetime of the upper laser level $^5I_7$, which has a lifetime of $\sim 1\,ms$. From this lifetime, the population of ions in $^5I_7$ is only expected to decrease by $\sim 1\%$ during the period of $10\,\mu s$. The decreasing efficiency for delays larger than $1\,\mu s$ can thus not be explained by "normal" $^5I_7$ decay. The decrease can neither be explained by PIQ as all holmium-ions pairs are expected to have undergone energy transfer upconversion at this point (pair lifetime was found to be 460 ns in Section 5.1). A high homogeneous ETU rate might be able to explain this observed efficiency reduction, together with other potential effects that will be further discussed in Section 5.3.2.

The efficiency in Figure 5.11 is lower than what it would have been had the fiber length been optimized to achieve maximum output power. Nevertheless, the efficiencies achieved here (even at long delays) are much higher than the reported efficiency of 16% by Holmen et al. [2] for the same holmium-doped fiber used here, but where CW 1950 nm pumping was utilized. However, the low 16% efficiency was found when operating at a repetition rate of 10 kHz and it is expected that the efficiency would be higher at a repetition rate of 100 kHz. The efficiency found in this work can thus not be directly compared to the results by Holmen et al.

Figure 5.11 show that by timing the seed pulses such that it comes immediately after the pump pulses can increase the optical conversion efficiency by $\sim 21\%$ (from 39% to 47%). However, it seems to be much more important simply to implement pulsed pumping instead of CW pumping, than the specific timing of the delay. This will be further discussed in Section 5.3.2.

5.3.2 Comparison with Simulations

Simulations of an equivalent holmium-doped amplifier scenario by solving the rate equations from Chapter 3 were done to compare with the experimental results. Figure 5.12 shows the experimental measurements from Figure 5.11 together with the result of the numerical simulation. In the simulation, a doubly-excited pair lifetime of $\tau_{pair} = 460\,ns$ was chosen. This is the pair lifetime found experimentally in Section 5.1. A $^5I_6$ lifetime of $1.4\,\mu s$ [23], and a large homogeneous ETU rate of $W_{11} = 10 \times 10^{-23}\,m^3s^{-1}$ was chosen. Lastly, the pair content was chosen to be $2k = 23\%$, only slightly larger than the estimate of 21% found for this specific holmium-fiber in Reference [2]. All other simulation parameters were as summarized in Table 3.1.

Figure 5.12 shows that the model has good agreement with the experimental measurements for the first microsecond, where the PIQ process dominates the population redistribution between states. A simple scaled up exponential decay is

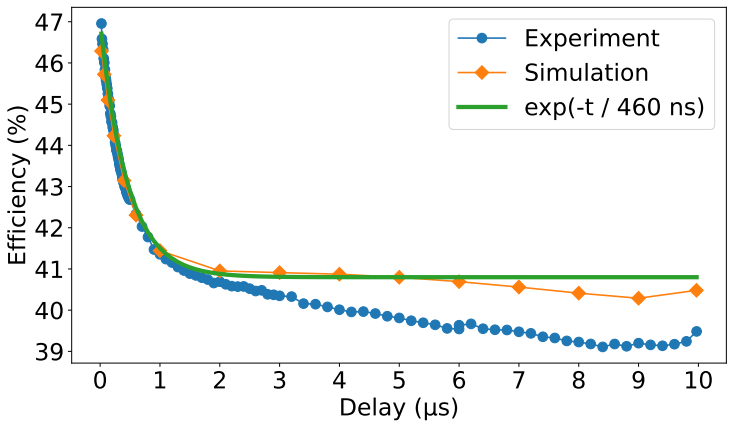

Figure 5.12: Efficiency of a holmium-doped fiber amplifier for different delays between the 1950 nm pump pulses and 2107 nm seed pulses. Results from a simulation of an equivalent scenario is plotted for comparison with the experimental measurements. Additionally, a simple scaled up exponential decay with a time constant of 460 ns is shown.

shown in the figure to illustrate how both the experimental measurements and simulation data follow a decay that is dominated by PIQ for the first microsecond of delays. However, for longer delays than ~ 1 µs, the simulations differ significantly from the experiments. The simulation data flattens almost completely for delays between 2 µs and 5 µs. In this range of delays, the experimental measurements decreases significantly. This decrease continues to a little over 8 µs. For delays between 5 µs and 8 µs, the simulated efficiency seems to decrease at a similar rate to the experimental measurements. In the numerical model, this decrease is attributed to homogeneous ETU of single ions. The reason for why the efficiency is almost flat for the delay range 2-5 µs is attributed to the fact that one of the ions in a pair that undergoes ETU becomes excited to $^5I_6$, and will decay back down to $^5I_7$ at a rate decided by the $^5I_6$ fluorescence lifetime (1.4 µs in the simulation). The upconverted ions decaying back down and the homogeneous ETU process counteracts each other, thus providing a plateau in Figure 5.12.

The reason why this plateau does not emerge in the experimental data is likely due to one or several energy transfer mechanisms that are not accounted for by the numerical rate equations of the model described in Chapter 3. For instance, energy migration can transport excitation from ion to ion until it reaches an ion-pair, which then undergoes the rapid ETU process. This would transfer energy from single ions to pairs, essentially re-creating doubly-excited ion-pairs at

a later time that is determined by an unkown energy migration rate. This effect is neglected in the numerical rate equations.

Additionally, larger clusters of holmium-ions could explain the observed efficiency decrease. The numerical model assumes that all ion-clusters only contain two holmium-ions. It is possible that many of the ion-clusters contain more ions than this. The rate of inhomogeneous ETU between two excited ions in a larger cluster is expected to be the same as the doubly-excited pair lifetime (460 ns), because the ions could still be approximated as being in immediate vicinity. However, a larger ion-cluster would mean that the ETU process could occur multiple times over an extended period of time. Say a cluster contains three holmium-ions, all of which become excited by a pump pulse. Two of the ions would interact with each other rapidly at the rate of the inverse pair lifetime. Thus, the third ion would stay excited until the upconverted ion decays back to $^5I_7$ from $^5I_6$, essentially creating a doubly-excited pair. Similar to the case of energy migration, this would mean that doubly-excited ion-pairs would be produced at a time after all ion-pairs have undergone ETU in the numerical rate equations.

The model assumption that single ions and ion-pairs can not interact with each other might also explain the observed difference. In reality, an ion-pair that only has one of its ions excited to $^5I_7$ acts equivalently to a single ion. Thus, such singly-excited pairs can interact with other single ions through homogeneous ETU. This effect is not accounted for by the numerical model, but it is expected to lead to a slighly higher decay, as the singly-excited ion-pairs take part in the homogeneous ETU quenching of $^5I_7$ as well. These three effects could explain the observed discrepancy in the simulation seen for delays beyond $\sim 1\,\mu s$.

Incorporating the effect of energy migration into the numerical model would be challenging, as its transition rate is unknown and inherently difficult to measure. Incorporating larger clusters such as a cluster of three or four holmium-ions would be relatively straightforward, following the same procedure as for an ion-pair. With the now known doubly excited pair-lifetime, this could be used for the upconversion rate of larger clusters as well. However, incorporating larger clusters would drastically increase the complexity of the model, as many more states of the larger clusters would need to be accounted for and this would create many more rate equations that would increase the computational power needed to solve the equations. Additionally, it would become increasingly difficult to make conclusive comparisons between simulations and experiments as the number of phenomenological parameters and energy transfer processes accounted for by the numerical model grow. Incorporating the effects of singly-excited pairs interacting with single ions would not increase the number of rate equations, only give an additional term to a few of the equations. This effect should thus be relatively simple to incorporate.

It can be seen in Figure 5.12 that the efficiency of both the experimental

measurements and the numerical simulations slightly increase when going from a delay of 9000 ns to 9978 ns. Although the effect is weak, it was confirmed to be real through numerous repeated measurements. It is speculated that it is caused by a favorable excitation distribution between single ions and pairs. When the delay becomes this long, the 2107 nm pulses comes shortly before the 1950 nm pump pulses, and importantly within the doubly-excited pair lifetime. The seed pulse could excite some holmium-pairs, such that these pairs are unable to absorb photons from the pump pulse. Thus, more of the pump pulse is "used" to excite single ions instead. It is possible that this would create a small increase in total degree of excitation to $^5I_7$, thus giving a higher efficiency. This effect was however not investigated any further.

A holmium-doped fiber amplifier utilizing CW pumping was simulated as well to compare with the simulation of pulsed pumping. The simulated CW pump has a power of 10.1 W, which corresponds to the average power of 20 ns, 100 kHz pump pulses. This simulation resulted in an optical convertion efficiency of 33%. This is significantly lower than both the simulation with pulsed pumping and the experimental measurements, that showed an efficiency ranging from 39% to 47% depending on the delay. Without PIQ, one would intuitively expect that a CW pump would produce an efficiency that would lie somewhere inbetween the minimum and maximum efficiency achieved by pulsed pumping, because the pump power is delivered continously over the period. However, the simulations show that this efficiency is much lower, even for the longest delays. The reason that the efficiency is much lower for CW pumping, even compared to pulsed pumping with a long delay (i.e. $\sim 10\,\mu s$) can be explained by multiple ETU processes occuring for a pair when pumped by CW light. When pumped by a short pulse (i.e. 20 ns), it is unlikely that the same ion-pair becomes doubly-excited, undergoes ETU and again becomes doubly-excited during the width of the pump pulse. However, when the amplifier is pumped continously, an ion-pair is likely to become doubly-excited by absorption of pump light multiple times during a period. Thus, a lot of pump power is "wasted" on absorption that will not be available for extraction by the seed pulses. It is important to note that utilizing pulsed pumping instead of CW pumping does come at a cost of increased complexity of the laser source.

In essence, these results reveal that the power conversion efficiency of nanosecond-pulsed holmium-doped fiber amplifiers can be improved considerably by using a pulsed pump source instead of CW pumping, since this will limit the PIQ process to occur at most one time per pair per pulse.

5.3.3 Summary

A holmium-doped fiber amplifier implemented with pulsed 1950 nm pumping has been developed and used to investigate the dynamic effects of PIQ in high power nanosecond-pulsed holmium-doped fiber amplifers. The amplifier can output

5.4 W average 2107 nm power for 17.7 ns near square pulses at 100 kHz repetition rate. It was found that the optical conversion efficiency depends on the delay between the 1950 nm pulses and the 2107 nm pulses. The efficiency varied from 47% to 39%, generally decreasing with longer delays. For delays below 1 µs, wherein the PIQ process is expected to dominated the quenching of the gain, the simulations and experimental measurements showed good agreement. However, for longer delays a discrepancy in the numerical model became apparent. It is suggested that this discrepancy is caused by energy transfer mechanisms not accounted for in the numerical model of Chapter 3, such as energy migration and larger cluster sizes. Importantly, it was found that implementing pulsed pumping instead of the most commonly used CW pumping is a powerful method for mitigating gain reduction caused by PIQ. Implementing pulsed pumping over CW pumping was shown with simulations to increase the optical conversion efficiency by more than 23% percent.

Chapter 6

Conclusion

The goal of this work has been to study pair induced quenching in holmium-doped optical fibers, with particular emphasis on gaining knowledge on dynamical aspects of the process, and its practical impact on nanosecond-pulsed fiber amplifiers.

Numerical Rate Equation Model

A numerical rate equation model was developed that incorporates the effects of holmium-ion pairs. This was done by separating the holmium-ions into two classes; single ions and ion-pairs. The two classes have their own set of energy states and related rate equations. The ion-pairs can rapidly undergo inhomogeneous energy transfer upconversion with a rate that is decided by the doubly-excited pair lifetime. In essence, the numerical model can be considered as an extension to several simpler models reported in literature, where the PIQ process is assumed to occur instantaneously. The rate equation model has been used and evaluated extensively throughout this work, by comparing experimental results with simulations of equivalent scenarios. Overall, the numerical model has offered good agreement between simulations and experiments, and notably, it has been successful in capturing key phenomenological aspects of PIQ that strongly affect laser behaviour on timescales relevant for nanosecond-pulsed fiber amplifiers. The model is therefore expected to become a valuable tool during development of next-generation pulsed holmium-doped fiber amplifiers, by allowing optimization and evaluation of various PIQ mitigation strategies at the computer design stage.

Spectroscopic Measurements

Spectroscopic measurements of holmium-doped fibers were done to study important propterties of PIQ. Time-resolved fluorescence measurements were done

for twelve different fiber samples to measure the doubly-excited pair lifetime of holmium-ion pairs. An average doubly-excited pair lifetime of 460 ns was measured, with variations of only a few percent observed for all twelve fibers samples. This lifetime was for reference compared to the lifetime of doubly-excited erbium-pairs, which has been reported in literature to be an order of magnitude lower ($\sim$ 50 ns). This somewhat surprisingly long holmium-pair lifetime has several important implications, such as the interpretation of non-saturable absorption measurements that is mentioned below. The fluorescence measurements furthermore revealed that holmium-doped fibers, even those produced by leading commercial manufacturers contain a considerable amount of clusters.

Measurements of non-saturable absorption of holmium-doped fibers were done in order to estimate the amount of pairs in a fiber sample that was expected to have a high pair content. With this method it was estimated that the fiber had 18% of its holmium-ions residing in pairs. This method has been used for decades to determine the pair-content in erbium-doped fibers. However, in the case of holmium, the results from numerical simulations revealed that the central assumptions that this method is based upon break, because of the significantly longer holmium-pair lifetime. The method of measuring non-saturable absorption to determine the pair-content in holmium-doped fibers likely provides a significant underestimation. The numerical simulations suggest the pair-content of the fiber sample studied in this work to be 30%, much higher compared to the estimate of 18% when following the conventional approach. It is concluded that the standard method does not give accurate estimates of pair-content, and that more complex numerical simulations are required for accurately determining the pair content in holmium-doped optical fibers.

PIQ in a High Power Holmium-doped Fiber Amplifier

The practical impact of PIQ in a high power holmium-doped fiber amplifier was investigated both experimentally and numerically. The fiber amplifier used 20 ns pump pulses with wavelength of 1950 nm and signal pulses with wavelength of 2107 nm, at 100 kHz repetition rate. This was done to investigate how the optical conversion efficiency depended on the delay between the seed and pump pulses. The amplifier delivered 5.4 W average power for the shortest delay, which corresponded to an efficiency of 47%. For longer delays, the efficiency was generally reduced, being only 39% for the longest delay. Importantly, it was found that the efficiency decreased rapidly on a timespan that corresponds to the time-course of the energy transfer upconversion process within a holmium-pair (460 ns). The numerical simulations were in good agreement with the experimental measurements in this short timespan.

However, the simulations and experiment did not agree well for delays longer than $\sim$ 1 µs. The origin of the observed discrepancy have been discussed, where

potential contributors that have not been accounted for in the numerical model are energy migration, more complex behaviour of homogeneous ETU, and the potential presence of holmium-clusters larger than two ions (i.e. a pair). All of these effects might individually, or combined, explain the experimental effects that the numerical model is unable to reproduce.

Additionally, a simulation was done where the holmium-doped fiber amplifier was pumped continously with the same average power as the 20 ns pulses at 100 kHz repetition rate. This simulation found a low 33% conversion efficiency. This result showed that implementing pulsed pumping greatly improved the efficiency of the nanosecond-pulsed holmium-doped fiber amplifier, although at the cost of a significantly more complex laser system.

The combined results of this work have improved the short-timescale understanding of pair induced quenching occurring in holmium-doped optical fibers. Notably, the lifetime of doubly-excited holmium-ion pairs measured in this project has, to the best of my knowledge, not been previously reported in published literature, despite the fact that this specific parameter appears to be essential for correctly interpreting the manifestations of PIQ on sub-microsecond timescales. The practical significance of this pair lifetime has been demonstrated through various independent experiments and numerical simulations in this work – among them a nanosecond-pulsed fiber amplifier that showed a greatly improved efficiency by pumping it with pulses significance shorter than the measured pair lifetime.

6.1 Suggestions for Future Work

To build upon this thesis, multiple different experiments and numerical investigations can be done. Listed below are only what I consider to be the most interesting and important future investigations:

- Experiment of CW pumping in addition to pulsed pumping, for the same seed pulses and repetition rate should be done to allow for direct experimental comparison of the efficiency between CW and pulsed pumping for the holmium fiber amplifier discussed in Section 5.3.

- Incorporation of additional effects into the numerical model, such as adding larger ion clusters and allowing singly-excited clusters to undergo homogeneous ETU with excited single ions.

- Precise measurements of the energy level manifolds in holmium and erbium, to allow for direct comparison of the degree of resoncance for the ETU processes. Measurements such as these could explain the reason for the order of magnitude longer pair lifetime of holmium compared to erbium.

- During the experiments it was observed that stimulated Raman scattering amplified the 2.1 µm pulses with a higher efficiency in the thulium-doped fiber than what was achieved through "regular" amplification in the holmium-doped fiber. Further investigations should be done to conclude whether or not a Raman amplifier, only utilizing a thulium-doped fiber, is a better approach for achieving high power nanosecond pulses with wavelength of 2.1 µm, compared to using a holmium-doped fiber for the final amplification step.

Appendices

Appendix A

Code Example of Non-saturable Absorption Simulations

The numerical rate equation model described in Chapter 3 has been used extensively throughout the thesis to simulate the impact of pair induced quenching in holmium-doped optical fibers. These equations have in this work been solved in a straightforward manner by alternatingly evolving the Equations (3.5)-(3.14) for one temporal step dt, before propagating the optical power of the involved pump and signal beams one spatial step, dz, according to Equations (3.15) and (3.16). This process in then repeated until the end of the simulation is reached.

For reference, the code example shown below corresponds to the code used to simulate the 1950 nm transimission of Fiber 8, which produces the simulation results shown in Figure 5.8. The code is written in the programming language *Python*, and uses the python-package *numba* for so-called *just-in-time* compilation which speeds up the computing time considerably.

```
import numpy as np
import matplotlib.pyplot as plt
from time import time

hc = 1.9865e-25 # Planck's constant times the speed of light [kgm^3/
    s^2]

'''Cross sections'''
sigma01p = 4.6e-25
sigma10p = 4.4e-25
sigma01s = 0.19e-25
sigma10s = 1.25e-25

'''Transition rates'''
tau_pair = 480e-9
tau_10 = 800e-6
```

```
x7to8 = 0.48
x6to8 = 0.828
x6to7 = 0.172
tau_2RD = 11.46e-3
tau_21NR = 4.0e-6
W_pair = 1 / tau_pair
W10 = 1 / tau_10
W20 = 1 / tau_2RD * x6to8
W21 = 1/tau_2RD*x6to7 + 1/tau_21NR
W11 = 4.5e-23

'''Fiber parameters'''
N_Ho = 7.8e25
k = 0.15
r = 5e-6
NA = 0.18
A = np.pi*r**2 # area of fiber core

"""Optical field parameters"""
pumpWavelength = 1950e-9
signalWavelength = 2107e-9
Vpump = 2*np.pi*NA*r/pumpWavelength
Vsignal = 2*np.pi*NA*r/signalWavelength
w0pump = r*(0.65 + 1.619*Vpump**-1.5 + 2.876*Vpump**-6)
w0signal = r*(0.65 + 1.619*Vsignal**-1.5 + 2.876*Vsignal**-6)
Gammap = 1 - np.exp(-2*(r/w0pump)**2)
Gammas = 1 - np.exp(-2*(r/w0signal)**2)

@jit(nopython=True)
def RK4step_P(f, y1, h, N):
    k1 = f(y1, N)
    k2 = f(y1+h*k1/2, N)
    k3 = f(y1+h*k2/2, N)
    k4 = f(y1+h*k3, N)
    return y1 + h*(k1 + 2*k2 + 2*k3 + k4)/6

@jit(nopython=True)
def RK4step_N(f, N, h, a, b):
    k1 = f(N, a, b)
    k2 = f(N+h*k1/2, a, b)
    k3 = f(N+h*k2/2, a, b)
    k4 = f(N+h*k3, a, b)
    return N + h*(k1 + 2*k2 + 2*k3 + k4)/6

@jit(nopython=True)
def dNdt(N, Pp, Ps): # rate equations
    W01p = Gammap*sigma01p*pumpWavelength*Pp / (hc*A)
    W10p = Gammap*sigma10p*pumpWavelength*Pp / (hc*A)
    W10s = Gammas*sigma10s*signalWavelength*Ps / (hc*A)
    W01s = Gammas*sigma01s*signalWavelength*Ps / (hc*A)

    # Single ions
```

```
    dN0dt = W11*N[1]**2 + (W10+W10p+W10s)*N[1] + W20*N[2] - (W01p+W01s)*N[0]
    dN1dt = (W01p+W01s)*N[0] + W21*N[2] - (W10+W10p+W10s)*N[1] - 2*W11*N[1]**2
    dN2dt = - dN1dt - dN0dt

    # Paired ions
    dN3dt = (W10+W10p+W10s)*N[4] + W20*N[6] - 2*(W01p+W01s)*N[3]
    dN4dt = 2*(W01p+W01s)*N[3] + 2*(W10+W10p+W10s)*N[5] + W21*N[6] + W20*N[7] - (W01p+W01s+W10+W10p+W10s)*N[4]
    dN5dt = (W01p+W01s)*N[4] + W21*N[7] - 2*(W10+W10p+W10s)*N[5] - W_pair*N[5]
    dN6dt = W_pair*N[5] + (W10+W10p+W10s)*N[7] - (W21+W20+W01p+W01s)*N[6]
    dN7dt = - dN3dt - dN4dt - dN5dt - dN6dt

    return np.array([dN0dt, dN1dt, dN2dt, dN3dt, dN4dt, dN5dt, dN6dt, dN7dt])

@jit(nopython=True)
def dPpdz(Pp, N):
    return Gammap*(sigma10p*(N[1]+N[4]+2*N[5]+N[7]) - sigma01p*(N[0]+2*N[3]+N[4]+N[6]))*Pp

@jit(nopython=True)
def dPsdz(Ps, N):
    return Gammas*(sigma10s*(N[1]+N[4]+2*N[5]+N[7]) - sigma01s*(N[0]+2*N[3]+N[4]+N[6]))*Ps

"""This function saves the power at each fiber segment at time t_end (used for non-saturable absorption simulations)"""
@jit(nopython=True)
def simulate_NSA(Nz, t_end, dt, pumpPower, L, N0):
    dz = L/Nz
    N_b = N0
    Pp_b = np.zeros(Nz+1)
    Ps = 0.0
    t = 0.0
    while t < t_end:
        Pp_a = Pp_b
        N_a = N_b
        Pp_b[0] = pumpPower
        for j in range(Nz):
            Pp_b[j+1] = RK4step_P(dPpdz, Pp_b[j], dz, N_b[j])
            N_b[j] = RK4step_N(dNdt, N_a[j], dt, Pp_b[j], Ps)
        t += dt
    return N_a + (N_b-N_a)*(t-t_end)/dt, Pp_a + (Pp_b-Pp_a)*(t-t_end)/dt

def transmission_vs_pump_power(Nz, L):
    k = 0.15
    N0 = np.zeros((Nz, 8))
```

```
110     N0[:,0] = (1-2*k)*N_Ho
111     N0[:,3] = N_Ho*k
112     dt = 60e-9
113     t_end = 90e-3
114     DT = 3e-3
115     DTnumb = int(t_end/DT)
116     N = np.zeros((DTnumb, Nz, 8))
117     Pp = np.zeros((DTnumb, Nz+1))
118     p = np.logspace(np.log10(1e-4), np.log10(100), DTnumb)
119     t1 = time()
120     for i in range(DTnumb):
121         N[i], Pp[i] = simulate_NSA(Nz, DT, dt, p[i], L, N0)
122         print('Data point', i+1)
123     t2 = time()
124     print(f'Simulation time = {np.round(t2-t1, 2)} s')
125     return N, Pp
126 
127 def nonsaturable_absorption(Pp, L1, L2, L3, Nz, Ltot):
128     dz = Ltot / Nz
129     lenList = np.array([L1, L2, L3])
130     Plist = np.zeros((3, Pp.shape[0]))
131     P_a = np.zeros((Pp.shape[0], 1))
132     P_b = np.zeros((Pp.shape[0], 1))
133     for i in range(lenList.size):
134         length = 0.0
135         c = 0
136         while length < lenList[i]:
137             P_a = Pp[:,c]
138             P_b = Pp[:,c+1]
139             length += dz
140             c += 1
141         Plist[i] = P_a + (P_b-P_a)*(lenList[i]-(length-dz))/dz
142     return Plist[0], Plist[1], Plist[2]
143 
144 def NSA(): # Non-saturable absorption
145     Nz = 100
146     Ltot = 0.15
147     N, Pp = transmission_vs_pump_power(Nz, Ltot)
148     Pp30, Pp69, Pp121 = nonsaturable_absorption(Pp, 0.03, 0.069,
        0.121, Nz, Ltot)
149 
150     fig, ax = plt.subplots()
151     ax.set_xlabel('Input power (dBm)')
152     ax.set_ylabel('Transmission (dB)')
153     ax.plot(10*np.log10(1e3*Pp[:,0]), 10*np.log10(Pp30/Pp[:,0]),
        label='30 mm')
154     ax.plot(10*np.log10(1e3*Pp[:,0]), 10*np.log10(Pp69/Pp[:,0]),
        label='69 mm')
155     ax.plot(10*np.log10(1e3*Pp[:,0]), 10*np.log10(Pp121/Pp[:,0]),
        label='121 mm')
156     plt.show()
157 
```

```
158 def main():
159     NSA()
160 
161 if __name__ == "__main__":
162     main()
```

Appendix B

Stimulated Raman Scattering

Theory

Stimulated Raman scattering (SRS) is a nonlinear optical effect that transfers energy from one EM wave (called the pump wave) to a second EM wave, either with longer wavelength (called the Stokes wave) or with shorter wavelength (called the anti-Stokes wave). This effect can be noticed if e.g. two highly intense laser pulses of different wavelengths propagate together simultaneously inside an optical fiber (a nonlinear medium). The Raman effect can be described as one pump photon with energy $\hbar\omega_\mathrm{p}$ becomes converted into a lower energy Stokes photon $\hbar\omega_\mathrm{s}$, and the difference in energy between the two photons is absorbed by the medium to excite a phonon. Also possible is the effect where a pump photon becomes converted to a anti-Stokes photon with higher energy, where the difference in energy comes from a phonon that has been absorbed in the process. The process that creates the anti-Stokes wave is however less likely than the process that creates the Stokes wave, thus the latter process will be considered here.

The Raman scattering process can occur spontaneously, or it can be stimulated by propagating two EM waves together where the longer wavelength wave (Stokes) has a wavelength that matches the Raman gain of the shorter wavelength wave (pump). The initial growth of the Stokes wave can be described by [12]

$$\frac{\mathrm{d}I_\mathrm{s}}{\mathrm{d}z} = g_\mathrm{R} I_\mathrm{p} I_\mathrm{s}, \tag{B.1}$$

where I_p and I_s are the pump intensity and the Stokes intensity, respectively. g_R is the Raman-gain coefficient. The gain coefficient $g_\mathrm{R}(\Omega)$ is a function of the frequency difference between the pump and Stokes wave $\Omega = \omega_\mathrm{p} - \omega_\mathrm{s}$, and depends on the medium that the light propagates through. For optical fibers, $g_\mathrm{R}(\Omega)$ depends on the composition of the fiber core. In silica fibers, the Raman

gain $g_{\mathrm{R}}(\Omega)$ extends over a large frequency range ($\sim 40\,\mathrm{THz}$) and has a broad peak located at about 13 THz [12]. In this work, intense pulses of 1950 nm and 2107 nm were used. It so happens that the frequency shift between these two wavelengths is $\sim 11.5\,\mathrm{THz}$ which is close to the peak of the Raman gain spectrum. Thus, if these optical pulses propagate together inside an optical fiber, energy will be transferred from the 1950 nm pulses to the 2107 nm pulses.

Equation (B.1) is only valid in the initial growth of the Stokes wave, when depletion of the pump is negligible. However, when the pump depletion can not be neglected, Equation (B.1) becomes coupled with an equation describing the depletion of the pump wave given as [12]

$$\frac{\mathrm{d}I_{\mathrm{p}}}{\mathrm{d}z} = -\frac{\omega_{\mathrm{p}}}{\omega_{\mathrm{s}}} g_{\mathrm{R}} I_{\mathrm{p}} I_{\mathrm{s}}. \tag{B.2}$$

Equation (B.1) describes how the Stokes wave grows as it propagates through the fiber, and as a function of the Raman gain, the pump intensity and the Stokes intensity itself. Equation (B.2) describes how the pump becomes depleted as it propagates, and as a function of the frequency ratio $\omega_{\mathrm{p}}/\omega_{\mathrm{s}}$ (which corresponds to the energy ratio), the Raman gain, the Stokes intensity and the pump intensity itself.

Experimental Findings

As discussed in Section 4.3, it was not possible to study the impact of PIQ on a holmium-doped fiber amplifier when the delay between the 1950 nm pump pulses and the 2107 nm seed pulses was such that the pulses overlapped. When the two pulses overlap inside the thulium-doped fiber, and because their intensities are large, the 1950 nm pulse begins to transfer its energy to the 2107 nm pulse by the process SRS.

Figure B.1 shows the average power of the amplified 2107 nm and 1950 nm pulses output from the thulium-doped fiber at delays where the pulses begins to overlap. As both pulses are $\sim 20\,\mathrm{ns}$ wide, they begin to overlap at a delay of $\sim -20\,\mathrm{ns}$ (corresponding to a delay of 9980 ns). From this delay, the amplification of the 2107 nm pulses increases drastically from when the pulses do not overlap. The maximum amplification occurs at zero delay where the pulses are completely overlapping. The average power of the 2107 nm pulses increases from $\sim 800\,\mathrm{mW}$ up to $\sim 4\,\mathrm{W}$. This increase in power is virtually fully attributed to the SRS gain. Simultaneously, the average power of the 1950 nm pulses decreases from $\sim 10\,\mathrm{W}$ down to $\sim 6\,\mathrm{W}$. This is attributed to the same effect, where power is transferred from the 1950 nm pulses to the 2107 nm pulses. Interestingly, but also as expected, the shape of the average power-increase for delays where the pulses overlap is a triangle. This is because the pulse shapes of the overlapping pulses

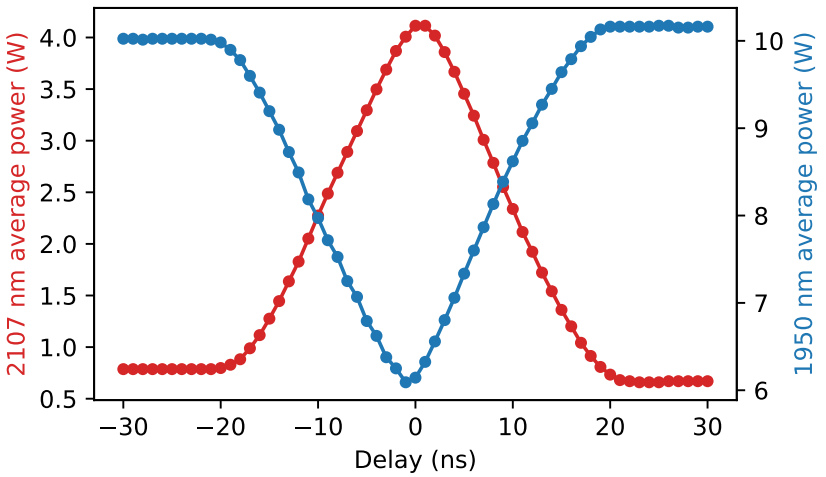

Figure B.1: Measurements of the average power of the 2107 nm pulses and 1950 nm pulses output from the thulium-doped fiber, and for delays that corresponds to where the pulses begin to overlap.

are nearly square (see Figure 5.10), and the convolution between two squares (which corresponds to the overlap) is a triangle shape.

These results reveal that even without purposely building a Raman amplifier, considerable energy transfer to 2107 nm from the 1950 nm pump is observed. A conversion efficiency above 30% is obtained, and this can likely be considerably improved by optimizing the Raman amplifier for example by increasing the fiber length. A thorough study of such a Raman amplifier would be an interesting topic for future research.

Appendix C

Measurements of Thulium-fiber Output

Figure C.1 shows five different "delay sweep" measurements of the average power 1950 nm pulses and the 2107 nm pulses output from the thulium-doped fiber in Figure 4.7, when the input 2107 nm pulses are being compensated for the experienced gain in this fiber. By comparing the five sweeps, we see that the output drifts differently each time. This is attributed to thermal fluctuations resulting in slightly different conditions for each time the experiments are performed. However, the fluctuations are small in magnitude and will not discourage the results of the experiment performed on the holmium-doped fiber amplifier. In the analysis of the optical convertion efficiency of the holmium-doped fiber amplifier in Section 5.3, the average of these five measurements at each delay point is taken as the input optical power to the holmium-doped fiber.

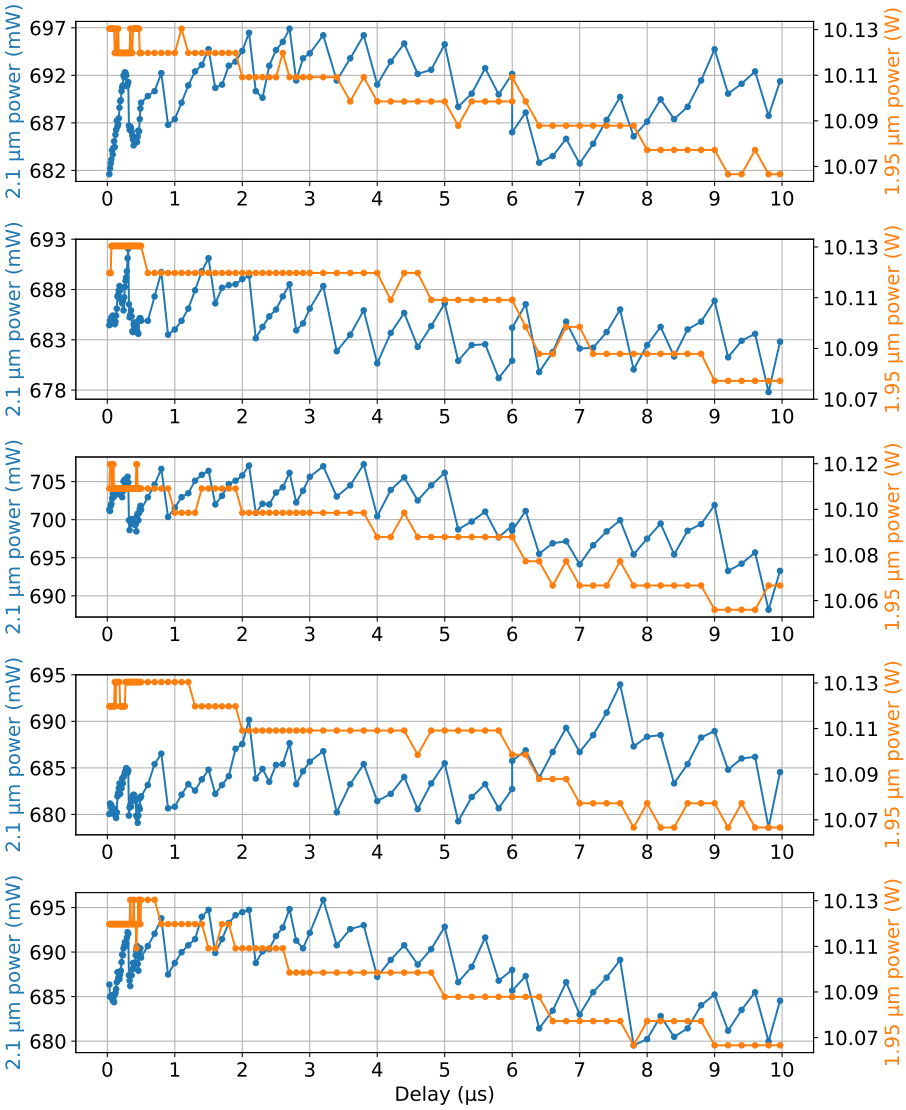

Figure C.1: Five measurements of the average output power from the thulium-doped fiber for different delays and when the input 2107 nm power is compensated for the gain it experiences in this fiber.

Bibliography

[1] A. W. Edvardsen. "Study of ion-cluster interaction dynamics in holmium-doped optical fibers". In: *Project report, Norwegian University of Science and Technology* (2021).

[2] L. G. Holmen and H. Fonnum. "Holmium-doped fiber amplifier for pumping a $ZnGeP_2$ optical parametric oscillator". In: *Opt. Express* 29 (6 2021), pp. 8477–8489.

[3] T. Maiman. "Stimulated optical radiation in ruby". In: *Nature* 187 (1960), pp. 493–494.

[4] L. Dong and B. Samson. *Fiber Lasers*. CRS Press, 2017. ISBN: 9781498725545.

[5] J. Wang et al. "Numerical modeling of in-band pumped Ho-doped silica fiber lasers". In: *J. Lightwave Technol.* 36 (24 2018), pp. 5863–5880.

[6] J. Wang et al. "Effects of ion clustering and excited state absorption on the performance of Ho-doped fiber lasers". In: *Opt. Express* 27 (10 2019), pp. 14283–14297.

[7] J. Gouët et al. "Realization and simulation of high-power holmium doped fiber laser for long-range transmission". In: *Opt. Express* 28 (15 2020), pp. 22307–22320.

[8] P. Myslinski, J. Fraser, and J. Chrostowski. "Nanosecond kinetics of up-conversion process in EDF and its effect on EDFA performance". In: *OSA Optical Amplifiers and Their Applications* (1995).

[9] P. Myslinski, D. Nguyen, and J. Chrostowski. "Effects of concentration on the performance of erbium-doped fiber amplifiers". In: *J. Lightwave Technol.* 15 (1 1997), pp. 112–120.

[10] R. Paschotta. *Optical Fiber Technology*. SPIE, 2010. ISBN: 9780819480903.

[11] E. Hecht. *Optics 5th ed.* Pearson, 2017. ISBN: 9781292096933.

[12] G. Agrawal. *Nonlinear fiber Optics 5th ed.* Academic press, 2013. ISBN: 9780123970237.

[13] O. Svelto. *Principles of Lasers 5th ed.* Springer, 2010. ISBN: 9781489977137.

[14] C. B. Layne, W. H. Lowdermilk, and M. J. Weber. "Multiphonon relaxation of rare-earth ions in oxide glasses". In: *Phys. Rev. B* 16 (1 1977), pp. 10–20.

[15] A. Einstein. "Zur Quantentheorie der Strahlung". In: *Phys. Z.* 18 (1917), pp. 121–128.

[16] G. Liu and B. Jacquier. *Spectroscopic Properties of Rare Earths in Optical Materials*. Springer, 2005. ISBN: 3540238867.

[17] D. McCumber. "Einstein relations connecting broadband emission and absorption spectra". In: *Phys. Rev.* 136 (1964), pp. 954–957.

[18] S. D. Jackson. "The spectroscopic and energy transfer characteristics of the rare earth ions used for silicate glass fibre lasers operating in the shortwave infrared". In: *Laser Photonics Rev.* 3 (5 2009), pp. 466–482.

[19] M. Kamrádek et al. "Holmium-doped fibers for efficient fiber lasers at 2100 nm". In: *OSA High-Brightness Sources and Light-driven Interactions* (2020).

[20] L. G. Holmen. *Development of* 1.5 µm *and* 2 µm *fiber lasers and applications in 3D-imaging and mid-infrared generation.* University of Oslo, 2021.

[21] N. Simakov et al. "A cladding pumped, tunable holmium doped fiber laser". In: *Opt. Express* 21 (23 2013), pp. 28415–28422.

[22] B. Peng and T. Izumitani. "Blue, green and 0.8 µm Tm^{3+}-, Ho^{3+}-doped upconversion laser glasses, sensitized by Yb^{3+}". In: *Electron. Lett.* 4 (6 1995), pp. 701–711.

[23] S. D. Jackson and T. A. King. "CW operation of a 1.064 µm pumped Tm-Ho-doped silica fiber laser". In: *IEEE J. Quantum Elect.* 34 (9 1998), pp. 1578–1587.

[24] B. Peng and T. Izumitani. "Optical properties, fluorescence mechanisms and energy transfer in Tm^{3+}, Ho^{3+} and Tm^{3+}-Ho^{3+} doped near-infrared laser glasses, sensitized by Yb^{3+}". In: *Opt. Mater.* 4 (6 1995), pp. 797–810.

[25] G. Turri et al. "Temperature-dependent spectroscopic properties of Tm^{3+} in germanate, silica, and phosphate glasses: A comparative study". In: *J. Appl. Phys.* 103 (093104 2008).

[26] C. Huang et al. "Theoretical modeling of Ho-doped fiber lasers pumped by laser-diodes around 1.125 µm". In: *J. Lightwave Technol.* 30 (20 2012), pp. 3235–3240.

[27] M. Kamrádek et al. "Nanoparticle and solution doping for efficient holmium fiber lasers". In: *IEEE Photonics J.* 11 (5 2019).

André Wean Edvardsen

Study of Pair Induced Quenching in Nanosecond-pulsed Holmium-doped Fiber Amplifiers

NTNU
Norwegian University of
Science and Technology